JAERI-M
88-100

REPORT OF THE JOINT SEMINAR ON HEAVY-ION NUCLEAR PHYSICS AND NUCLEAR CHEMISTRY IN THE ENERGY REGION OF TANDEM ACCELERATORS (III)

June 1988

(Eds.) Yasuharu SUGIYAMA, Akira IWAMOTO and Sumiko BABA

日本原子力研究所
Japan Atomic Energy Research Institute

JAERI-Mレポートは，日本原子力研究所が不定期に公刊している研究報告書です。
入手の問合わせは，日本原子力研究所技術情報部情報資料課（〒319-11茨城県那珂郡東海村）あて，お申しこしください。なお，このほかに財団法人原子力弘済会資料センター（〒319-11 茨城県那珂郡東海村日本原子力研究所内）で複写による実費頒布をおこなっております。

JAERI-M reports are issued irregularly.
Inquiries about availability of the reports should be addressed to Information Division Department of Technical Information, Japan Atomic Energy Research Institute, Tokai-mura, Naka-gun, Ibaraki-ken 319-11, Japan.

編集兼発行　日本原子力研究所
印　　刷　いばらき印刷㈱

JAERI-M 88-100

Report of the Joint Seminar on Heavy-Ion Nuclear Physics and Nuclear Chemistry in the Energy Region of Tandem Accelerators (III)

(Eds.) Yasuharu SUGIYAMA, Akira IWAMOTO and Sumiko BABA+

Department of Physics
Tokai Research Establishment
Japan Atomic Energy Research Institute
Tokai-mura, Naka-gun, Ibaraki-ken

(Received May 12, 1988)

A meeting of the third joint seminar on "Heavy-Ion Nuclear Physics and Nuclear Chemistry in the Energy Region of Tandem Accelerators " was held at Tokai Research Establishment of JAERI in the period from 7 to 9 January, 1988, being attended by 74 participants. The meeting aimed at:

1) making an opportunity for discussions by experimentalists and theorists on nuclear reaction, nuclear structure, nuclear instrumentation and nuclear chemistry,
2) presenting the results newly obtained by means of the JAERI tandem accelerator.

This report is the proceedings of the meeting and comprises 43 papers.

Keywords: Heavy-ion, Tandem Accelerator, Nuclear Reaction, Nuclear Structure, Nuclear Chemistry

---

Organizing Committee

Y. Sugiyama (Department of Physics, JAERI)
A. Iwamoto (Department of Physics, JAERI)
S. Baba (Department of Radioisotopes, JAERI)
+ Department of Radioisotopes

JAERI－M 88－100

タンデム領域の核物理・核化学の研究会（Ⅲ）
報 告 集

日本原子力研究所東海研究所物理部
（編）杉山康治・岩本 昭・馬場澄子+

（1988年5月12日受理）

第3回目の「タンデム領域の核物理・核化学の研究会」が1988年1月7日から9日にかけて，日本原子力研究所東海研究所において開催され，74人の所内及び所外の研究者が参加した。この研究会は，原子核反応及び構造，研究装置，核化学など広い範囲の研究に携わる理論研究者達と実験研究者達が討論する場を提供することと，JAERIタンデム加速器により得られた新しい研究結果を紹介することを開催目的としている。この報告書は，研究会で発表された43の研究報告をまとめたものである。

研究会世話人 杉山康治（日本原子力研究所物理部）
岩本 昭（ 〃 ）
馬場澄子（日本原子力研究所アイソトープ部）
東海研究所：〒319－11 茨城県那珂郡東海村白方字白根2－4

+ アイソトープ部

Contents

Speakers in paper of collaboration are denoted by underlines.

目　　次

1. Nuclear Structure at High Spin States

Teruo Kishimoto*, Shin-ichi Kinouchi*, Hideo Sakamoto* and Tetsuo Kammuri**

*Insitute of Physics, University of Tsukuba and **Department of Physics, Osaka University

The present status of our study on nuclear structures at high spin states is briefly reported. In particular, the couplings between particle and rotational motions arising from shape changes at high spin states as well as those from velocity dependent terms in an average nuclear potential are discussed, which can crucially modify the conventional cranking term.

Let us first analyze a model Hamiltonian in order to see the effect of shape changes on the particle-rotation coupling. The Hamiltonian to start with is that of the SU_3 model expressed by

$$H = H_0 - \frac{\chi}{2} \sum_{\mu} Q_{\mu}^{\dagger} Q_{\mu} \quad , \quad Q_{\mu} = \sum_{i=1}^{A} (Q_{\mu})_i \quad ,$$

where H_0 is a Hamiltonian for a spherical harmonic oscillator and Q_{μ} an SU_3 quadrupole operator. According to the Hartree approximation, the intrinsic Hamiltonian is known to be that of a deformed harmonic oscillator potential and it may be expressed with a deformation parameter a_{ν} as

$$H_{def} = H_0 - \sum_{\nu} a_{\nu} Q_{\nu} \equiv \sum_{i=1}^{A} (h_{def})_i \quad ,$$

and in the quanta representation as

$$h_{def} = \hbar\omega_x (c_x^{\dagger} c_x + \frac{1}{2}) + \hbar\omega_y (c_y^{\dagger} c_y + \frac{1}{2}) + \hbar\omega_z (c_z^{\dagger} c_z + \frac{1}{2}) \quad .$$

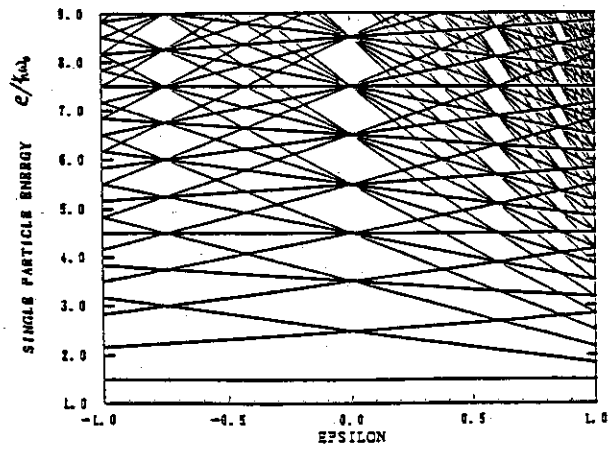

Fig.1

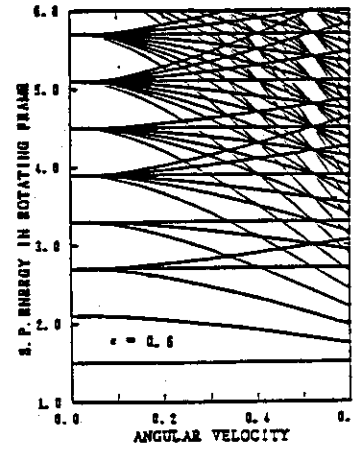

Fig.2

The single particle energies as a function of deformation parameters are nothing but Nilsson diagrams for this model, and they are shown in Fig.1 assuming a prolate deformation. Impressive shell closures at ε=0.6 corresponging to 2:1 ratio in nuclear radii can be seen. Degenerate orbits here have major oscillator quantum numbers differing by one and the unperturbed excitation energies for a ΔK=1 octupole mode is zero near the deformed closed shell indicating a possible octupole instability.

In a rotating system, the intrinsic Hamiltonian in the cranking model is given by

$$\tilde{h}_{def} = h_{def} - \Omega\cdot\ell_x = \sum_{\kappa=x,y,z} \omega_\kappa (c^\dagger_\kappa c_\kappa + \frac{1}{2}) - \Omega\cdot(c^\dagger_y c_z + c^\dagger_z c_y) \quad ,$$

which can be expressed in terms of new quanta for normal modes as

$$\tilde{h}_{def} = \sum_{\alpha=1,2,3} \omega_\alpha (c^\dagger_\alpha c_\alpha + \frac{1}{2}) \quad .$$

The single particle energies as a function of the angular velocity Ω are shown in Fig.2 for a fixed deformation of ε=0.6. The effect of rotational disturbances on single particle energies are quite dramatic and such an effect on charged particles would only be produced by an equivalent magnetic field of 10^{17} Gauss for $\hbar\Omega$≅1Mev. The approach here is called as the cranked Nilsson model and has been used quite extensively in realistic calculations. The model can predict the termination of a rotational angular momentum at a certain value.

In order to follow a detailed change in nuclear shapes, one has to take the self-consistent mechanism seriously. Minimization of the cranked Hartree energy $\tilde{E} = \langle H - \Omega\cdot L_x \rangle$ is equivalent to the self-consistency condition in a rotating system given by $a_\nu = \chi \langle Q_\nu \rangle$, which in fact insures the canonicity relation $\partial\tilde{E} / \partial\Omega = - \langle L_x \rangle$. Therefore for each Ω, the deformation parameters must be determined by the self-consistency condition, which then determine ω_κ (κ=x,y,z) and finally ω_α (α=1,2,3). The self-consistent single particle energies in the present model turn out to be constant for all Ω, and therefore the level crossings seen in Fig.2 is completely spurious when shape changes are taken into account. Such a drastic result, of course, is because of the simple model we have employed here, and is consistent with the SU_3 model where the particle and rotational degrees of freedom are decoupled completely.

The induced particle-rotational coupling arising from shape changes can now be expressed as the modification to the cranking term:

$$\tilde{H}'_{def} = H_0 - \sum_\nu a_\nu(\Omega_0)Q_\nu - \Omega_0 \cdot L_x + \delta\Omega \cdot \left[L_x + \sum_\nu \left[\frac{\partial a_\nu}{\partial \Omega} \right]_0 Q_\nu \right] ,$$

where the additional term arises just in order to satisfy the self-consistency relation with a new deformation parameter $a_\nu(\Omega_0+\delta\Omega)$ when the angular velocity changes as $\Omega_0 \rightarrow \Omega_0+\delta\Omega$, which indeed guarantees the complete attenuation of the particle-rotation coupling in the SU_3 model.

The above formulation expanded about a certain classical Ω_0 togather with the canonicity relation mentioned above enables us to formulate the modified cranking model in a quantal description even in triaxial rotational motions at high spin states. The effective quadrupole moment and transition operators under rotational disturbances are derived and tested successfully against exact SU_3 results at least in low spin states.

The requirement of self-consistency in a nuclear system has played quite important roles in our derivation of the higher-order effective interactions and the higher-order particle-collective couplings. The most unique features of effective interactions in rotating nuclei arise from velocity dependences in the realistic single particle potential, such as $(\ell \cdot s)$, ℓ^2, a paring potential and a cranking term, and the time reversal violation in the rotating intrinsic system. The general framework has been developed and the model is being tested in several examples. The application to recently observed high-spin states of super-deformed nuclei has yielded the modification of moments of inertia as much as 40% in apparently good agreement with experimental observations. The study of giant resonances at high-spin states is also initiated with a new type of interaction. The spectroscopic studies of high-spin states will provide us with valuable informations to explore unique properties of a nuclear system so far unaccessible.

The detailed explanation of the present discussion can be found in ref.1, and will be reported elsewhere.

Reference:

1. S.-I. Kinouchi, Ph.D. Thesis, University of Tsukuba, 1988.

2. Multiple Coulomb Excitation in the Nd-Sm Nuclear Region

Hideshige KUSAKARI*, Masumi OHSHIMA** and Yoichi ONO*

*Faculty of Education, Chiba University, Chiba, 260, and **Physics Division, Japan Atomic Energy Research Institute, Tohkai, Ibaraki, 319-11

The experimental data on B(E2) values in the even-mass Nd, Sm and Gd isotopes with $N \approx 90$ are limitted to those for low-spin states below the 6^+ or the 8^+ state. However, these B(E2) values in the yrast band (ground-state band) seem to show a very interesting feature[1,2,3]: the B(E2) values in ^{150}Nd, ^{152}Sm and ^{154}Gd increase more rapidly with increasing spin I than predictions based on a rigid-rotor model. The $B(E2;8^+ \rightarrow 6^+)$ is about 130 % of a rigid-rotor model prediction (see Fig. 1). Discussions on these B(E2) values have been done and explanation was made as a effect of band mixing with the beta-vibrational band[1,2,3].

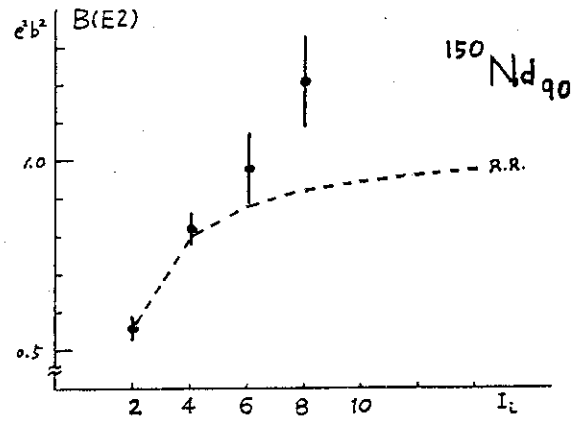

Fig. 1 Experimental B(E2) in ^{150}Nd (from ref. 3) and a rigid-rotor model prediction.

We intended to check up such a interesting feature and to get new information about B(E2) values for higher-spin states. We measured the gamma-gamma coincidences and gamma-ray angular distributions for ^{148}Nd and ^{150}Nd. As shown in Fig. 2, new levels of 8^+ in ^{148}Nd and of 10^+ and 12^+ in ^{150}Nd were observed in the present Coulomb excitation experiment. We also obtained the integrated yields of multiple-Coulomb excitation for ^{148}Nd and ^{150}Nd using the 230 MeV ^{58}Ni beam and the thick ^{148}Nd and ^{150}Nd targets (18 mg/cm^2 and 20 mg/cm^2). This incident energy of ^{58}Ni beam is safe for the Coulomb excitation experiment. The ^{58}Ni beam was stopped in the target.

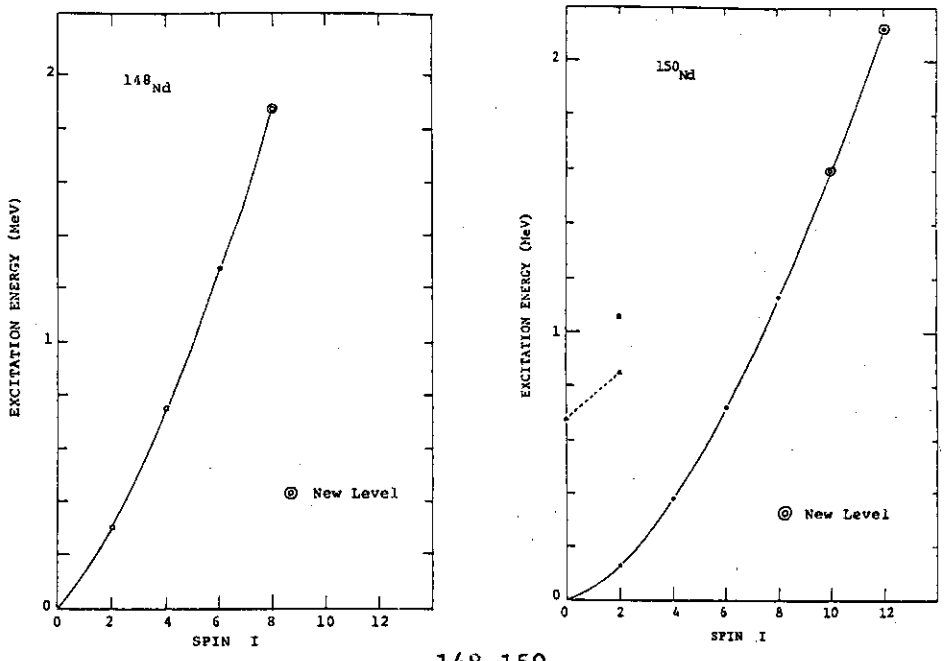

Fig. 2 Observed excited levels of ^{148,150}Nd in the present Coulomb excitation experiment.

The relation between the cross sections of Coulomb excitation, $\sigma(I^+)$, and the measured values $I_0(I^+)$ are schematically shown in fig. 3. The total yields of transitions, $I_0(I \rightarrow I-2)$, are corrected for conversion electrons and are compared with the theoretical values, $\sigma_{tot}(I^+)$, as follows:

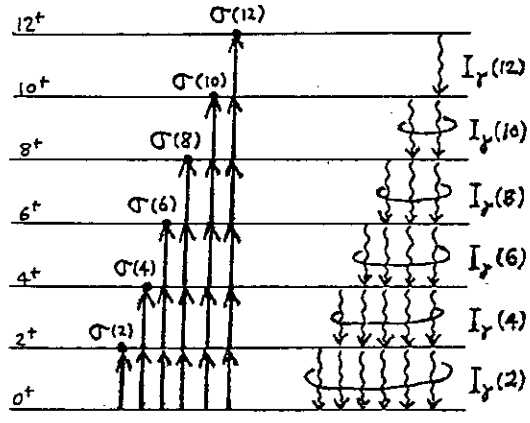

Fig. 3 Schematic explanation for cross sections of multiple-Coulomb excitation and gamma-ray yields.

$$\frac{I_0(I \rightarrow I-2)}{I_0(2^+ \rightarrow 0^+)} = \frac{\sigma_{tot}(I^+)}{\sigma_{tot}(2^+)} ,$$

$$\sigma_{tot}(I^+) = \sigma(I) + \sigma(I+2) + - - - - - + \sigma(I_{max}) ,$$

$$\text{and} \quad \sigma(I^+) = \int \sigma(I^+, E(x))\, dx ,$$

where E(x) is an average energy of ^{58}Ni beam at the depth x in the thick target, and each value of E(x) was estimated with a step of 1 mg/cm^2 using Ziegler's table[4]. The cross sections of Coulomb excitation, $\sigma(I^+, E(x))$,

were calculated using the deBoer-Winther code[5]. For simplification in comparison, the rigid-rotor model is adopted in the calculations. Used values of the intrinsic static quadrupole moment Q_0 are 5 [b] and 7 [b] for ^{148}Nd and ^{150}Nd, respectively, which were deduced from the experimental values of the static quadrapole moment $Q(2^+)$. Fig. 4 shows comparison between the present experimental data and the calculations in ^{148}Nd and ^{150}Nd. Obvious diferences between the experimental values and the calculated values are seen for higher-spin ($I \geq 6$) states in the both cases of ^{148}Nd and ^{150}Nd. It means that the experimental B(E2) values for the higher-spin states are smaller than the rigid-rotor model predictions. The discrepancy between the present result (based on " thick target + multiple-Coulomb excitation ") and the previous data proposes a very important problem.

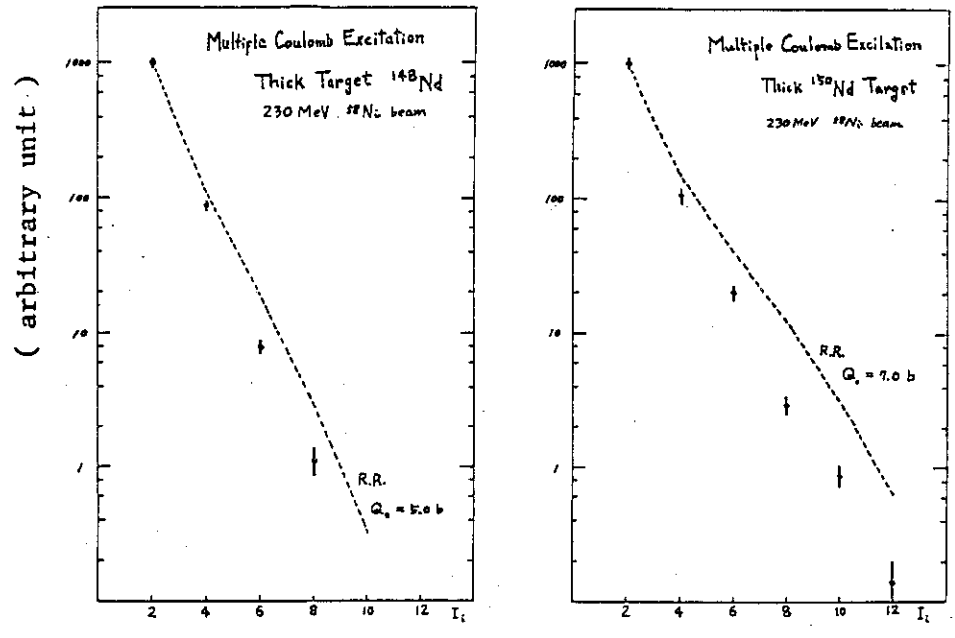

Fig. 4 Comparison between the experimental yields of transitions following to the multiple-Coulomb excitation using a thick target and the rigid-rotor model predictions. (left: ^{148}Nd, right: ^{150}Nd)

References

1) N. Rud et al., Nucl. Phys. A191 (1972) 545
2) H.J. Wollersheim and Th.W. Elze, Nucl. Phys. A278 (1977) 87
3) S.W. Yates et al., Phys. Rev. C17 (1978) 634
4) Ziegler, "Table of Stopping Power and Range" pp.394
5) A. Winther and J. de Boer, "Coulomb Excitation" (Academic Press) pp.394

3. G-factors along the yrast levels in Er isotopes from A=158 to 170

K. Sugawara-Tanabe and K. Tanabe*
Dept. of Physics, Univ. of Tokyo, Tokyo, 113 Japan
* Dept. of Physics, Saitama Univ., Urawa, Saitama,338 Japan

Recently experimental data of g-factors along the yrast line and also for γ-vibrational 2^+ states have become available[1]. The most interesting data is the difference between the behavior of g-factors along the yrast line for ^{166}Er and that for ^{168}Er. For ^{166}Er, the g-factor decreases monotonically with an increasing angular momentum, while for ^{168}Er it keeps nearly constant. In the backbending plot the former nucleus shows gradual increase and the latter much more modest increase. This indicates there is a delicate change in spin alignment between these two nuclei. For ^{158}Er it is measured around spin 16^+ and becomes nearly negative or zero, indicating the alignment comes from ν i13/2 level. Since one-body field is well approximated by the cranked HFB equation[2], we apply our calculation to g-factors along the yrast line. The yrast state is calculated from the variational principle of the hamiltonian with three constraints of $\hat{N}_\pi$, $\hat{N}_\nu$ and $\hat{J}_x$. Our hamiltonian has spherical single particle energy and residual pairing, quadupole-pairing, and quadrupole-quadrupole interactions. The spherical single particle levels over two major shells for each of proton and neutron shells are fixed from the spherical Nilsson levels without adding any additional energy shift. The quadrupole-quadrupole interaction between π-π is the same value with that between ν-ν and that between π-ν is set free. The quadrupole-pairing interaction is chosen to be proportional to pairing interaction and the ratio is fixed. Thus we have only 3 free parameters, and change them nearly monotonically from A=158 to 170. We got quite nice fit to the experimental data for both the energy levels and the g-factors systematically over these isotopes. In Fig.1 we show both the backbending curves and g-factors up to spin 20 over Er isotopes.

Fig.1

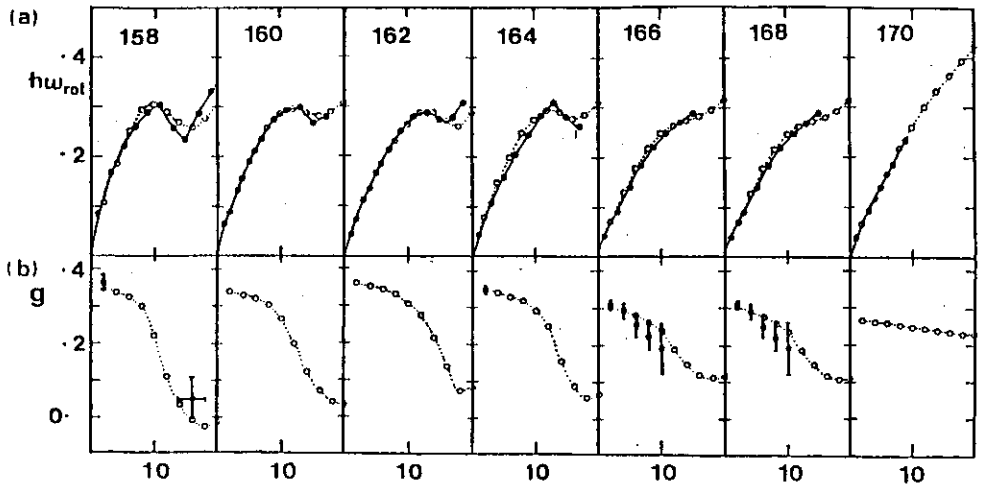

I

Fig.1(a)shows rotational angular frequency $\hbar\omega_{rot}$ versus I over Er isotopes. The vertical axis is $\hbar\omega_{rot}$ in units of MeV, and the horizontal axis is I in common with Fig.1(b). The experiments [1] are plotted by solid circles connected with the solid line and the theoretical values are by open circles with dotted lines. The numerals inside of each figure are mass number A, which is common in Fig.1(b) shows g-factors without reduction factor versus I over Er isotopes. The vertical axis is g-factor. Solid circles with error-bar are experimental values. The theoretical values are shown by open circles connected with dotted line.

The g-factor is defined by,

$$g = \frac{g_l \langle \hat{J}^{\pi}_x \rangle + g^{\pi}_s \langle \hat{s}^{\pi}_x \rangle + g^{\nu}_s \langle \hat{s}^{\nu}_x \rangle}{\langle \hat{J}^{\pi}_x + \hat{J}^{\nu}_x \rangle} , \qquad (1)$$

where $\hat{J}^{\pi}_x$ ($\hat{J}^{\nu}_x$) is the proton(neutron) angular momentum operator, $\hat{s}^{\pi}_x$ ($\hat{s}^{\nu}_x$) the proton(neutron) spin operator and the gyromagnetic ratios of a free nucleon are denoted by g_l , g^{π}_s and g^{ν}_s. For low spin state the expectation value of s_x is small, and (1) becomes $\langle J^{\pi}_x \rangle / \langle J^{\pi}_x + J^{\nu}_x \rangle$. Thus the variation of g-factors as a function of I is directly related to the rotational alignment mechanism which comes from the collapse of the nucleon pairs near the Fermi surface.

Now we see the detail mechanism of spin alignment over these isotopes. In Fig.2 we show a change of a few quasi-particle energies of ν+ shell which are smalller than 2.2 MeV according as an increase of I over Er isotopes. Fig. 2 shows the quasiparticle energy E_i versus I over Er isotopes. The numerals inside the figures are mass number A. The horizontal axis is I and the vertical axis is E_i in

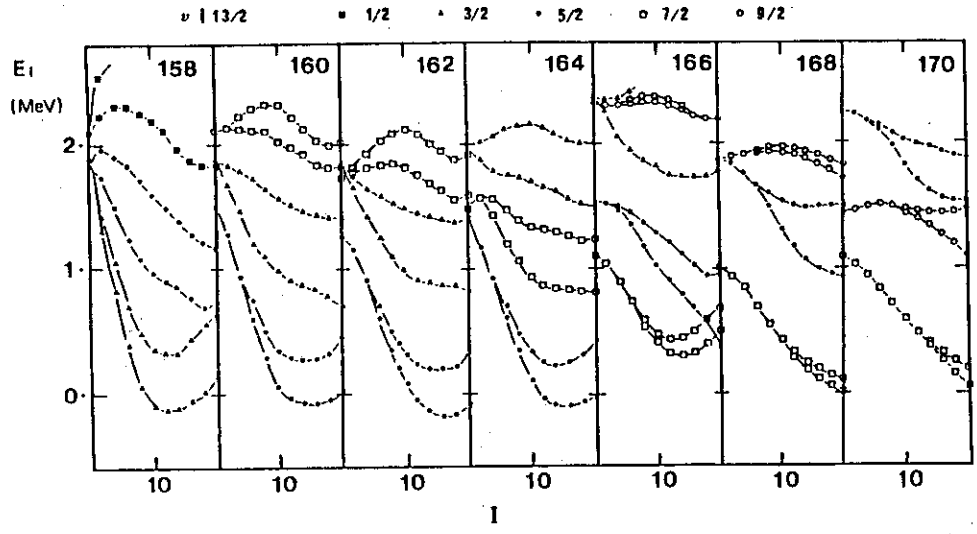

units of MeV. The solid squares denotes j_z =1/2, the solid triangles 3/2, the solid circles 5/2, the open squares 7/2 and the open circles 9/2. From A= 158 to 164, the quasiparticle energy E_i becomes negative nearly around the b. b. point in Fig.1a, showing the gapless superconducting state[3].

We see the splitting of E_i for j_z and its time reversed state when I or $\hbar\omega_{rot}$ becomes large. The lowest E_i shows the position of fermi surface. The spin of the lowest quasi-particle energy changes from j_z =3/2 to 9/2 from A=158 to 170. The second lowest spin state follows this change. Thus we can conclude that the fermi surface at ν i13/2 changes gradually from j_z=3/2 to 9/2 according as A=158 to 170 and it influences the delicate change of backbending.

Refs.[1] observes g-factors of 2^+_γ states. Then we must apply RPA calculation[4]. However whithin RPA approximation, the expectation value of one-body operator in 1-phonon 2^+ state does not differ from that in cranked HFB ground state, i.e. $\langle J_x \rangle = \langle O_n J_x O_n^\dagger \rangle_{RPA}$, where $O_n^\dagger$ is the creation operator of 1-phonon with n-th eigenvalue from RPA ground state. Thus we get the same g-factor value as that in the ground state. If we want to get the different value, we must go beyond RPA to HRPA. Experimentally the error-bar is large and there are no difference from the ground state value for a moment.

In conclusion the energy level behaviour(b. b.) is closely related to g-factor behaviour, which originates from the pairing collapse at ν_+ i13/2 level.

References

[1] C.E.Doran, H.H.Bolotin,A.E.Stuchbery,A.P.Byrne & G.J.Lampard, Proc. of Int.Conf.on Nuclear structure through static and dynamic moments, Melbourne,Aug.(1987)vol.2,169.:Z.Phys.A325(1986)285.: C.Ryan & H.H.Bolotin, private communication.:A.Alzner et al, Proc. of Int. Conf.on Nuclear structure through static and dynamic moments, Melbourne Aug.(1987)vol.2,165.

[2] K.Sugawara-Tanabe & K.Tanabe, Phys.Lett.192B(1987)268; 135B(1984) 353.

[3] B.Banerjee H.J.Mang & P.Ring, Nucl.Phys.A215(1973)366.

[4] K.Sugawara-Tanabe & A.Arima, Proc.of Int.Conf.on Nuclear structure through static and dynamic moments, Melbourne,Aug.(1987)vol.2,71.

4. Electromagnetic Transition Probabilities for One-Quasineutron Natural-Parity Rotational Bands

Masumi Oshima,[*] Eisuke Minehara,[*] Shin-ichi Ichikawa,[**] Hideki Iimura,[**] Takashi Inamura,[***] Akira Hashizume[***] and Hideshige Kusakari[****]

[*]Department of Physics, [**]Department of Chemistry, Japan Atomic Energy Research Institute, [***]RIKEN(The Institute of Physical and Chemical Research) and [****]Faculty of Education, Chiba University.

Rotational perturbation effect which causes signature dependent level energies and transition moments has been well established theoretically and experimentally for the case of high-spin orbitals such as $i_{13/2}$[1-3] and $h_{11/2}$.[4,5] This effect is caused by the Coriolis force which strongly acts on high-spin orbitals. In contrast the effect on lower-spin orbitals is not well known because it is believed to be rather weak. It is, however, desirable to study in detail how the Coriolis force affects the rotational levels based on the low-spin orbitals. For this purpose we undertook multiple Coulomb excitation experiments on ^{163}Dy, ^{173}Yb and ^{157}Gd with a 250-MeV ^{58}Ni beam from the tandem accelerator at Japan Atomic Energy Research Institute. Information on levels and electromagnetic transition probabilities for the ground-state rotational bands was obtained up to high spins. The main component of the ground state in ^{163}Dy is $h_{9/2}$ and those in ^{173}Yb and ^{157}Gd are $f_{7/2}$.[6] A part of this work has been reported elsewhere.[7]

Since the low-spin orbital bands have a natural parity in nature, j-mixing is the most distinct properties of these bands; Simple rules (single-j model) for the signature dependences of the B(M1) values and of the quasiparticle energies,[8] which has been well established for the high spin orbital bands, are not expected to hold. In fact, we have observed quite a large signature dependent staggering of B(M1) values and its phase contradicts with a prediction of the single-j model for $j = \frac{9}{2}$. A small mixing of the $f_{7/2}$ orbital is considered to be sensitive to the B(M1).

The ground state of $^{173}_{70}Yb_{103}$ is the $\nu\frac{5}{2}$[512] single-particle state and the main component is assumed to be $f_{7/2}$. The B(M1;I → I-1), B(E2;I → I-2) and B(E2;I → I-1) values are plotted in units of predictions of rigid-rotor model[7] in Figs. 1-3, respectively. An intrinsic quadrupole moment,

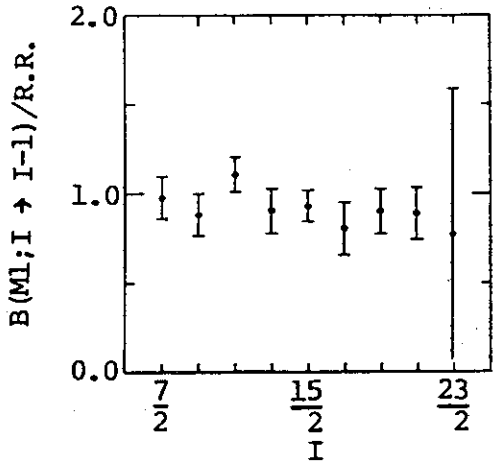

Fig. 1 B(M1;I → I-1) values of the gound band of ^{173}Yb in units of rigid-rotor model prediction.

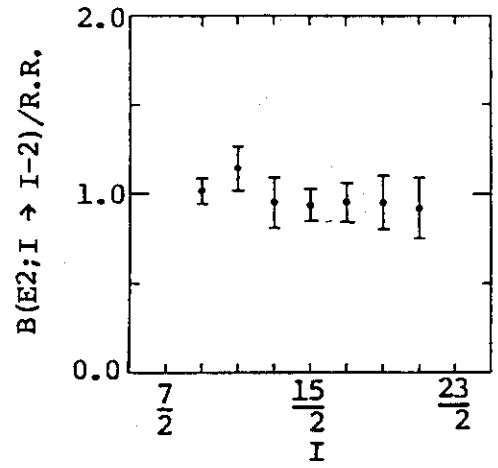

Fig. 2 B(E2;I → I-2) values of the ground band of ^{173}Yb in units of rigid-rotor model prediction.

Fig. 3 B(E2;I → I-1) values of the ground band of ^{173}Yb in units of rigid-rotor model prediction.

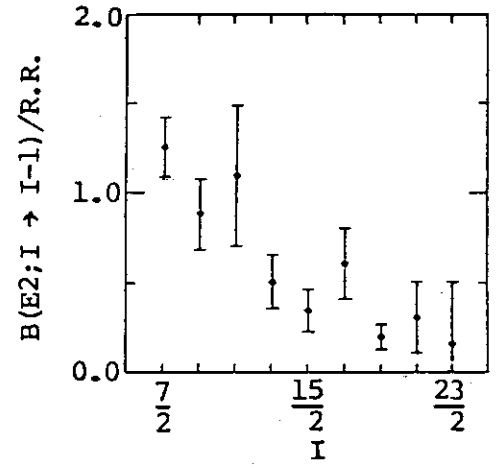

Q_0 = 7.4 b, and g-factors, $g_k - g_R = -0.77$, were assumed for the rigid-rotor model predictions.[6] The B(M1;I → I-1) and B(E2;I → I-2) values are close to the rigid-rotor model predictions and they show almost no signature dependence. This observation reflects the fact that the rotational perturbation due to the Coriolis force is weak for the predominant $f_{7/2}$ orbital. An interesting feature is that the B(E2;I → I-1) values deviate significantly from the rigid-rotor model predictions at high spins (see Fig. 3).

A preliminary analysis for $^{157}_{64}Gd_{93}$ shows that the B(M1) and B(E2) values have a similar tendency to those of ^{173}Yb: While the B(M1) values do show larger signature dependence than those of ^{173}Yb, the amplitude of the zigzag is still rather small as compared to those of the high-spin orbital (It should be noted that the phase of the staggering coincides with the single-j model prediction for $j = \frac{7}{2}$.); and the B(E2;I → I-1) values tend

to decrease with increasing spin and their absolute values are always smaller than rigid-rotor model predictions.

We summarize the experimental results as follows. The signature dependence of B(M1) values are small but, as the neutron number decreases, it becomes appreciable. The signature dependence may indicate a significant γ deformation because in the region of $N \sim 90$ the nucleus in general becomes γ-unstable and it is known that the γ deformation is much concerned with the signature dependence. The reduction of the $B(E2;I \rightarrow I-1)$ values observed at high spins may coincide with the results obtained for ^{165}Lu[2] and ^{161}Dy.[3] In order to understand the experimental results for ^{173}Yb and ^{157}Gd theoretical calculation taking into account of the γ degrees of freedom and j-mixing should be necessary. The theoretical study is in progress.

References

1) M.Ohshima, E.Minehara, M.Ishii, T.Inamura and A.Hashizume, Nucl. Phys. A436 (1985) 518
2) J.Kownacki, J.D.Garrett, J.J.Gaardhøje, G.B.Hagemann, B.Herskind, S.Jonsson, N.Roy, H.Ryde and W.Walus, Nucl. Phys. A394 (1983) 269
3) M.Oshima, E.Minehara, S.Ichikawa, H.Iimura, T.Inamura, A.Hashizume and H.Kusakari, submitted to Phys. Rev. C (1987)
4) G.B.Hagemann, J.D.Garrett, B.Herskind, J.Kownacki, B.M.Nyako, P.L.Nolan and J.F.Sharpey-Schafer, Nucl. Phys. A424 (1984) 365
5) S.Jonsson, J.Lyttkens, L.Carlen, N.Roy, H.Ryde, W.Walus, J.Kownacki, G.B.Hagemann, J.D.Garrett, B.Herskind and P.O.Tjøm, Nucl. Phys. A422 (1984) 397
6) A.Bohr and B.R.Mottelson, Nuclear Structure Vol. 2 (Benjamin, New York, 1975)
7) E.Minehara, M.Oshima, S.Kikuchi, T.Inamura, A.Hashizume and H.Kumahora, Phys. Rev. C35 (1987) 858
8) I.Hamamoto, Phys. Lett. 106B (1981) 281; Proc. Niels Bohr Centennial Conf. on Nuclear Structure, Copenhagen 1985, ed. R.Broglia, G.B.Hagemann and B.Herskind (North-Holland, Amsterdam-London, 1985) p.129

5. Effects of Particle-Rotation Interaction in Normal-Parity Bands

Akitsu Ikeda
Physics Department, Tokyo Institute of Technology
Oh-okayama, Meguro, Tokyo

Rotational motion of a nucleus influences its own internal structure in various ways: it may change the nuclear shape or reduce the pairing correlation. Among the various effects, rotation-alignment of particles is important and has been observed in many nuclides. It manifests itself conspicuously in the rotation-aligned bands of odd-A nuclides and the backbend of yrast bands of even nuclides. These are caused by rotation-alignment of a particle or particles in unique-parity orbitals such as $i_{13/2}$ and $h_{11/2}$. As is seen from the examples, the effect of rotation-alignment is strong for particles in unique-parity orbitals, because the Coriolis interaction, which is responsible for it, has large matrix elements when those orbitals are involved. The effect of rotation alignment gives rise to a characteristic feature in rotational bands based on unique-parity orbitals in odd-A nuclides. Such a rotational band is split into two sequences of levels with spin difference of two unit, each of which has a definite quantum number called signature, $s = \frac{1}{2}(-1)^{I-\frac{1}{2}}$. The signature is related to the symmetry of a deformed intrinsic state under rotation of 180 degrees around an axis perpendicular to the symmetry axis. The symmetry holds not exactly but approximately when the nucleus is triaxially deformed. One of the two sequences consists of levels with spin equal to j+2n, and the levels of the other sequence have spins equal to j+2n+1. The former is shifted downward in energy and, therefore, called the favored band. The latter is called the unfavored band. Thus the signature has one to one correspondence to favoredness of the energy shifts. Another important property of such rotational bands is that magnetic transitions from I to I-1 is stronger when I is a favored level than when it is an unfavored level.

Recently energy spectra and M1 transition probabilities have been measured for a rotational band in ^{163}Dy by Minehara et al. by using the Tandem accelerator at JAERI.[1,2] The band is not based on unique-parity

orbitals but is considered to largely involve a natural-parity orbital 5/2[523]. The result is remarkable in that the excitation energies are quite smooth with spin, indicating a regular rotational motion, but that the M1 transitions show rather strong oscilation with spin, indicating appreciable rotational perturbation.

It is natural to attempt to understand the data by assuming the dominance of orbitals of a specific j-value. Since M1 probabilities are strong for the 11/2→9/2, 15/2→13/2, 19/2→17/2 transitions but weak for 9/2→7/2, 13/2→11/2,and 17/2→15/2 transitions, the dominant j is considered to be $f_{7/2}$ in view of what is known in the case of unique-parity orbitals. A close look at the energy spectrum, however, shows us that it is not really smooth with spin but deviates slightly from a smooth line. The 9/2, 13/2, 17/2,... levels are shifted downward in energy and this suggests the dominance of $h_{9/2}$. Thus, the energy spectrum and M1 transitions suggest different values for the dominant j and the idea of the dominance of specific single-j orbitals has a difficulty.

The involvement of different j's seems to be essential to understand the experimental data. What is expected is the following: the rotational motion gives rise to a rotation-alignment in this situation also. We should remember that the rotation-alignment has produced two kinds of structure, favored and unfavored in the case of unique-parity orbitals. In the present situation, the rotation-alignment will let orbitals j form a favored structure in I=j+2n levels and an unfavored structure in I=j+2n+1 levels. To be more concrete, $h_{9/2}$ will contribute to form a favored structure in I=9/2, 13/2, 17/2... and an unfavored structure in I=11/2, 15/2,... while the opposite applies to $f_{7/2}$. The system will be able to make its energy lower by increasing the favored structure and by reducing the unfavored structure. Consequently $h_{9/2}$ will be involved more in I=9/2, 13/2, 17/2,...and $f_{7/2}$ more in I=7/2, 11/2, 15/2, and so on. Thus the two different structures must develope alternatively with spin in the seemingly single rotational band. It is then quite probable that the energy spectrum is not disturbed very much because the 7/2, 11/2, 15/2,....levels and the 9/2, 13/2, 17/2,...levels will gain negative energy shifts of similar size from $f_{7/2}$ and $h_{9/2}$, respectively.

With these physical pictures in mind, numerical calculations have been carried out in terms of a particle - symmetric rotor model in which $p_{1/2}$, $p_{3/2}$, $f_{5/2}$, and $h_{11/2}$ are taken into account in addition to $f_{7/2}$ and $h_{9/2}$.

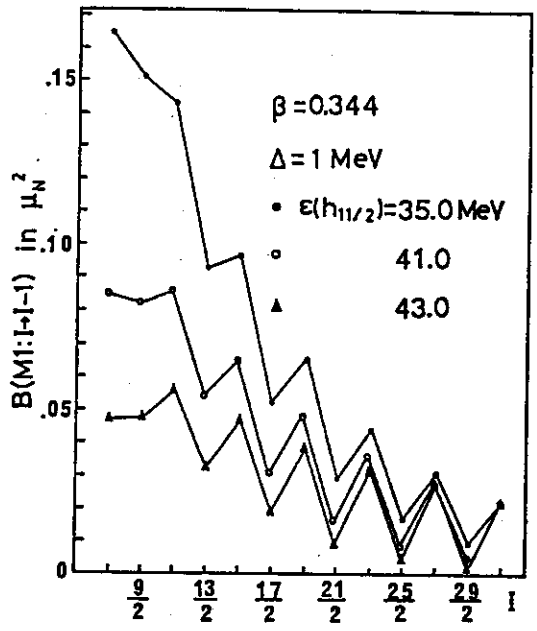

Fig. 1 B(M1:I→I-1)'s vs I. Spherical single particle energies are: $\varepsilon(p_{1/2})$=53.29, $\varepsilon(p_{3/2})$=51.94, $\varepsilon(f_{5/2})$=52.31, $\varepsilon(f_{7/2})$=49.01, $\varepsilon(h_{9/2})$=49.69 MeV. The chemical potential is placed between 5/2[523] and 3/2[521], and 1 MeV is chosen for the energy gap. The deformation, ß, is 0.344. $\varepsilon(h_{11/2})$ is varied to see its effect. When $h_{11/2}$ is located higher in energy, its effect is larger and B(M1)'s are found to be more suppressed.

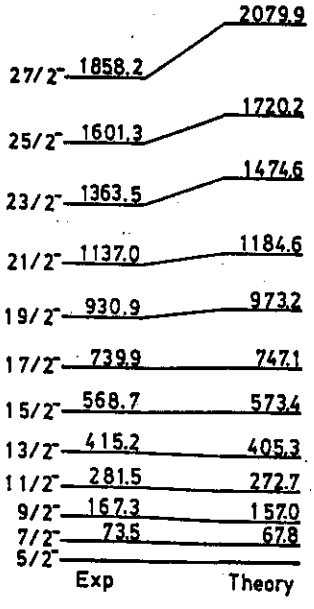

Fig. 2 The experimental and theoretical energy spectra. The energies are given in keV. The theoretical energy grows too fast for larger spins due to the assumed rigid rotor.

Two figures are presented to show that the characteristic features can be understood by the present calculation. In Fig.1 B(M1:I→I-1)'s are plotted against angular momentum for a few different locations of $h_{11/2}$ relative to the other orbitals. It should be noted that the observed variation of B(M1)'s with respect to spin are well reproduced by the calculation. We observe also that the effect of $h_{11/2}$ orbitals is remarkable in reducing the transition probabilities. This effect has been noted for the first time with an experimental evidence. We should be careful when employing the widely accepted idea that the interaction between $h_{11/2}$ and the other normal-parity orbitals is negligibly small. Although we have obtained very weak transition probabilities, they are still larger than the experimental data by almost an order of magnitude. Since the reduction of the B(M1)'s is a result of delicate cancellation, a more careful numerical analysis has to be done.

The calculated energy spectrum is illustrated in Fig.2 together with the experimental data. The calculation well reproduces the rather smooth increase of the energy with spin, though the staggering is slightly stronger in the theoretical results than in the experimental data.

In conclusion, the present model and calculations are found capable to describe the experimental data of ^{163}Dy. Thus we can be confident in the wave functions obtained. What remains to be done is to analyse them and to see if our physical picture described at the beginning of this report really applies to the data. Such a detailed study is now under progress.

This work was partially supported by the Grant-in-aid for Scientific Research of Japan Ministry of Education, Science and Culture under Grant No.62540198.

References

[1] E.Minehara, M.Oshima, S.Kikuchi, T.Inamura, A.Hashizume, and H.Kumahora, Phys. Rev. C35 (1987) 858.

[2] M.Oshima, E.Minehara, S.Kikuchi, T.Inamura, A.Hashizume, M.Matsuzaki, and H.Kusakari, preprint RIKEN-AF-NP-62.

6. Signature Dependence of Electromagnetic Transitions and the Interacting Boson-Fermion Model

Nobuaki Yoshida*, Hiroyuki Sagawa**, Takaharu Otsuka** and Akito Arima**

*Department of Information Science, University of Tokyo, **Department of Physics, University of Tokyo

The recent development of gamma-ray spectroscopy provides us with new information on energy levels and electromagnetic transitions in deformed nuclei.[1,2] Especially, the signature dependence observed in odd-A nuclei has inspired studies on triaxiality of nuclear shape.

In this report, we present a result of calculation using the interacting boson-fermion model (IBFM). In the present study, we restrict ourselves to the IBFM with an odd particle in an orbital j. The hamiltonian is $H = H^B + H^F + V^{BF}$, where H^B is a usual hamiltonian of the interacting boson model 1 (IBM1), and V^{BF} is the boson-fermion interaction

$$V^{BF} = \Gamma\, Q\, [a_j^{\dagger} \tilde{a}_j]^{(2)} - \frac{\Lambda}{\sqrt{2j+1}} :[[d^{\dagger} \tilde{a}_j]^{(j)} [a_j^{\dagger} \tilde{d}]^{(j)}]^{(0)}: .$$

Since the odd particle always occupies the orbital j, the effect of the fermion hamiltonian H^F is trivial.

We consider three types of boson hamiltonian corresponding to the three limits of the IBM, i.e., SU(3), O(6) and U(5) limits which correspond respectively to the axially-symmetric rotor, the γ-unstable rotor, and the vibrator. The O(6) limit with a finite number of bosons also corresponds to the triaxial rotor[3] of $\gamma=\pm 30^0$. The number of bosons is fixed to N=12. Typical values are taken for the parameters in each limit.

The proton odd particle in $0h_{11/2}$ is considered. In each limit of the core, we use three sets of parameters in the boson-fermion interaction: (a) Γ=0.1MeV, Λ=0; (b) Γ=0.5MeV, Λ=0; (c) Γ=0.5MeV, Λ=12MeV. The larger (smaller) value of Γ corresponds to the strong (weak) coupling through the quadrupole-quadrupole interaction. On the other hand, Λ is changed to see the role of the exchange interaction in the strong coupling case.

The boson effective charge is assumed to be a typical value; e^B=0.11eb. The effective charge of 2e is assumed for the odd proton. In

calculating B(M1) values, we take $g^B=0.4\mu_N$ as a typical value. The g_s contribution of the odd particle is quenched by 0.7, giving $g^F=1.26\mu_N$.

The calculated B(E2) and B(M1) values are shown in Figs. 1 and 2. B(E2) values are presented in terms of the dynamical quadrupole moments, normalized by rigid rotor values with K=7/2. As seen in the figure, the signature dependence depends sensitively on the exchange interaction and the nature of the boson core. Above all, in O(6) nuclei, which may be interpreted as having triaxial shape, the effect of the exchange interaction on electromagnetic transitions is remarkable. The signature dependence of experimental data should be studied in the present framework.

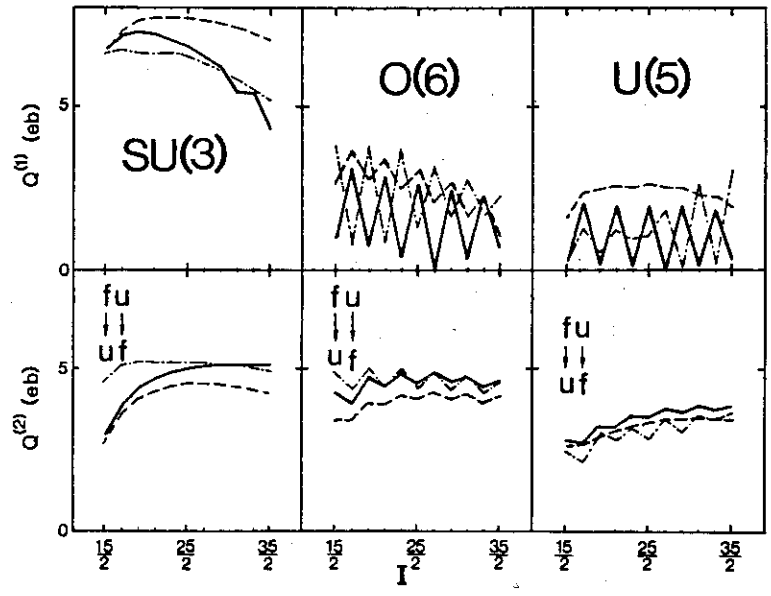

Fig. 1 Dynamical quadrupole moments calculated by the IBFM with boson cores in three limits. Solid lines correspond to the case (a), dashed lines to (b), and dash-dotted lines to (c).

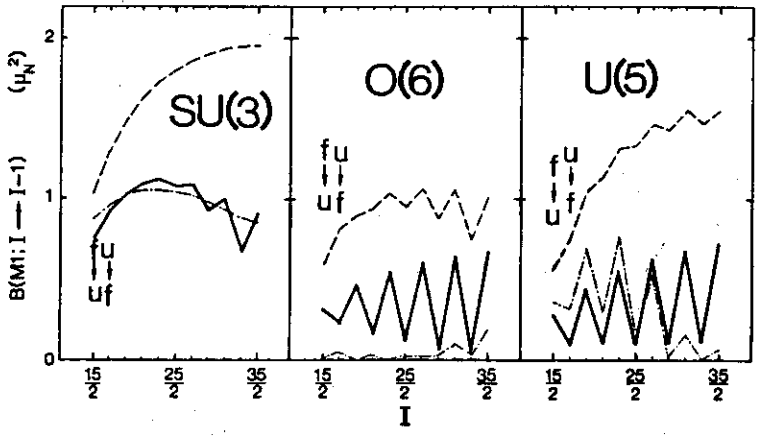

Fig. 2 B(M1) values calculated by the IBFM. See the caption of Fig. 1.

References

1) G. B. Hagemann, in Proc. of Int. Conf. on Nuclear Structure through Static and Dynamic Moments, (Melbourne, 1987); and references therein.

2) M. Oshima (private communication).

3) T. Otsuka and M. Sugita, Phys. Rev. Lett. 59 (1987) 1541.

7. Proton-Neutron s-d-g IBM and Spherical-Deformed Phase Transition

Takaharu Otsuka and Michiaki Sugita*

Department of Physics, University of Tokyo, Hongo, Tokyo, 113, Japan

*Japan Atomic Energy Research Institute, Tokai, Ibaraki, 319-11, Japan

The proton-neutron sdg interacting boson model is proposed as the underlying scheme for quadrupole collective states, and is applied to the description of the spherical-deformed phase transition. The sdg Hamiltonian consists of the boson single particle energies and the proton-neutron quadrupole interaction. Thus, this Hamiltonian is a modeling of the pairing and quadrupole interactions between nucleons. We analyzed, as an example, the phase transition in Samarium isotopes. The single boson enrgies are fixed by the pairing gap as ε_d=1.3 MeV and ε_g=1.8 MeV for both proton and neutron bosons. The strength of the quadrupole interaction is also kept constant as κ=0.15 MeV, assuming the SU(3) quadrupole operators. The diagonalization of the sdg Hamiltonian is difficult, and hence the existing approach to this model is only the cranking calculation [1] which can be applied to strongly deformed nuclei only. We solve the Hamiltonian in terms of the variation of the intrinsic state with the angular momentum projection, assuming the axial symmetry. Because of this variation-after-projection, one can expect a good approximation in vibrational, rotational and transitional situations. Fig. 1 shows excitation energies, their ratios, two-neutron separation energies, and E2 moments. The E2 moments are calculated with the proton and neutron boson charges as 0.150 and 0.075 eb, respectively. Experimental data showing the phase transition are reproduced by the present calculation remarkably well. The proton-neutron s-d-g IBM thus describes the phase transition as a function of the numbers of the proton and neutron bosons, keeping all parameters fixed at constants which are reasonable from the shell model estimate. The driving force of the phase transition is the proton-neutron quadrupole interaction. Since the phase transition occurs as a consequense of increasing number of bosons (or valence nucleons), this work should be related to the empirical systematics by Casten et al.[2].

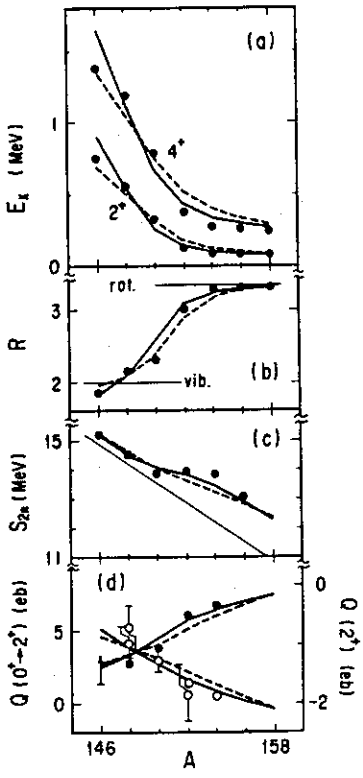

Fig. 1. Properties of the first 2^+ and 4^+ states of Samarium isotopes. Points are experiments, solid lines are proton-neutron s-d-g calculations, and dashed lines are s-d-g IBM-1 results, for (a) energy level, (b) ratio $R= E_x(4^+)/E_x(2^+)$, (c) two neutron separation energy, (d) transition E2 moment of $0^+ \rightarrow 2^+$ (closed circles), and static E2 moment of 2^+ (open circles). The thin line in (c) indicates the linear term which comes from outside the IBM.

1) S. Pittel et al., Phys. Lett. 144B (1984) 145.
2) R.F. Casten et al., Phys. Rev. Lett. 58 (1987) 658

8. Structure of high-spin isomers in the framework of the particle-rotor model

Naoki Tajima and Naoki Onishi

College of General Education, University of Tokyo, Komaba, Meguro-ku, Tokyo

On account of the K-selection rule, states which have large expectation values of K-quantum number are likely to become long-lived isomers in axially symmetric deformed nuclei[1]. But recently observed high-K isomers in neutron deficient Os isotopes have lifetimes much shorter than those predicted by the K-selection rule[2)3)]. In this report attention is concentrated on the $K^P=10^+$ isomer in ^{184}Os which has a very simple configuration, that is, a purely intruder orbital ($\nu i_{13/2}$) one-particle one-hole (9/2[624], 11/2[615]) state[4)5)].

The $K^P=10^+$ isomer decays into I=10 and I=8 members of the g-band with a half life of 20 ns. In the isotone ^{182}W, the isomer which has presumably the same configuration decays with a half life of 1.4 us, which is 70 times as long as that of the isomer in ^{184}Os. This difference in the lifetime can be attributed to the difference of the softness toward γ-deformation: γ-deformation mixes the K-quantum number and the K-selection rule breaks down. The degree of the γ-softness can be known from the ratio of the excitation energy of the I=2 state of the γ-band to that of the I=2 state of the g-band. The ratio is about 8 in the case of ^{184}Os while it is about 12 in the case of ^{182}W. Thus ^{184}Os is more γ-soft than ^{182}W.

We reproduced the lifetimes of these isomers in a model calculation in which the γ-degree of freedom is taken into account as a dynamical variable. We used a particle-rotor model in which we employed a γ-soft Bohr model (with β fixed)[7)8)] or triaxial rotors (with β, γ fixed) for the "rotor" (or "core"). For the "particle", full { $\nu(i_{13/2})^n$; n=0,2,4,...,14 } configurations are utilized. For the interactions between the $i_{13/2}$ neutrons and the core, we assumed a Quadrupole-Quadrupole interaction and a Cooper pair exchange interaction. The former is responsible for the effect of nuclear deformed potential on the $i_{13/2}$ neutrons. The latter is approximated by a pairing field for the $i_{13/2}$ neutrons. States are described in a laboratory frame for the benefit of the dynamical treatment of the γ-degree of freedom. For the formulation of the model, see refs.[9)~14)]

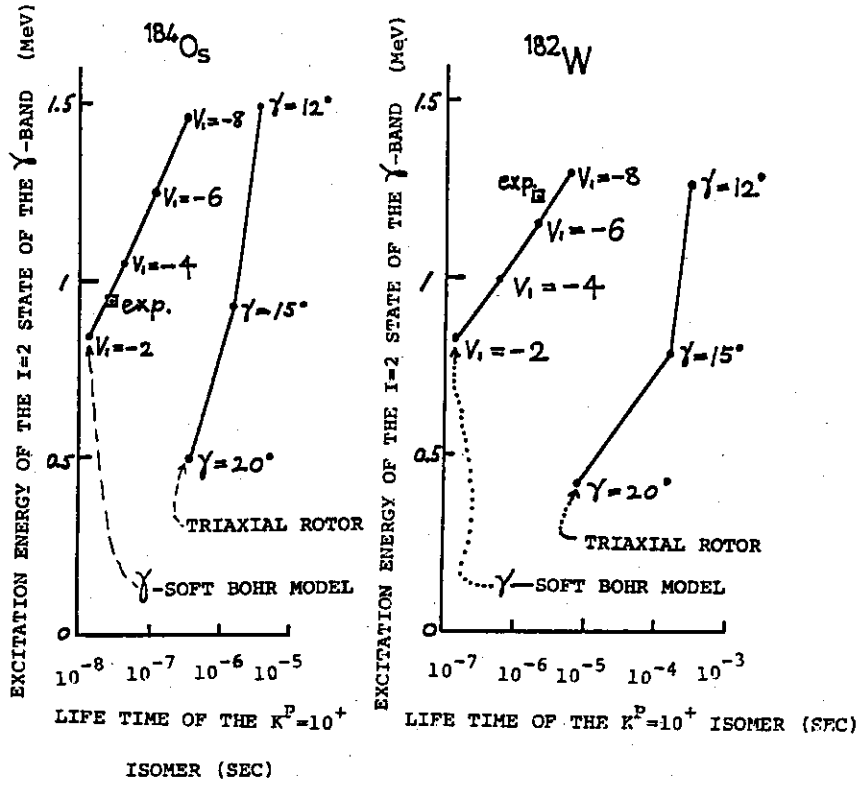

Fig. 1 The lifetime of the $K^P=10^+$ isomer and the excitation energy of the I=2 state of the γ-band for ^{184}Os and ^{182}W. The potential energy for γ-deformation used in the calculation takes on the form

$$V(\gamma) = (2\hbar^2/B\beta^2)\, V_1 \cos(3\gamma)$$

where $(2\hbar^2/B\beta^2)$ = 0.197 (when V_1=-2) ~ 0.229 (when V_1=-8) (MeV) for ^{184}Os and $(2\hbar^2/B\beta^2)$ = 0.175 (when V_1=-2) ~ 0.196 (when V_1=-8) (MeV) for ^{182}W. To estimate the effective γ-potential of the total system, the contribution from $i_{13/2}$ neutrons must be added to the V(γ) of the bare core. The γ-driving force of $i_{13/2}$ neutrons can be simulated effectively by a γ-potential with V_1≈-4 in the case of these parameter sets.

The Quadrupole deformation β is fixed to the value 0.20 (0.22) for ^{184}Os (^{182}W). The energy scale of the core $(2\hbar^2/B\beta^2)$ is varied from core to core so as to fit the excitation energy of the I=2 state of the g-band to the experimental value. The Fermi level is fixed so that the expectation value of number of neutrons in the $i_{13/2}$ orbital become 10. The strength of the Cooper pair exchange interaction is fixed so that the excitation energy of the $K^P=10^+$ isomer is reproduced. The neutron-neutron interaction in the $i_{13/2}$ orbital is assumed to be delta-interaction

$$V_{\nu\nu} = -4\pi\, G\, \delta^{(2)}(\Omega_1-\Omega_2)$$

where G = 22/(mass number) = 0.12 [MeV].

The results of numerical calculations are shown on the left-side of the Fig.1 for ^{184}Os and on the right-side for ^{182}W. Parameters of the model are given in the caption of Fig.1. Calculated lifetimes of the isomers are in quantitative agreement with experimental ones if we use a γ-soft Bohr model with γ-potentials proportional to cos(3γ) and whose heights are determined by adjusting the excitation energies of the I=2 states of the γ-band to the observed value. If we use (γ-fixed) triaxial rotor, the lifetimes are overestimated by a factor of order 2.

references

1) K.E. Loebner, Phys. Lett. B26 (1968), 369.
2) J. Pedersen, B.B. Back, S. Bjørnholm, J. Borggreen, M. Diebel, G. Sletten, F. Azgui et al., Phys. Rev. Lett. 54 (1985), 306.
3) J. Pedersen et al., Z. Phys. A321 (1985), 567.
4) J. Pedersen et al., private communication.
5) Tord Bengtsson, private communication.
6) B.D. Jeltema, F.M. Bernthal et al., Nucl.Phys. A280 (1977), 21.
7) I. Hamamoto and N. Onishi, Phys. Lett. B150 (1985), 6.
8) N. Onishi, I. Hamamoto, S. Aberg, and A. Ikeda, Nucl. Phys. A452 (1986), 71.
9) N. Tajima and N. Onishi, Phys. Lett. B179 (1986), 187.
10) P.J. Evans and S.M. Harris, Nucl. Phys. A277 (1977), 109.
11) A. Ikeda, M. Kitajima, M. Miyawaki, and N. Onishi, Phys. Lett. B85 (1979), 172
12) F. Gruemmer, K.W. Schmidt, and A. Faessler, Nucl. Phys. A326 (1979), 1.
13) M. Reinecke, H. Herold, H. Ruder, and G. Wunner, Nucl. Phys. A361 (1981), 435.
14) A. Ikeda and N. Onishi, Progr. Theor. Phys. 70 (1983), 128.

9. STUDY OF NUCLEAR STRUCTURE IN VERY LIGHT RARE-EARTH NUCLEI

Mitsuhiko Ishii
Department of physics, JAERI, Tokai, Ibaraki, Japan

Before talk about the subject, I would like to mention in brief the memory of late Professor Hiroshi Taketani, the Tokyo Institute of Technology. He helped us at an early stage of in-beam experiments at the JAERI tandem accelerator laboratory.

It was one day in spring in 1968 that I met him. He visited the JAERI to see Dr H. Takekoshi (Professor of the Kyoto University). They discussed on nuclear physics, especially neutron-captured γ-rays and γ-ray resonance fluorescence. Their talk ran on the Li-drifted germanium detector which had just been commercially available; only several Ge(Li) detectors had been imported in Japan. In order to observe neutron captured γ-rays, we had fabricated some Ge(Li) detectors. So he was so much interested in them and wanted to get their own ones. A few months later he sent M. Ogawa, one of his first graduate students and now Professor of the Tokyo Institute of Technology, to learn our fabrication techniques. One year after this, they succeeded in making a Ge(Li) detector by themselves. Then they applied it to the study of nuclear structure through the (p,nγ) reactions.

From time to time I have helped the Professor since. In 1977 to 1978 I worked with T. Matsuzaki (RIKEN) to construct a γ-ray linear polarimeter composed of two high-purity Ge crystals. By use of this polarimeter, he studied the band structure in Se-74 and -76, and earned his science Ph. D. degree.

In 1982 the JAERI tandem accelerator was completed in construction and put into operation for experiments. Then A. Makishima (Dr.; the Defence Medical College) joined us. Our first experiment at the tamdem accelerator facilities was to observe the E0 transition in Se-74 [1]. During that time we made plans for new experiments of in-beam γ-ray spectroscopy. We planned to develope a charged-particle multiplicity filter "Silicon Box"; it consists of ten Si ΔE counters which cover the target with almost 4π solid angle and count the number of emitted charged particles each fusion event. We chose the luminosity rather than the resolving

power in particle identification. Prof. Taketani was afraid of its performance. In fact few supported our plan and some people insisted that the neutron multiplicity filter was much more promissing which was being constructed at the Daresbury Laboratory in U. K. Prof. Taketani was not so willing to accept our plan but was too gentle to discourage us. So our plan was put into practice. It took a few years to bring the Si-box to completion. Then the new instrument turned out to be a powerful tool for in-beam γ-ray spectroscopy via heavy-ion fusion reaction [2]: Its compact size permits the particle γ-γ coincidence with a good efficiency. Furthermore, because it is separable into two parts, we can place between them a simple plunger system for the lifetime measurement or a magnetizing device for the g-factor measurement.
Any way our success is greatly in debt to his generosity.

Now to return, I will give a short review of our study on very light rare-earth nuclei. Then our recent topics will be presented.

We bigin with search for well-deformed Sm and Ce isotopes. We have identified the transitions in Sm-134 and Ce-124: In Sm-134 the excitation energis of the 2^+ and 4^+ states are $E(2^+)$ = 163 keV and $E(4^+)$ = 480 keV, respectively and in Ce-124 $E(2^+)$ = 142 keV and $E(4^+)$ = 448 keV. The empirical formula for the E2 transition probability [3] and the β-dependency of B(E2) have shown that those nuclei have a large deformation around β~.3 in their ground state bands. Recently we have observed candidates for the $2^+ \rightarrow 0^+$ and $4^+ \rightarrow 2^+$ transitions in Sm-132, which will be mentioned later.

In spite of a large deformation in their ground state bands, Ce-126 and Ce-124 show anomaly in the B(E2): In Ce-126 the $8^+ \rightarrow 6^+$ and $6^+ \rightarrow 4^+$ transitions are hindered by a factor of 2 or more in comparison with the theoretical predictions, and so are those in Ce-124 [4]. We have not yet found any plausible explanation of this anomaly.

Another interesting result is the fact that two quasiproton state $(\pi h11/2)^2_{10^+}$ drops at such a low excitation energy as to compete with the quasineutron one $(\nu h11/2)^2_{10^+}$. In Sm-138 the yrast 10^+ state was found to have a halflife of 0.55 ns [5]. Its g-factor has been measured to be $g(10^+) \sim +1.0$ by observing the larmor precessions of the γ-rays involved. This result supports a picture of two quasiprotons aligned to collective motion. In a similar way the 10^+_2 state in Ce-126 has turned out to be a proton-like isomer with a halflife of 8 ps, but the result is not so conclusive as the yrast 10^+ state in Sm-138 [6].

Finally we report our recent experiments.

Experiment 1.

We have saught γ-ray transitions in Sm-132 excited by the reaction: Cd-106 (160MeV S-32, α2n) Sm-132. The cross section for this reaction is about 3 mb so that we have taken no γ-γ coincidence. The γ-rays of interest have been saughted by comparison with the spectra taken in other excit channels. Additionally we have relied on the IBM-2 and the systematics of the $E(2^+)$ and $E(4^+)$ observed in Ba, Ce, Nd, Sm and Gd with $N < 82$. Our IBM parameters were determined so as to reproduce the excitation enrergies of the 2^+ to 12^+ states, on the average, in Ba to Gd isotopes with $N < 82$. So the present IBM prediction has a trend to give slightly higher $E(2^+)$ and $E(4^+)$ than the experimental ones. Thus we obtain a criterion for the 2^+ state: $125\ \text{keV} \leq E(2^+) \leq 129\ \text{keV}$. As for the 4^+ state, we adopted instead the ratio $E(4^+)/E(2^+)$ as the criterion because this is more reliable than $E(4^+)$:

$$E(4^+)/E(2^+) = 3.13 \qquad \text{(the IBM-2)}$$
$$3.15 \pm 0.05 \qquad \text{(the systematics)}$$

The prediction of $E(4^+)$ can be obtained by multiplying this ratio by $E(2^+)$ experimentally obtained. In fig.1 a γ-ray spectrum taken in the αxn reaction is compared with the one taken in the αpxn reactions. The regions for the candidates to be saught in are indicated by the horizontal segments. Thus we have found the candidates of $2^+ \rightarrow 0^+$ and $4^+ \rightarrow 2^+$ transitions with energies of 126 keV and 266 keV, respectively.

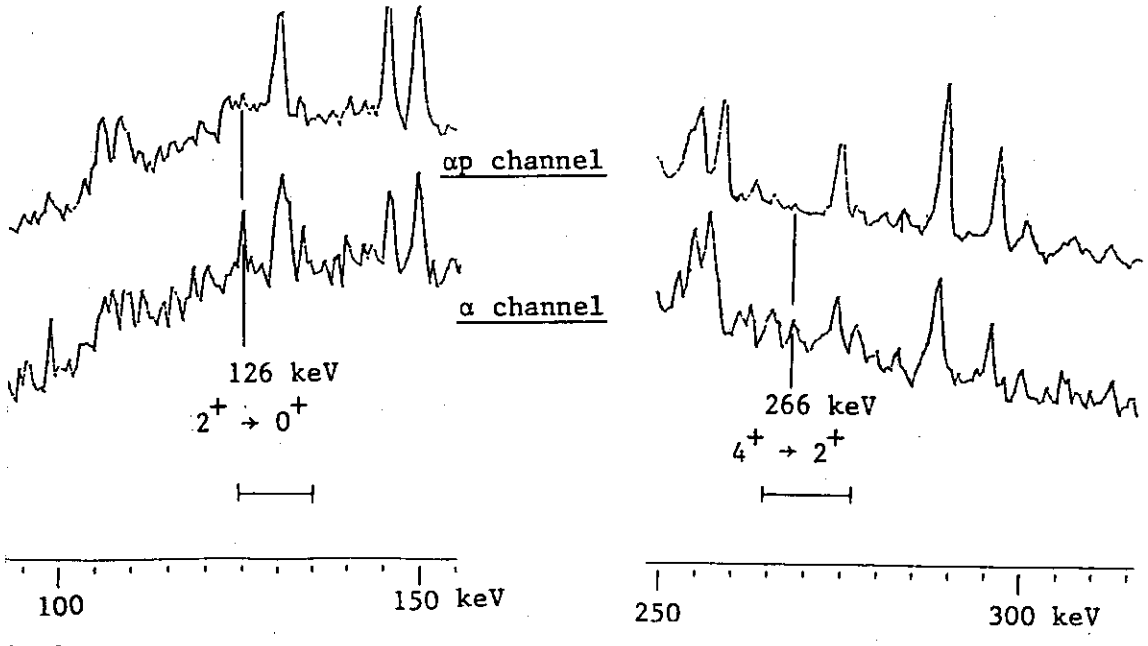

Fig.1 Gamma-ray spectra to seek the transirions in Sm-132.

Experiment 2.

We found that in Nd-134 the 2^+, 4^+ and 6^+ states are fed via an unidentified isomer with a halflife of 13 ps. Along the same line as the yrast 10^+ state in Sm-138, it is interesting to examine whether the isomer is proton-like or not. For this purpose we have measured its g-factor relative to that of the 4^+ state in Nd-132.

The experiment has been done as follows: Nd-132 and -134 nuclei were produced by the same fusion reaction: Ag-107 + S-32 with different exit channels: αp2n and 3p2n, respectively; they recoiled into Gd host where the strength of the static hyperfine interaction was about -1.4 M gauss. As a result the g-factors involved were measured at the same time and under the same condition. The 4^+ state in Nd-132 has a lifetime of 15 ps but its g-factor is unknown; assumedly $g(4^+) \cong +0.35$. If the isomer possesses a g-factor around this value, it rotates by almost the same angle as the 4^+ state in Nd-132 under the influence of the hyperfine interaction. There is no significant delay in de-excitation from the isomer to the 2^+ state so that the 4^+ state in Nd-134 inherits the larmor precession from the isomer.

The result has shown that the isomer concerned rotates by a small angle in comparison with the 4^+ state in Nd-132. This means that the isomer has a small g-factor and is not due to two quasiprotons : $(\pi h11/2)^2_{10}+$. It possesses either the neutron configuration: $(\nu h11/2)^2_{10}+$ or some complicated proton one else.

The author thanks my colleague Dr T. Ishii and Dr A. Makishima, the Defence Medical College, for their hard work in instrumentation and experiment. He acknowledges collaboration in experiment of Prof. M. Ogawa, M.S. M. Hoshi and M.S. K. Yanagida, the Tokyo Institute of Technology.

References

[1] A. Makishima et al., Nucl. Phys. A425(1984)1.

[2] M. Ishii et al., Nuclei off the Line of Stability (ed. R.A. Meyer and D.S. Brenner, A.C.S., Washington D.C., 1986) ch.75.

[3] L. Grodzins, Phys. Lett. 2(1962)88.

[4] M. Ishii et al., Int. Nucl. Conf., Harrogate U.K., 1986.

[5] A. Makishima et al., Phys. Rev. C 34(1986)576.

[6] T. Ishii et al., Int. Conf. on Nucl. Structure, Melbourne, 1987.

10. A UNIFIED DESCRIPTION OF $K^{\pi}=0^{+}$ AND $K^{\pi}=0^{-}$ BANDS FROM OCTUPOLE VIBRATIONAL TO OCTUPOLE DEFORMED NUCLEI

Takaharu OTSUKA and Michiaki SUGITA[1)]

Department of Physics, University of Tokyo,
Hongo, Bunkyou-ku, Tokyo, 113, Japan

[1)]Department of Physics, Japan Atomic Energy Research Institute,
Tokai, Ibaraki, 319-11, Japan

The $K=0^{+}$ and $K=0^{-}$ bands in actinide nuclei are described in terms of an extended interacting boson model. The model comprises of s, p, d and f bosons which represent bosons of $L^{\pi}=0^{+}$, 1^{-}, 2^{+}, 3^{-}, respectively. We include p as well as f bosons on the basis of a microscopic investigation presented in Ref. [1]. We assume that the Hamiltonian consists of single particle energies and a multipole-multipole interaction of quadrupole, dipole and octupole type. The parameters of the Hamiltonian are optimized so that main features of those nuclei are reproduced. Similarly to the sd IBM, the number of bosons is equated to the half of the number of valence nucleons outside the ^{208}Pb core.

The diagonalization of this Hamiltonian is extremely difficult, and probably impossible from a practical point of view. Instead we use a mean field approximation where the axially-symmetric and parity-mixed intrinsic state is introduced as

$$\Phi \propto (s^{\dagger} + x\, p_0^{\dagger} + y\, d_0^{\dagger} + z\, f_0^{\dagger})^{n} |0),$$

where x, y, z are variational parameters. The parity is mixed since the quadrupole and octupole motions are coupled. The variation with respect to x, y, z is performed after the projection of both the angular momentum and parity. As a result, the intrinsic state is, in principle, varied from state to state for a fixed nucleus.

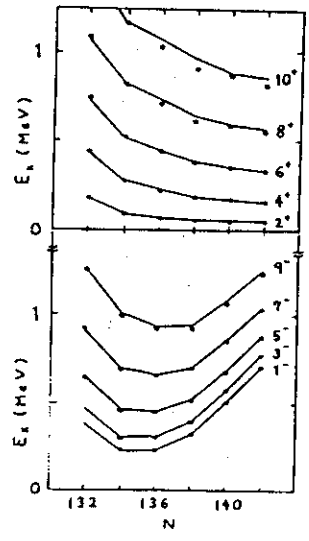

Fig. 1 Experimental [2] (points) and theoretical (lines) energy levels of lowest states of the Th isotopes.

By varying values of a few parameters of the Hamiltonian smoothly with respect to N and Z, we can describe various situations of actinide nuclei within the same model. As an example, the Th isotopes are

considered. The experimental [2] and theoretical excitation energies of the states of the $K=0^+$ and $K=0^-$ bands are shown in Fig. 1. One finds a good agreement between experiment and theory. It turned out that the functional dependence of the above parameters is nearly linear on N (Z is constant). A typical pattern of the static octupole deformation can be observed around N=134-136, while the situation is like the octupole vibration around N=142. In fact, the octupole correlation is largest around N=134-136, whereas the quadrupole deformation evolves continuously as N increases.

We further calculated the electric transitions, such as E1, E2 and E3, as well as the energy splitting between the positive and negative parity bands, that is, Energy Displacement. As usual, the Energy Displacement is given by [3]

$$\delta E_I = E(I) - \{ (I+1)E(I-1)+I\cdot E(I+1) \}/(2I+1).$$

Since these two observables, in particular, are fairly sensitive to the wave function, the quality of the present model can be checked rigorously. In Fig. 2 and 3, the results are shown and compared with experiment. We can obtain a good reproduction of experiment also on these quantities.

In conclusion, we point out that the present spdf boson model provides a clue to understanding the actinide nuclei quantitatively.

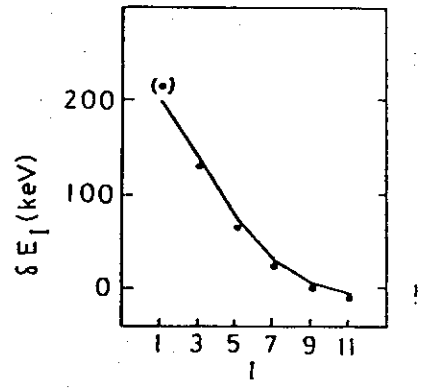

Fig. 2 Experimental (points) and theoretical (lines) Energy Displacement for ^{224}Th.

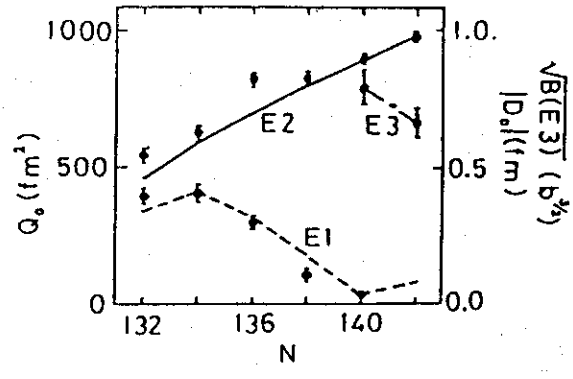

Fig. 3 Experimental (points) and Theoretical (lines) moments for the Th isotopes.

References

[1] T. Otsuka, Phys. Lett. 182B (1986) 256.
[2] P. Schuler et al., Phys. Lett. 174B (1986) 241.
[3] W. Nazarewicz and P. Orlanders, Nucl. Phys. A441 (1985) 420.

11. Intrinsic Properties of the Superdeformed State Predicted by the Self-consistent Calculation

Kosai Tanabe

Department of Physics, Saitama University, Urawa, Saitama 338

1.- Recent dicoverly of the superdeformed rotational bands in ^{152}Dy[1], and subsequently in $^{146,\ 148}Gd$[2], ^{132}Ce[3], ^{135}Nd[4], $^{134,136}Nd$[5] and other nuclei are quite attractive from viewpoint of testing microscopic nuclear theory in the extremity of large deformetion, large rotational frequency and high excitation. Our attempt here is to reproduce the superdeformed band (s.-d. b.) as well as the ground band (g. b.) and the s. band (s. b.) in $^{132}_{74}Ce_{58}$ on the basis of the self-consistent solution to the cranked Hartree-Fock-Bogoliubov equation. The usefulness of this type of approach consists in (1) the spontaneous creation of deformation starting from spherical single-particle basis together with the residual interaction with rotational symmetry, (2) relating the collective properties directly to single-particle behaviour and (3) the self-consistent description of stepwise evolution of intrinsic structure associated with vanishing of pairing gaps and rotational alignment of spins.

In order to describe large prolate deformation, we must take into account enough range of single-particle space to cover thoroughly the relevant orbitals. Therefore our single-particle space exteds over almost three major shells both for proton and neutron. The assumed residual interaction includes the monopole-pairing, quadrupole-pairing[6]

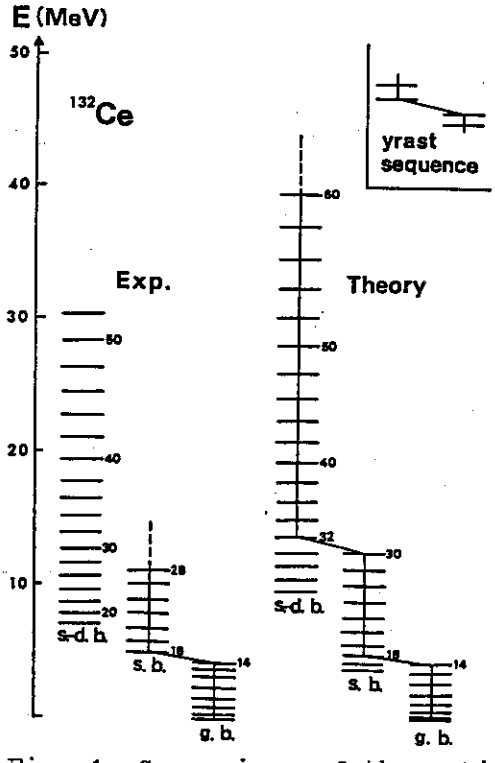

Fig. 1 Comparison of theoretical and experimental level schemes.

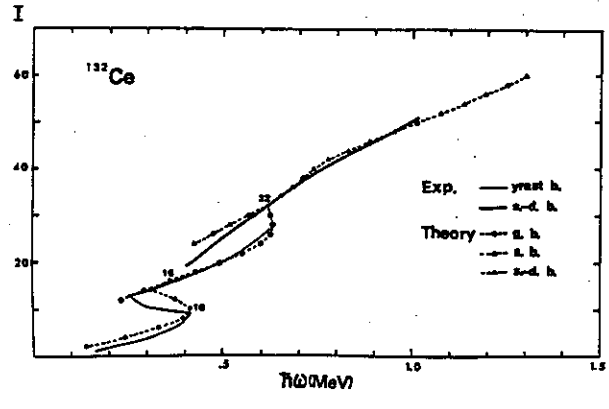

Fig. 2 Theoretical ω-I curve compared with experiment for ^{132}Ce

and quadrupole-quadrupole forces, whose interaction strengths are adjusted to reproduce well the level schemes both for the g. b. and the s. b. up to spin 32.

2.- The calculated level scheme is compared with experimental one in Fig. 1. The theory predicts that the yrast is composed of the g. b. up to spin 14, and the s. b. from spin 16 to 30, and the s.-d. b. becomes yrast from spin 32. Since the band head energy and the spin-parity assignment are not known yet, the energy of the experimental level assumed to have spin 24 is adjusted to coincide with the corresponding theoretical level in Fig. 1. The theoretical ω-I curve is compared with the experimental yrast bands (the thin curve) and the experimental s.-d. b. (the thick curve). We observe that the theory reproduces quite well the s.-d. b. as well as the g. b. and the s. b.. Therefore, as seen in Fig. 3, the moments of inertia $\mathcal{J}^{(1)}$ along these three bands are also well explained by the theory.

3.- The level-dependent pairing gaps are calculated to analyze details of the intrinsic structure evolution along different bands. As shown in Fig. 4, along the s. b. the average gap Δ_n for neutron shell vanishes and

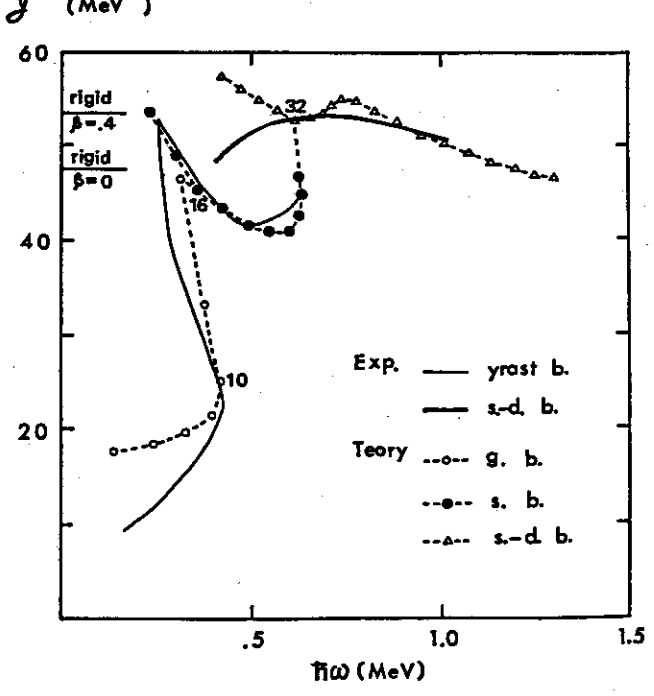

Fig. 3 Theoretical kinetic moment of inertia $\mathcal{J}^{(1)}$ compared with experiment.

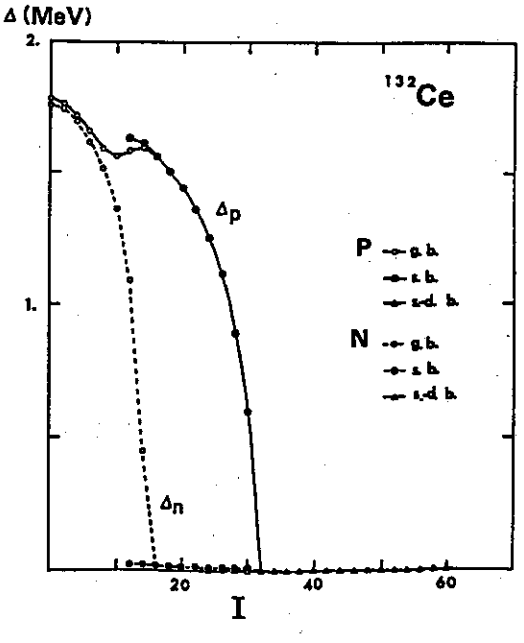

Fig. 4 Calculated average gaps vs spin for ^{132}Ce.

and Δ_p for proton shell is still finite, while both Δ_n and Δ_p vanish along the s.-d. b.. Thus our result predicts that the s.-d. b. is realized by the perfect "rigidification" of the deformed nuclear system resulting from the Coriolis antipairing effect (i. e. the Mottelson-Valatin effect[7]). Along the yrast band the gapless superconducting state which is indicated by negative quasiparticle energy is generated in the positive parity neutron shell $\nu i_{13/2}$ at spin 8, and subsequent spin alignment is caused by the Stephens-Simon mechanism in the occupied single-particle levels with small j_z (= Ω) near Fermi surface. This mechanism creates the s. b. from spin 16 to 30. The s.-d. b. is characterized by decoupled nucleaon pairs in many levels so that it is rather shared by many nucleon in the rigid rotor. Thus the interband transition from one of the s.-d. b. level tharacterized with many quasiparticles to the s. b. level (2-quasiparticle character) or the g. b. level (0-quasiparticle character) must be very much suppressed as inferred from experiments.

4.- Microscopic theory describes the phase transition from the superconducting phase partially with gapless superconductivith to the oormal phase with large deformation at spin 32 along the yrast sequence. It must be natural to assume that the rigidification occurs also in the core portion of $Z_c = 28$ and $N_c = 50$, which is artificially introduced in the present calculation. Therefore, we have

$$\langle r^2 \rangle_{total} = \langle r^2 \rangle_{HFB} + \langle r^2 \rangle_{core},$$

where $\langle r^2 \rangle_{core}$ is a constant contribution from the core part, i. e.

$$\langle r^2 \rangle_{core} = 3/5\ (Z_c R_p^2 + N_c R_n^2)/(Z_c + N_c)$$

with $R_p = 4.6$ fm and $R_n = 6.0$ fm. Furtheremore, the effect of the defor-

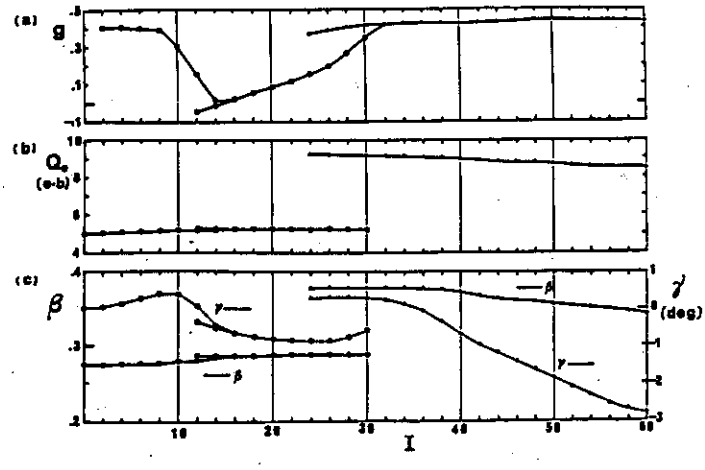

Fig. 5 (a) G-factor,
(b) Intrinsic quadrupole moment Q_0 ,
(c) Deformation parameters β and γ.

mation of the core and the polarization caused by the coupling between single-particle and giant E2 resonance are assumed to be accounted for by a single effective charge, i. e. the isoscalar polarization tharge e_{pol}. Our result shows that the intrinsic quadrupole moment Q which is roughly a constant along the s.-d. b. agrees with the experimental value 8.8 e.b when we take $e_{pol}/e = 0.34$. Theoretical predictions for some collective properties are summarized in Fig. 5, i. e. (a) the g-factors, (b) the intrinsic quadrupole moment Q_0 , and (c) the deformation parameters β and γ.

5.- Above deformation parameters are microscopically calculated from

$$\beta = (\langle r^2Y_{20}\rangle^2 + 2\langle r^2Y_{22}\rangle^2)/\langle r^2\rangle,$$

$$\tan\gamma = 2\langle r^2Y_{22}\rangle/\langle r^2Y_{20}\rangle$$

with taking account of the renormalization effect described by the effective charge. The calculation yields $\beta = 0.27$ at the groung state, and increases slightly up to 0.29 at 14^+ state, but β takes an almost constant value 0.29 along the s. d. up to 30^+ state. Along the s.-d. b., we have $\beta = 0.38$ at spin 32, 0.37 at spin 42 and 0.36 at spin 52. It is quite noticeable that our β microscopically calculated is smaller than the experimental β determined from observed Q_0. Furthermore, the slight decrease of $\mathcal{J}^{(1)}$ with increasing I along the s.-d. b. is accounted for by the decrease of β and also slight increase of γ, which may correspond to small admixture of the oblate configuration as expected from local minimum in the potential surface at very high spins[8].

In conclusion the s.-d. b. in ^{132}Ce is a manifestation of the rigidification of the deformed nuclear system. Apparent large value of β does not necessarily mean elongation in the nuclear shape, but the deformation of rigidified total system and the increase of charge density in the nuclear periphery. Detailed account of our results will be published elsewhere[9].

1) P. J. Twin et al., Phys. Rev. Lett. 57(1986), 811.
2) G. Hebbinghaus et al., Phys. Rev. Lett. 59(1987), 2024.
M. W. Drigert et al., Phys. Lett. 201B(1988), 223.
3) P. J. Nolan et al., J. Phys. G11(1985), L17.
A. J. Kirwan et al., Phys. Rev. Lett. 58(1987), 467.
4) E. M. Beck et al., Phys. Rev. Lett. 58(1987), 2182.
5) M. E. Beck et al., Phys. Lett. 195B(1987), 531.
6) K. Tanabe and K. Sugawara-Tanabe, Phys. Lett. 135B(1984), 353.
7) B. R. Mottelson and J. G. Valatin, Phys. Rev. Lett. 5(1960), 511.
8) S. Frauendorf and F. R. May, Phys. Lett. 125B(1983), 245.
9) K. Tanabe and K. Sugawara-Tanase, On the rigidification of nuclear system in the superdeformed rotational band, to be published (1988).

12. Laser-Nuclear Spectroscopy for Unstable Nuclei Far From the Stability Line

S. Matsuki
Institute for Chemical Research, Kyoto University, Kyoto

1. Introduction

Important spectroscopic informations on unstable nuclei far from the stability line have been achieved recently with laser-nuclear spectroscopy[1]. These experiments have been performed with quite a small number of unstable nuclei produced with accellerators (less than 100 atoms/sec.). Various methods for improving the sensitivity of atom detection have been applied in these investigations:1)coincidence measurements between the fluoreacence and the ion[2],2)application of the resonance ionization spectroscopy[3], and 3)radiation-detected optical pumping (RADOP) and the NMR measurements[4]. With these improved methods for laser-nuclear spectroscopy, for example, anomalous even-odd staggering in the light Sr isotopes[2], sudden shange of nuclear shape in the neutron deficient Au isotopes[3], and precise magnetic moments of rare gas (Xe, Rn) nuclei[4] have been revealed.

Although great improvements for the sensitive detection scheme in the laser-nuclear spectroscopy have been obtained recently as mentioned above, still more elaborate methods are required for further investigation of the nuclei far from the stability region of which the production rate is lower than 100 atoms/sec.. We are developing a new method for efficient and sensitive measurement of nuclear spin and/or magnetic moment with the RADOP in solids, i.e., achievement of significant nuclear polarization with laser optical pumping in solids and its detection with the RADOP method[5]. In the following section, the method and the first results on the unstable ^{170}Tm in SrF_2 are presented.

2. Nuclear polarization of unstable ^{170}Tm with optical pumping in solids

As proposed and demonstrated by Jeffries and collaborators[6], polarization of nuclei by optical pumping in solids can be achieved with the following principle; the magnetic circular dichroism of Tm^{2+} in alkarine earth fluoride hosts is so large that the electron-spin polarization can be sufficiently enhanced by pumping with circularly polarized laser light. The electron polarization enhanced by pumping the 4f-5d band is transferred to the nuclei by hyperfine coupling and/or selective spin-lattice relaxation processes. Usually the number of unstable nuclei in crystal is so quite small that it is extremely difficult to detect the nuclear polarization

with the normal magnetic resonance (NMR and ESR) and even with more sensitive optical methods. The method of the beta- and gamma-RADOP has thus to be invoked to achieve enough sensitivity for the detection of the polarization.

The electron polarization can be also transferred to nuclei by inducing microwave transition (dynamic nuclear polarization). The observation of the enhancement and/or the destruction of the polarization due to this microwave transition with RADOP is a sensitive detection method for measuring the hyperfine coupling constant A, thereby enabling us to know the relevant structure of the nuclei such as the spin and the magnetic moment.

The overall experimantal setup is shown in Fig.1. A sample of 3x3x1mm thick crystal of SrF_2 containing 0.02% stable ^{169}Tm was irradiated by thermal neutrons from the Kyoto University Reactor. About one part in 10^6 of ^{169}Tm was converted to unstable ^{170}Tm(half-life 128d and nuclear spin 1-). The sample was mounted in a helium cryostat in the dc field of an electromagnet. The pumping source used was a laser light of about 590 nm wave length from a dye-laser pumped by an Ar ion laser. The temperature of the sample was about 2.0 K. The beta-rays emitted in the decay of ^{170}Tm were detected with a caF_2(Eu) scintillator set just behind the sample in liquid helium and the scintillation light was transmitted via a light guide to a photomultiplier outside of the cryostat. The sign of the circular polarization of the pumping light was changed in every 45 seconds and the experimental asymmetry A_{exp} of beta-ray distribution defined by

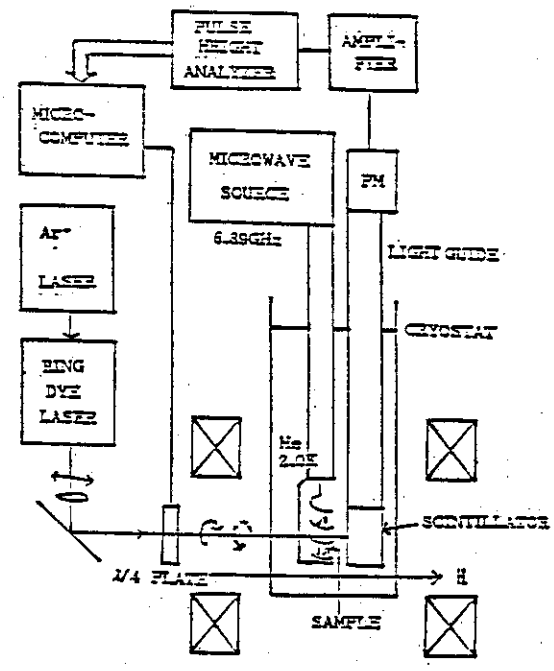

Fig. 1 Experimental arrangement for β-ray radiation-detected optical pumping in solid.

$$A_{exp}=(N(\sigma^+)-N(\sigma^-))/(N(\sigma^+)+N(\sigma^-)),$$

was thus measured. The magnetic field dependence of the observed beta-ray asymmetry is shown in Fig.2. The asymmetry increases with increasing magnetic field up to about 500 Gauss and then decreases monotonously. It is estimated that the maximum value of A_{exp} at about 500 Gauss corresponds to the nuclear polarization of about 4%.

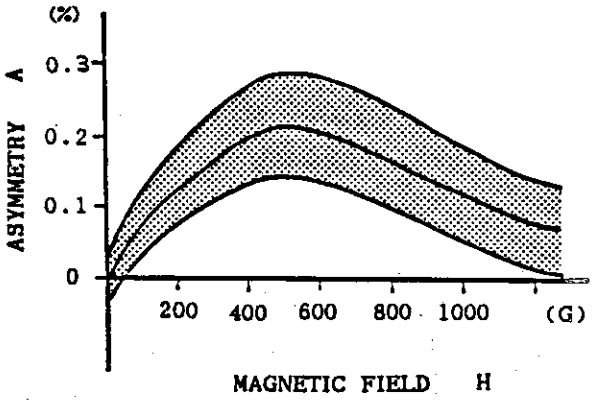

Fig. 2 Magnetic field H dependence of the observed β-ray asymmetry A_{exp} for optical pumping of $^{170}Tm^{2+}$: SrF_2. Shadowed area shows the limit of local variation of A_{exp} with H.

3. Observation of the enhanced nuclear-polarization with an applied rf-field

In addition to the optical pumping, an rf-field of 6.89 GHz was applied to the sample and the enhancement of the polarization due to the saturation of the forbidden transition between the substates 2 and 6 ($\langle M_s=+1/2, M_I=0\rangle$ to $\langle M_s=-1/2, M_I=+1\rangle$) was observed. In Fig.3 shown are the results of the observed resonance with varying magnetic field H. The observed resonance indicates that the microwave transition enhances the polarization by about 4 to that from the optical pumping only.

By fitting the resonance shape to a Gaussian curve, the magnetic field at the resonance was obtained. The hyperfine coupling constant A_{170} of ^{170}Tm was thus deduced as 589(18)MHz and the magnetic moment of ^{170}Tm was obtained from the known A and magnetic moment of the stable ^{169}Tm with the relation,

$$\mu_{170}=(\mu_{169} \times 1/A_{169} \times 1/2)\times A_{170}$$
$$=0.247(8)\ nm,$$

which is in good agreement with the value from the atomic beam magnetic resonance experiment[7], 0.2448(36) nm.

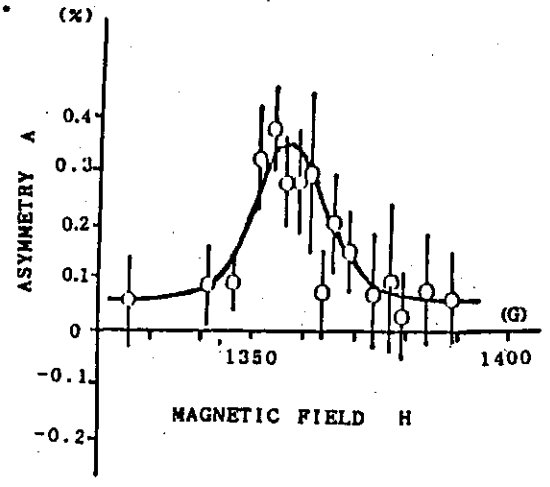

Fig. 3 Resonant enhancement of β-ray asymmetry A_{exp} observed in inducing microwave forbidden (6.890 GHz) transition between (M_S=+1/2, M_I=0)-(-1/2, 1) sublevels of $^{170}Tm^{2+}$.

4. Conclusion

We have shown that the nuclear polarization of unstable nuclei in soilds (^{170}Tm in SrF_2) can be achieved and efficiently detected by beta-ray radiation detected optical pumping. The experiment is the first to achieve and observe directly the significant nuclear polarization due to optical pumping in soilds. The observed enhancement of the polarization by appling an rf-field resonant to the forbidden transition provides a new powerful method to measure the magnetic moment of unstable nuclei in rare-earth region. A project for the experimental research on the nuclear structure of Tm isotopes far from the stability line are in progress along with the RADOPS method described above.

This experiment was performed in collaboration with K.Shimomura, S.Uemura, T.Kohmoto, Y.Fukuda and T.Hashi.

References

1) S.Matsuki, Nihon Butsuri Gakkaisi (in Japanese),43(1988)136, and refs. cited therein.
2) D.A.Eastham et al., Phys. Rev. C36(1987)1583, and refs. cited therein.
3) K.Wallmeroth et al., Phys. Rev. Lett. 58(1987)1516, and refs. cited therein.
4) F.P.Calaprice et al., Phys. Rev. Lett. 54(1985)174; M.Kitano et al., Phys. Rev. C34(1986)1974.
5) K.Shimomura, S.Matsuki, S.Uemura, T.Kohmoto, Y.Fujuda and T.Hashi, Contribution to the Int. Conf. on Quantum Electronics (Tokyo, July, 1988), and S.Matsuki et al., to be Published.
6) W.B.Grant et al., Phys. Rev. B4(1971)1428.
7) See "Table of Isotopes" ed. C.M.Lederer and V.S.Shirley(John Wiley & Sons, New York, 1978).

13. Multi-Cluster Structure in Highly-Excited States of Light Nuclei

Kiyoshi Katō

Department of Physics, Hokkaido University, Sapporo 060, Japan

It has now become evident that the cluster structure is one of the fundamental nuclear structures together with the shell structure in light nuclei.[1),2)] Many successful results for the low-lying states obtained by the cluster model interest us in further investigations of the cluster structure in the high excitation energy region. Since many cluster degrees of freedom activate with the increase of the excitation energy,[3)] one of the most interesting problem in the highly-excited states is the multi-cluster structure.

The prototype of the multi-cluster structure which has been known until now is the 3α structure of the 0_2^+ state (7.55 MeV) in ^{12}C.[4)] Furthermore, a strong possibility of the 4α linear-chain like structure has been suggested in the highly-excited states of ^{16}O,[5)] and the ^{12}C+2α cluster structure of the $K^\pi=0_3^+$ band starting at 7.20 MeV in ^{20}Ne has been discussed.[4)]

In this report, we discuss the multi-cluster structure such as α-^{16}O-α in the highly-excited states of ^{24}Mg. We solve the relative motion of the ^{16}O+2α system by using the orthogonality condition model(OCM).[6)]

The obtained energy spectrum is shown in Fig.1. In order to see properties of obtained states, we calculate α- and ^{8}Be-reduced widths of them. In Fig.2, we show the typical results of α-reduced widths of the 0^+

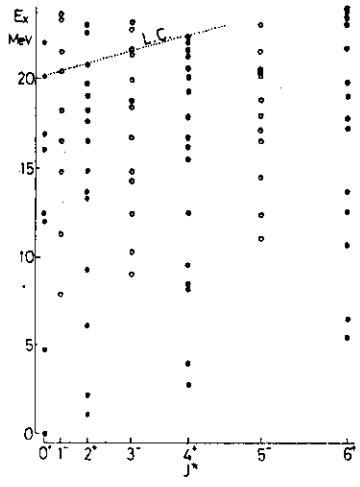

Fig.1 Energy spectra with $J^\pi \leq 6^+$ obtained by the ^{16}O+2α OCM for ^{24}Mg.

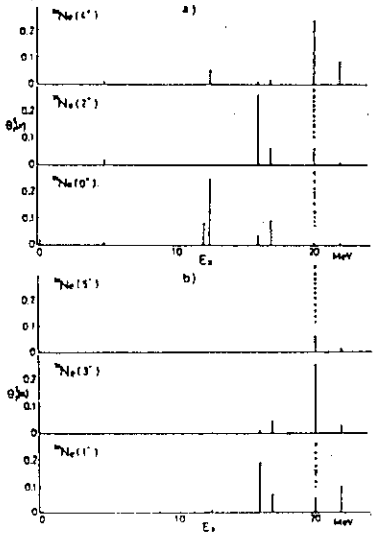

Fig.2 α-reduced widths of the 0^+ states obtained by the ^{16}O+2 α OCM.

states. The 7-th 0^+ state calculated at about 20 MeV has large α-reduced widths in both channels of positive and negative parity states of ^{20}Ne. These results suggest that the 0^+ state at about 20 MeV has a α-^{16}O-α linear-chain structure as shown in Fig.3; such a configuration can be reasonably understood to have a parity mixing configuration of the residual ^{16}O-α system (^{20}Ne) which is obtained by removing one alpha cluster from the α-^{16}O-α system. Furthermore we can see the linear-chain structure of the 0^+_7 state from the following results; 1) the dominant (λ, μ) component of the 0^+_7 state is (N,0) which describes a stretched intrinsic configuration, and 2) the ^{8}Be-reduced widths are very small. By larger model space calculation, we obtained the rotational states with the linear-chain structure starting at 18 MeV and decay widths of them for α-particles as shown in Table I.

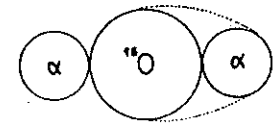

Fig.3 α-^{16}O-α configuration.

Table I

The α-width of the α-^{16}O-α linear-chain states. a_c is a channel radius.

J^π	0⁺		2⁺		4⁺	
l^π \ a_c(fm)	5.16	6.00	5.16	6.00	5.16	6.00
0^+	55 KeV	99 KeV	100 KeV	130 KeV	57 KeV	50 KeV
2^+	218	351	176	262	2.5	7.1
4^+	32	48	49	80	89	62
6^+	1.6×10^{-20}	4.9×10^{-20}	1.2×10^{-7}	2.7×10^{-7}	5.2×10^{-3}	1.9×10^{-2}
1^-	14	11	39	24	5.1	2.9
3^-	3.0×10^{-2}	2.7×10^{-2}	1.5	1.3	10	5.6
5^-	0	0	0	0	2.6×10^{-6}	2.2×10^{-4}

Such linear-chain states at the highly-excited energies of ^{24}Mg have not been investigated experimentally up to the present. It is strongly desired to make an experimental search for cluster states with attention to characteristic α decay widths.

References

1) Prog. Theor. Phys. Suppl. No.52 (1972).
2) Prog. Theor. Phys. Suppl. No.68 (1980).
3) K. Ikeda, N. Takigawa and H. Horiuchi, Prog. Theor. Phys. Suppl. Extra Number (1968), 464.
4) Y. Fujiwara, H. Horiuchi, K. Ikeda, M. Kamimura, K. Katō, Y. Suzuki, and E. Uegaki, Prog. Theor. Phys. Suppl. No.68 (1980), 29.
5) H. Horiuchi, K. Ikeda and Y. Suzuki, Prog. Theor. Phys. Suppl. No.52, (1972), 89.
6) K. Katō, H. Kazama and H. Tanaka, Prog. Theor. Phys. 76 (1986), 75.

14. Distribution of Isoscalar B(E2) Strength in Light Nuclei and Nuclear Structure

Yasuyuki Suzuki

Department of Physics, Niigata University

Giant quadrupole resonances (GQR) have been observed in inelastic hadron and electron scatterings. Systematic analysis has revealed the properties of the resonances including the excitation energy, total width and isoscalar B(E2) strength in percentage of the energy weighted sum rule (EWSR) for the nuclei with the mass number $A > 40$. The characteristics of the B(E2) strength for the nuclei with $A < 40$ is the existence of both a very strong low-energy transition and broad high-energy transitions fragmented over wide energy region. Also missing strength amounts to more than 30 % of the EWSR. This is illustrated in fig.1 which shows observed B(E2) strength up to 30 MeV excitation energy.

The cluster model succeeds in explaining the properties of low-lying levels of light nuclei, but in general reproduces only $20 \sim 30$ % of the EWSR. For example, the $^{16}O+2\alpha$ cluster model developed by Kato et al. reproduces 20 % of the EWSR. The insufficient strength is ascribed to the fact that the fragment clusters in the cluster model are assumed to be frozen to their ground states.

The nuclear symplectic model,[1] an extension of the SU(3) model to include core excitations, is a collective model for the GQR (and also giant monopole resonances) on the basis of the shell model. It has been developed[2] as a powerful and practical means of nuclear spectroscopy. The combined model of both the cluster and symplectic models has been worked out for ^{20}Ne[3] and ^{16}O[4] for reproducing the distribution of the B(E2) strength as well as the properties of the low-lying levels.

A recent experiment[5] has shown that the GQR of ^{40}Ca is split into two parts, one lying at $E_x = 13.5 \pm 1.5$ MeV with the strength of 40 % and the other lying at $E_x = 18 \pm 2$ MeV with the strength of 50 % EWSR. This splitting was not predicted in a shell model calculation of Hoshino and Arima.[6] Since the cluster-Sp(6,R) model calculation for ^{16}O predicts a splitting of the B(E2) strength at high excitation energy, it is interesting to see whether or not the observed splitting in ^{40}Ca is explained by the combined model as in ^{16}O.

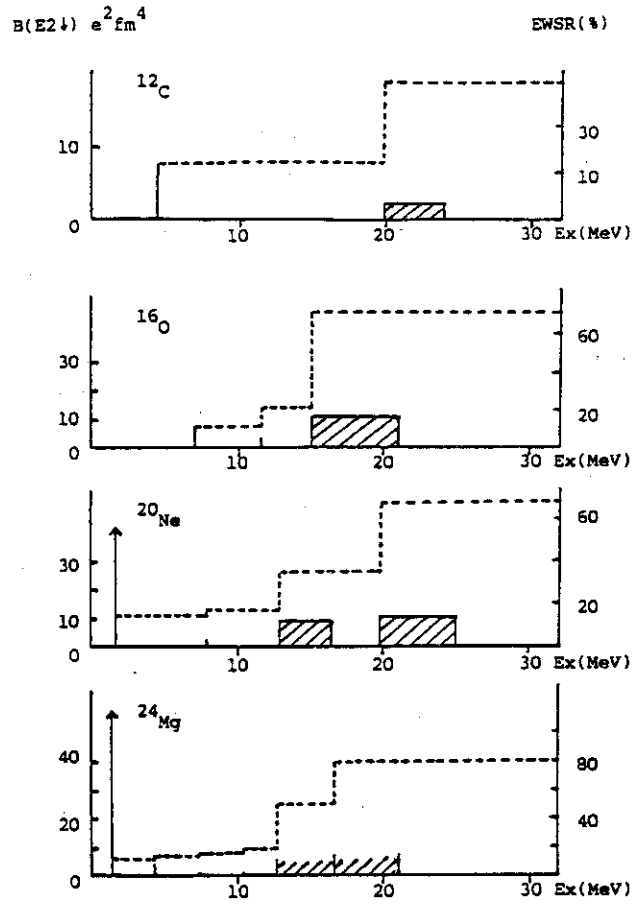

Fig. 1 Isoscalar E2 strength in liht nuclei

References

1) D.J. Rowe, Reports on Prog. in Phys. 48 (1985) 1419.
2) Y. Suzuki and K.T. Hecht, Nucl. Phys. A455 (1986) 315.
3) Y. Suzuki, Nucl. Phys. A470 (1987) 119.
4) Y. Suzuki and S. Hara, to be published.
5) F. Zwarts et al., Nucl. Phys. A439 (1985) 117.
6) T. Hoshino and A. Arima, Phys. Rev. Lett. 37 (1976) 266.

15. Study of the Short Half-Lived Nuclei by the Ion-Guide Isotope Separator On-Line at Tohoku University

T. Shinozuka and M. Fujioka

Cyclotron and Radioisotope Center, Sendai, Tohoku University

Abstract; The status of the ion-guide isotope separator on line at the Tohoku University Cyclotron is reported. Using the present ion-guide system together with a ΔE-E plastic counter telescope and a germanium detector we identified 16 short-lived nuclei including firstly mass separated nuclei ; ^{57}Cu, ^{45}V and so on. The efficiency of mass separation was $\varepsilon \sim 1$ %, where ε is defined as the number of atoms collected at the end of the separator divided by that recoiling from the target. Application of IGISOL to nuclear physics is being performed for Tz=-1/2 mirror nuclei in the $f_{7/2}$-$p_{3/2}$ shell regions and medium mass neutron-rich nuclei produced by proton-induced fission reaction with a uranium target.

The ion-guide method was firstly developed at University of Jyvaskyla of Finland[1]. It is based on the helium-jet technique, but uses a modified target chamber to provide recoil ions. These ions are guided into a conventional isotope separator for further acceleration. No ionizers are used; instead, natural charge creation mechanisms associated with nuclear reactions and recoil thermalization are exploited. These mechanisms, along with charge-exchange processes, create singly-charged atomic recoils in helium. With this approach, separation times and efficiencies are independent of the volatility of the element, and, in the case of refractory elements, separation times several orders of magnitude shorter than those typical of ion-source-based systems are achieved. The details of an IGISOL system has been described[2,3].

Our main interests in the study of short-lived nuclei have been concentrated on the superallowed β^+-decay of the mirror nuclei in the $f_{7/2}$ and $p_{3/2}$ shell regions since we mass-separated ^{59}Zn for the first time by using a conventional ion source of hollow cathode type[4]. The study of the decay of mirror nuclei is important because it is related with a fundamental problem of the quenching of the Gamow-Teller strength in nuclei. However, these mirror nuclei (^{57}Cu, ^{55}Ni, ^{45}V and so on) except for ^{59}Zn

have troublesome properties, i.e., melting points higher than 1000 ℃ and half lives shorter than 0.5 s, and are difficult to study with a conventional on-line mass separator, and we had not been able to mass separate these mirror nuclei. By using a high-speed target transport device TARO[5] we could discover one of these mirror nuclei ^{57}Cu, but of course, without mass separation.

After the development of our IGISOL as described above we began survey works on these mirror nuclei and others using this IGISOL. These experiments have successively been performed rather easily and in a straightforward way, i.e., only by changing the target for changing the nuclide to study. And, the ^{57}Cu and ^{45}V were mass-separated for the first time. In table 1, the obtained half-life values of six mirror nuclei in the $f_{7/2}$ shell-region are shown together with the other two mirror nuclei, ^{41}Sc and ^{43}Ti. Due to sufficient statistics supported by the stable operation of IGISOL, all the experimental errors are smaller than 2 % except that of ^{53}Co. The nucleus ^{45}V is firstly mass-separated in the present experiment, and the result is in good agreement with in Hornshoj[6]. For the half-life of ^{47}Cr, there was considerable discrepancy among several reports as described in Burrows[7]. The present result obtained with the

Table 1 Properties of the β-decay of mirror nuclei and GT matrix elements in the $f_{7/2}$-shell

Mirror Nucleus	Half-life (ms)	Q_{EC}[a] (keV)	Branching Ratio(%)	$B(GT)^{1/2}$ Exp.	$B(GT)^{1/2}$ Theory
^{41}Sc	596.3(17)[b]	6495(1)	99.963(13)	0.850(5)	1.134
^{43}Ti	513.0(80)[c]	6868(7)	(100)	0.739(15)	0.947
^{45}V	547.2(53)	7132(17)	95.7(15)	0.494(23)	0.523
^{47}Cr	472.0(63)	7452(14)	96.3(12)	0.432(23)	0.409
^{49}Mn	381.7(74)	7718(24)	93.6(26)	0.441(39)	0.487
^{51}Fe	305.0(43)	8022(15)	95.0(13)	0.483(23)	0.589
^{53}Co	267(109)	8304(18)	(100)	0.495(359)	0.614
^{55}Ni	212.1(38)	8696(11)	(100)	0.493(20)	0.716

a) Ref.13.

b, c) Refs. 14 and 15, respectively.

mass-separated ^{47}Cr, however, is apparently different from that of Burrows, 508(10) ms. This discrepancy seems to be an open problem to us. The mirror nucleus ^{49}Mn was mass-separated by Hardy[8] and ^{51}Fe and ^{55}Ni by Aysto[9]. The present results for those nuclei are in good agreement with their data.

From the present experimental results, we obtain the reduced Gamow-Teller matrix elements, $B(GT)^{1/2}$. The method of analysis is the same as in ref. 9. For $|g_A/g_V|$ we adopted the recent value[10] of 1.262(5). Table 2, also, shows the experimental GT matrix elements and the theoretical predictions from a shell-model calculation [11] using the modified Kuo-Brown interaction and permitting up to two particle excitation from the $f_{7/2}$-shell to the upper $p_{3/2}$, $f_{5/2}$ and $p_{1/2}$-shells. Figure 1 shows the quenching factor, for the eight mirror nuclei as well as the simple average (i.e., with equal weight) ρ = o.844 ± 0.042. It is remarkable that in the middle of $f_{7/2}$-shell the quenching factor is clearly larger than those of the beginning and end of the shell, and that the average value ρ is larger than the quenching factor[12], 0.76(3), derived for sd-shell nuclei by Wildenthal, and 0.75(3) derived for 25 GT transitions including the eight mirror ones by Miyatake[11]. The fact that the present value of ρ is larger than that derived also for the $f_{7/2}$-shell[11] is caused by; 1) we restricted to the mirror transitions, and 2) we used the present value of $T_{1/2}$ for ^{47}Cr which is considering shorter than that of Burrows[7], which was used in ref.11). It is therefore highly required to study further the mirror β-decays in the $f_{7/2}$-shell, especially around the middle of the shell, both experimentally and theoretically.

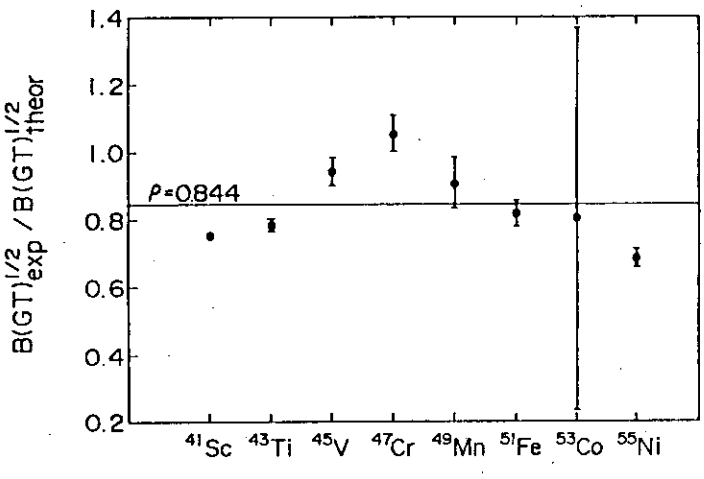

Fig.1 The quenching factors of the mirror nuclei in the $f_{7/2}$-shell.

Presently, application of IGISOL to the study of neutron rich nuclei produced by proton-induced fission reaction with a ^{238}U target has started recently. It seems that its experiment has much feasibility of finding

new nuclides in the neutron-rich side at the A～100 region which is the valley of mass distribution of fission induced by thermal neutron on ^{235}U.

The success of IGISOL machine at Sendai shows that the IGISOL has joined the research tools for looking for unknown nuclei far from the β-stability line. The IGISOL has many merits, i.e., speed of separation, versatility, simplicity and stable operation. It is, however, important to increase the yield of IGISOL in order to overcome the very small production cross section for nuclei far from the β-stability.

We would like to thank for powerful driving forces of our colleagues; Dr. H. Miyatake, Dr. M. Yoshii, Dr. M. Hama, Dr. J. Arje and Dr. J. Aysto.

References

1) J. Arje, J. Aysto, H. Hyvonen, P. Taskinen, V. Kopponen, J. Honkanen, K. Valli, A. Hautojarvi and K. Vierinen, Nucl. Instr. Meth. A247, 431 (1986).
2) J. Arje, Phys. Scripta T3 (1983) 37.
3) M. Yoshii, H. Hama, K. Taguchi, T. Ishimatsu, T. Shinozuka, M. Fujioka and J. Arje, Nucl. Instr. Meth. B26, 410 (1987).
4) Y. Arai et al., Phys. Lett. 104B (1981) 186.
5) T. Shinozuka et al., Phys. Rev. C30 (1984) 2111.
6) P. Hornshoj, J. Kolind and N. Rud, Phys. Lett. 116B, 4 (1982).
7) T. W. Burrows, J. W. Olness and D. E. Alburger, Phys. Rev. C31, 1490 (1985).
8) J. C. Hardy, H. Schmeing, E. Hagberg, W. Perry, J. Wills, E. T. H. Clifford, V. Koslowsky, I. S. Towner, J. Camplan, B. Rosenbaum, R. Kirchner and H. Evans, Phys. Lett. 91B, 207 (1980).
9) J. Aysto, J. Arje, V. Kopponen, P. Taskinen, H. Hyvonen, A. Hautojarvi and K. Vierinen, Phys. Lett. 138B, 369 (1984).
10) P. Bopp, D. Dubbers, L. Horning, E. Klemt, J. Last, H. Schutze, S. J. Fremen and O. Scharpf, Phys. Rev. Lett. 56, 919 (1986).
11) H. Miyatake, K. Ogawa, T. Shinozuka and M. Fujioka, Nucl. Phys. A470, 328 (1987).
12) B. H. Wildenthal, Prog. Part. Nucl. Phys. 11, 5 (1984).
13) A. H. Wapstra and G. Audi, Nucl. Phys. A432, 1 (1985).
14) D. E. Alburger and D. H. Wilkinson, Phys. Rev. C8, 657 (1973).
15) V. J. Janecke, Z. Naturforschg., 15a, 593 (1960).

16. Identification of the New Isotope ^{121}La and Decay Spectroscopy of ^{122,124,126}La and ^{128,130}Pr by Means of Selective Mass Separation

Toshiaki Sekine, Kentaro Hata, Yuichiro Nagame, Shin-ichi Ichikawa*, Hideki Iimura*, Masumi Oshima**, Naruto Takahashi*** and Akihiko Yokoyama***

Department of Radioisotopes, *Department of Chemistry, **Department of Physics, Japan Atomic Energy Research Institute and ***Faculty of Science, Osaka University

The neutron deficient isotopes with $50 \leqq Z, N \leqq 82$ are extensively studied as a frontier of unstable nuclei and as a testing field of nuclear deformation. For studying the nuclei in this region by means of a combination of heavy-ion reaction, isotope separation on line(ISOL) and nuclear spectrosopy, we have developed a new ion-source technique that strengthens elemental selectivity in ISOL. Using this technique, we have searched for a new isotope of ^{121}La and studied decays of ^{122,124,126}La and ^{128,130}Pr. In this paper, we summarize these experimental results. In addition, the properties of the low-lying states in their daughter even-even nuclei are discussed in connection with the prediction by Puddu et al.[1] based on the interacting boson model.[2]

1. Selective on-line mass separation with ionization of the monoxide of light lanthanoids

In order to strengthen elemental selectivity in ISOL for light lanthanoids, we attempted to use their monoxide ions possibly formed in a thermal ion source. The process expected to produce a monoxide ion MO^+ is as follows. A highly-ionized nuclear reaction product M^{x+} recoils into a catcher, and is evaporated by heating from there as a free atom M. Since some oxygen atoms are present as impurities inherently in an ionizing cavity, the species MO is produced with the chemical reaction M + O → MO. Then, MO and also M are ionized by surface ionization. In this process elemental selectivity is given by the difference between the dissociation energies of monoxides.

In off-line experiments with stable isotopes, the observed MO^+/M^+ ratio decreased by several orders of magnitude with atomic number from 57 (La) to 62 (Sm). It was also found that La and Ce give almost the same MO^+/M^+ ratio in the temperatures taken, 1900 - 2730 K; consequently, they are not separable from each other. It is, however, very important that they can be separated from other lanthanoids, Ba and Cs. In the studies described in the following sections, La isotopes were obtained as $La^{16}O^+$, being well separated from the Cs and Ba isobars, while Pr isotopes were obtained because most of the La and Ce isobars were in MO^+.

2. Identification of the new isotope ^{121}La

To search for a very unstable nucleus of ^{121}La, whose proton binding energy is predicted to be negative, an enriched ^{92}Mo target (3.06 mg/cm^2) was bombarded with a 4.7-MeV/u ^{32}S beam. Following mass separation, gamma-singles, gamma-gamma coincidence and beta-gamma coincidence measurements were performed for the A=137 ($^{121}La^{16}O^+$) fraction. From the measurement over a counting time of 12 h the gamma lines with energies of 97.8, 134.0, 138.7, 169.4, 239.8, 303.8 and 379.1 keV were assigned to the transitions associated with the decay of ^{121}La; its half-life was found to be 5.2±0.2 s.

The assignement of the radioactivity to ^{121}La was supported by the results of the gamma-gamma coincidence measurement: some gamma lines were found to be coincident with Ba X-rays that were emitted in an electron-capture decay of ^{121}La or in an internal conversion process associated with a transition in ^{121}Ba, the daughter of ^{121}La. Additionally, the observed half-life of ^{121}La is in good agreement with the predicted value 5 s by the gross theory of beta decay.[3)]

3. Decay spectroscopy of the odd-odd nuclei $^{122,124,126}La$ and $^{128,130}Pr$

A Mo target (4.1 mg/cm^2) and a Rh target (3.8 mg/cm^2) were bombarded with ^{32}S beams (5.0-6.2 MeV/u) to produce neutron deficient isotopes of La and Pr, respectively. The products were mass-separated as described before, and gamma-ray measurements were carried out for the masses 138 ($^{122}La^{16}O^+$), 140 ($^{124}La^{16}O^+$), 142 ($^{126}La^{16}O^+$), 128 and 130. From the gamma-ray data, we obtained the half-lives of

^{122,124,126}La and ^{128,130}Pr, and constructed their decay schemes. The half-lives and the estimated spin-parity values are listed in Table 1 together with the previouly reported ones. The half-lives obtained are more accurate in most cases than the previous values. In the decay schemes obtained, the levels in the gamma band are populated as well as those in the ground band. In addition, populations in the negative parity band were also seen in the decays of ^{124}La and ^{126}La. Further, in the decay of ^{122}La, the gamma-band head (2_2^+ state) in ^{122}Ba was newly identified with a level energy of 940 keV. This energy value is found to be very close to that predicted with IBM.[1)]

Table 1
Half-lives and spin-parity values

	Present work		Previous work	
Nuclide	$T_{1/2}$ (s)	I^π	$T_{1/2}$ (s)	I^π
^{121}La	5.2±0.2			
^{122}La	9.6±1.0	(3^+)	8.7±0.7[a)]	
^{124}La	29±2	(7)	29±3[b)]	(6,7)[c)]
^{126}La	54±2	(4)	60±18[d)]	
^{128}Pr	2.7±0.4	(3^+)	3.2±0.5[e)]	
^{130}Pr	31±2	(4)	28±6[f)]	
			44±4[g)]	

a) J. M. Nitschke et al., Z. Phys. A316 (1984) 249.
b) D. D. Bogdanov et al., Nucl. Phys. A307 (1978) 421.
c) K. Furuno et al., J. Phys. Soc. Japan 56 (1987) 1905.
d) I. L. Preiss et al., Phys. Rev. 129 (1963) 1284.
e) P. A. Wilmarth et al., Z. Phys. A321 (1985) 179.
f) D. D. Bogdanov et al., Nucl. Phys. A275 (1977) 229.
g) M. Korfelahti et al., Z. Phys. A327 (1987) 231.

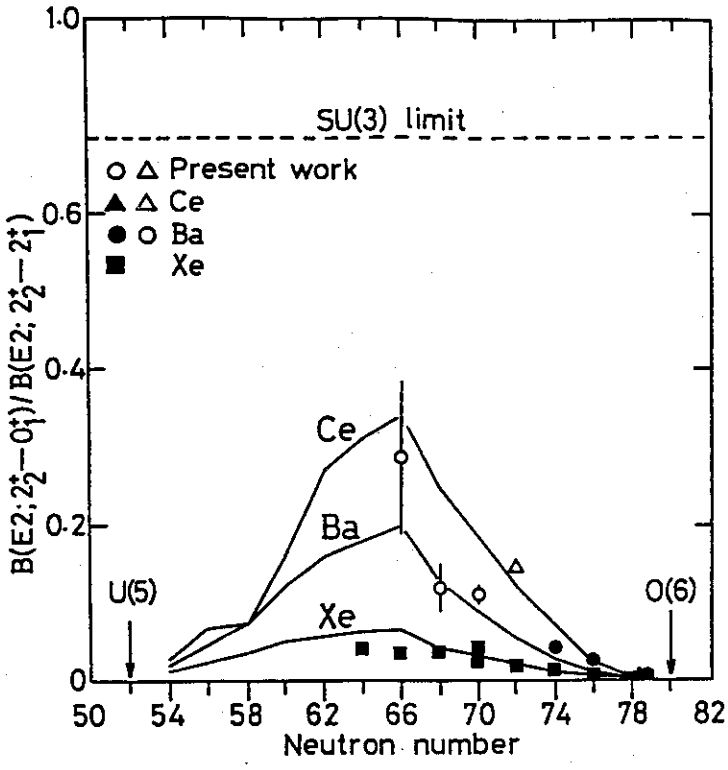

Fig. 1 Comparison between experimental and calculated values of the ratio $B(E2;2_2^+\rightarrow0_1^+)/B(E2;2_2^+\rightarrow2_1^+)$ in Xe, Ba and Ce. The lines are the calculted values taken from ref.[2] and the solid symbols are the previous experimental values cited in the same reference.

From the gamma-ray data, we have obtained the branching ratios of electromagnetic transition from 2_2^+, 3_1^+ and 4_2^+ states in ^{122,124,126}Ba and ^{130}Ce. The experimental branching ratios are found to be in good agreement with the theoretical E2 branching ratios calculated with IBM.[1] Assuming that the observed transitions $2_2^+\rightarrow0_1^+$ and $2_2^+\rightarrow2_1^+$ are a pure E2 transition, we plotted the experimental and theoretical ratios $B(E2;2_2^+\rightarrow0_1^+)/B(E2;2_2^+\rightarrow2_1^+)$ in Fig.1. This figure shows that the experimental result supports the predicted changes in the structure of the isotopic chains Ba and Ce in addition to Xe.[1,2]

References

1) G. Puddu, O. Scholten and T. Otsuka, Nucl. Pys. A348 (1980) 109.
2) F. Iachello and A. Arima, "The Interacting Boson Model," Cambridge Univ. Press, Cambridge (1987).
3) K. Takahashi, M. Yamada and T. Kondoh, At. Nucl. Data. Tables 12 (1973) 101.

17. Accelerator Mass Spectrometry Experiments at the RCNST Tandem Facility of University of Tokyo

Mineo Imamura

Institute for Nuclear Study, University of Tokyo

1. Introduction

Accelerator mass spectrometry (AMS) is a new type of mass spectrometry in which ions are accelerated to high energy compared with conventional mass spectrometry. It makes use of dissociation of interfering molecular ions by electron stripping and the subsequent particle identification of the accelerated atoms. Its extremely high sensitivity in detection of long-lived radioisotopes promises many new possibilities in various research fields of science. In ten years since the inspiring work by R. Muller (1977)[1], approximately 30 AMS facilities have been operated or planned in the world.[2]

Our AMS program started in 1980 using tandem Van de Graaff accelerator at the Research Center for Nuclear Science and Technology (RCNST), University of Tokyo. The first ^{10}Be measurements came out in 1982, but the earthquake in the early 1983 forced interruption of the program for two and half years due to the damage of accelerator tubes and their repair works. At present the system is capable of routine measurements of three isotopes, ^{10}Be, ^{14}C and ^{26}Al.

This paper presents a brief description of our AMS system and its application to measurements of nuclear reaction cross sections.[3-5]

2. AMS system at RCNST

The measurement system is schematically illustrated in Fig. 1. One of the important feautures in our AMS system is the monitor beam Faraday cup system which is also used for the terminal voltage stabilization by means of slit current feedback. The data taking is performed by an automatic data aquisition system interfaced to a small computor, PC-9801 (NEC Co.).

In the conventional method of AMS, the measurements of isotope ratios of radioactive/stable are performed by the sequential injection of radioactive and stable ions. The sequential method requires very stable operation of the accelerator because of the requirement of the stable beam-transmission efficiency. We apply an alternative and unique way of the injection, what we call the 'internal beam monitor method', which has been proved to be very effective for the improvement of the measurement precision.

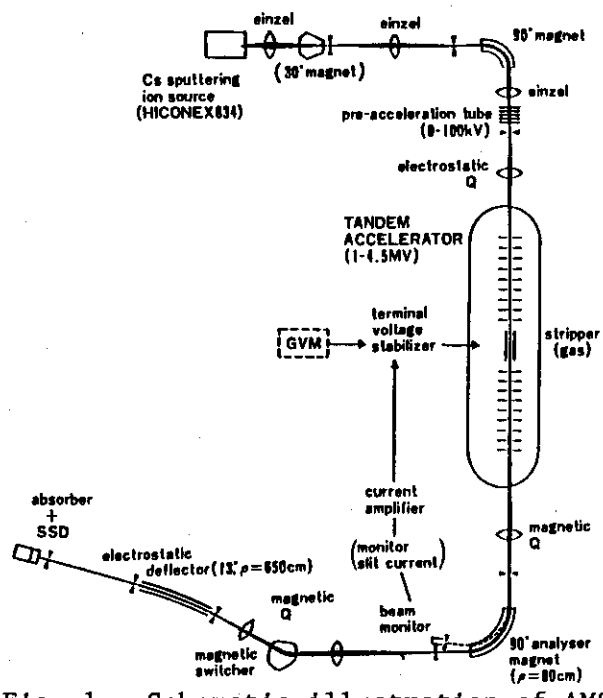

Fig. 1 Schematic illustration of AMS system at the RCNST tandem accelerator facility.

In this method negative ions with the same molecular weight as the radioactive one are injected simultaneously, instead of sequentially, and accelerated. The radioisotope ions are counted with the detector while stable ions are measured with a monitor Faraday cup. The radioactive/stable isotope ratio in the sample is calculated from the observed ratio of accelerated ions (radioisotope/monitor) and the relative ratio of the molecular (monitor) to the main beam (stable isotope) measured at the injection Faraday cup.

Our approach has advantages over the conventional sequential method in that it can avoid many factors affecting the precise measurements: fluctuation of the beam intensity and changes of parameters in the ion source and in the accelerator. In Table 1, perfomances of our AMS system are presented. Minimum sample sizes needed for measurements with reasonable counting statistics are 10^7, 10^5 and 10^7 atoms for ^{10}Be, ^{14}C and ^{26}Al, respectively.

Table 1 Performances of the AMS facility at RCNST

Nuclide ($t_{1/2}$)	Neg. Ion	Current uA	Charge State	Monitor Ion	Term. Volt.	Transm. Eff. %	Sensitivity [Reproducibility]
Be-10 (1.5×10^6y)	BeO^-	0.1-0.4	+3	$^9Be^{17}O^-$ ($^9Be^{3+}$)	3.5_{MV}	0.5-1.5	5×10^{-14}[2%]
C-14 (5.7×10^3y)	C^-	0.5-10	+3	$^{13}CH^-$ ($^{13}C^{3+}$)	3.0_{MV}	3 - 10	3×10^{-16}[2%]
Al-26 (7.2×10^5y)	Al^-	0.01-0.06	+3	$^{10}B^{16}O^-$ ($^{16}O^{2+}$)	2.5_{MV}	10	1×10^{-13}[7%]

3. Applications

The AMS measurements have been applied to studies of diverse fields

Table 2 Yield ratios ($^{10}Be/^{7}Be$) in photonuclear reactions

Target	E_{max}(GeV)	$^{10}Be/^{7}Be$
Cu	0.8	0.52 ± 0.11
	0.9	0.87 ± 0.39
	1.0	0.83 ± 0.17
O	0.55	0.27 ± 0.03
	0.85	0.22 ± 0.02
	1.05	0.22 ± 0.02

such as nuclear chemistry, nuclear cosmochemistry, geophysics and archaeology. In the followings I describe shortly some recent experiments applied to nuclear reaction cross section studies.

$^{10}Be/^{7}Be$ ratios in fragmentation

^{10}Be and ^{7}Be formation cross sections have been determined on Cu and O bombarded with bremsstrahlungs from the electron synchrotron accelerator at INS. The $^{10}Be/^{7}Be$ ratios are given in Table 2. The same ratios for proton-induced reactions of similar energy are in the range of 0.1-0.2 according to Raisbeck and Yiou (1976). The ratios in Cu are considerably larger by a factor of 5. This seems to show a difference in mass dependence of fragment yield i.e. $A^{-\lambda}$ or a difference in N/Z ratio of excited nuclei before fragmentation.

^{10}Be production cross sections from n + ^{14}N

The cross sections of the $^{14}N(n,x)^{10}Be$ reaction with $E_n \lesssim 40$ MeV have been measured for VN targets irradiated with a quasi-monoenergetic neutron beam from the $^{9}Be(p,n)^{9}B$ reactions. Fig. 2 is the obtained excitation function which shows a distinct difference from that of the proton-induced reaction. The above reaction is important in estimating the atmospheric production of ^{10}Be.

Acknowledgements I wish to thank our collaborators, who are M. Honda, K. Kobayashi, T. Kobayashi, H. Nagai, S. Shibata, H Yamashita, K. Yoshida and H. Yoshikawa.

References

1) R.A.Muller, Science 196(1977) 489.
2) Proc. 4th Int. Symp. on Accelerator mass spectrometry, Nucl Instr. Meth. B29 (1987).
3) M. Imamura et al., Nucl. Instr. Meth. B5(1984)211.
4) K. Kobayashi et al. ibid B29 (1987)173
5) H. Nagai et al. ibid B29(1987)266.

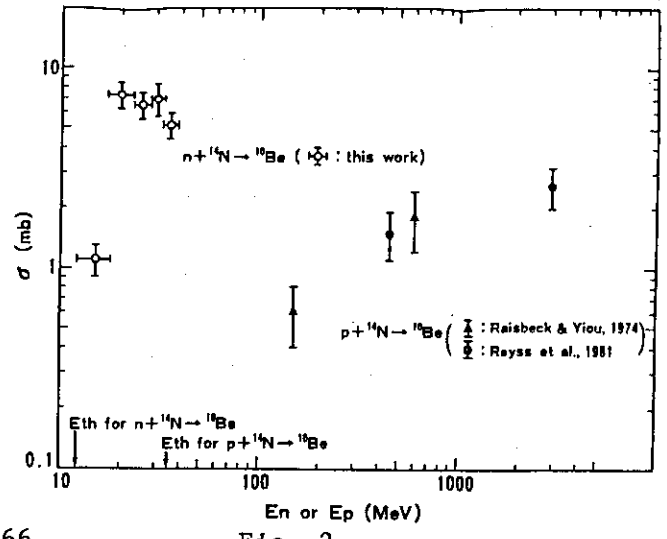

Fig. 2

18. Fusion and Quasi-Fission with High Angular Momenta

Hiroshi Baba

Faculty of Science, Osaka University

The excitation function of the heavy-ion fusion reaction is theoretically treated by several models. Among them, Bass model[1] and extra-push/extra-extra-push model[2] have advantages in their simplicity and yet giving clear presentation of the reaction mechanism. The former gives fairly good overall agreement with observed fusion cross sections for the reaction systems lighter than actinides, whereas the latter gives a persuasive feature with quantitative reproduction of the observation.

Bass model is constructed on a simple yet clear theoretical ground based on a spherically symmetric potential and reproduces well observed fusion cross sections σ_{fu} in most cases as long as the maximum orbital angular momentum of incident partial waves does not exceed the classical critical value l_{crit} for fusion. In the heavy-ion reaction, a part of the angular momentum is damped into internal spin due to the friction in the composite system of projectile and target. The damping of angular momenta causes fusion of partial waves with angular momenta greater than l_{crit} which would not result in fusion otherwise. Bass model proclaims therefore the fusion cross section σ_{fu} keeps increasing with energy untill the decreased angular momentum due to damping reaches l_{crit}.

In the reaction systems with which Bass model concerns, the fused nuclei decay into the final products via either fission or particle evaporation. The excitation function σ_{er} for the particle evaporation process is theoretically expected to be inversely proportional to the energy E for sufficiently high energies, and this is experimentally proved to be the case for systems heavier than Pb. For the compound nuclides lighter than Au, however, σ_{er} is scacely measured in the energy region where the $1/E$ dependence holds. Instead, the fission cross section σ_f is measured for a number of reaction systems. The subtracted value of the Bass model σ_{fu} by the amount of σ_f should then give σ_{er}, which shows a linear relationship with respect to the energy but does not decrease so much as to give the $1/E$ proportionality as shown in Fig.1. Moreover, the deviation from the $1/E$

18. Fusion and Quasi-Fission with High Angular Momenta

Hiroshi Baba

Faculty of Science, Osaka University

The excitation function of the heavy-ion fusion reaction is theoretically treated by several models. Among them, Bass model[1] and extra-push/extra-extra-push model[2] have advantages in their simplicity and yet giving clear presentation of the reaction mechanism. The former gives fairly good overall agreement with observed fusion cross sections for the reaction systems lighter than actinides, whereas the latter gives a persuasive feature with quantitative reproduction of the observation.

Bass model is constructed on a simple yet clear theoretical ground based on a spherically symmetric potential and reproduces well observed fusion cross sections σ_{fu} in most cases as long as the maximum orbital angular momentum of incident partial waves does not exceed the classical critical value $\underline{l}_{crit}$ for fusion. In the heavy-ion reaction, a part of the angular momentum is damped into internal spin due to the friction in the composite system of projectile and target. The damping of angular momenta causes fusion of partial waves with angular momenta greater than $\underline{l}_{crit}$ which would not result in fusion otherwise. Bass model proclaims therefore the fusion cross section σ_{fu} keeps increasing with energy untill the decreased angular momentum due to damping reaches $\underline{l}_{crit}$.

In the reaction systems with which Bass model concerns, the fused nuclei decay into the final products via either fission or particle evaporation. The excitation function σ_{er} for the particle evaporation process is theoretically expected to be inversely proportional to the energy $\underline{E}$ for sufficiently high energies, and this is experimentally proved to be the case for systems heavier than Pb. For the compound nuclides lighter than Au, however, σ_{er} is scacely measured in the energy region where the $1/\underline{E}$ dependence holds. Instead, the fission cross section σ_f is measured for a number of reaction systems. The subtracted value of the Bass model σ_{fu} by the amount of σ_f should then give σ_{er}, which shows a linear relationship with respect to the energy but does not decrease so much as to give the $1/\underline{E}$ proportionality as shown in Fig.1. Moreover, the deviation from the $1/\underline{E}$

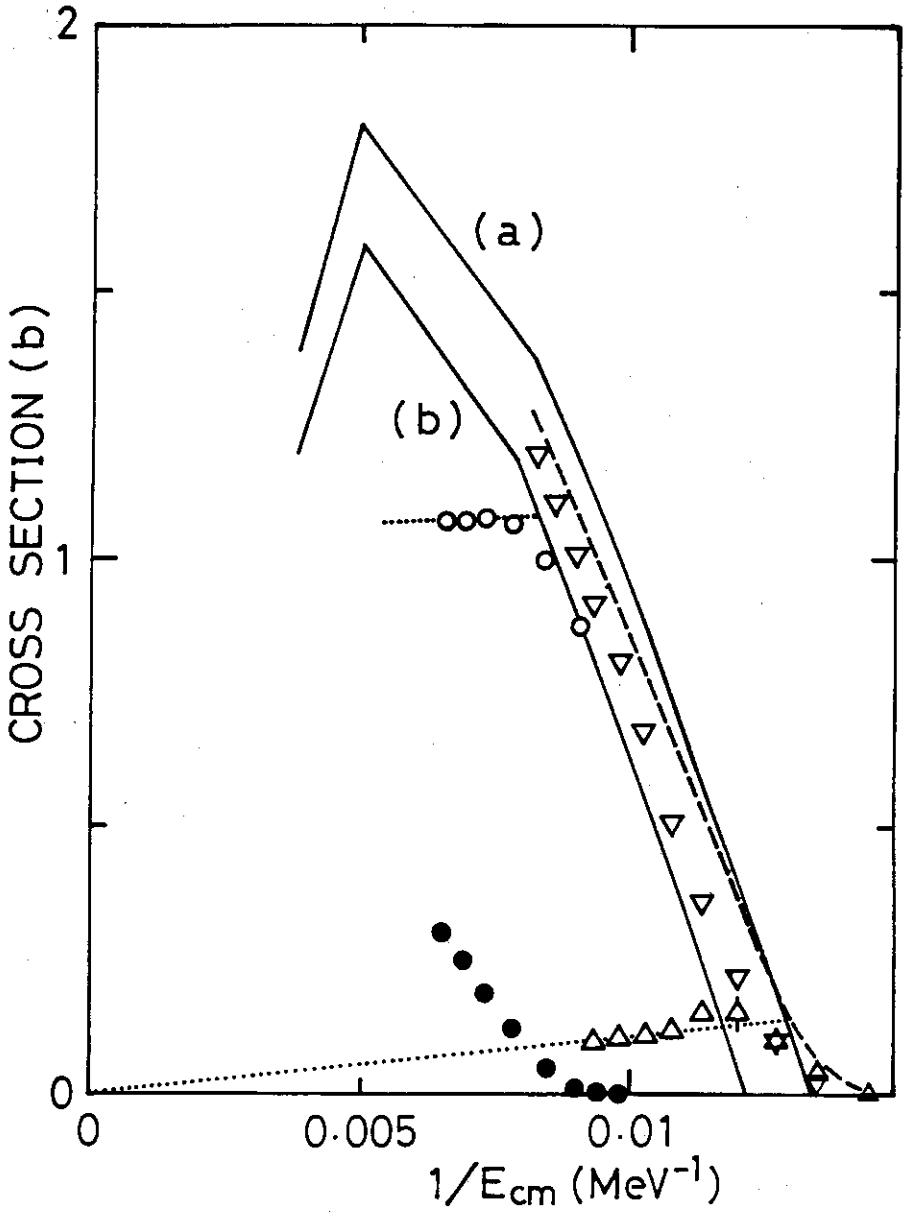

Fig.1 Fusion, fission, and evaporation cross sections plotted versus inverse of the center-of-mass energy for reaction systems of (a) ^{197}Au + ^{16}O and (b) ^{134}Ba + ^{24}Mg. Solid lines are the calculated fusion cross sections σ_{fu} by Bass model[1]. Downward and upward triangles represent observed σ_f[3] and σ_{er}[4], respectively, and the dashed line gives the sum of them, the fusion excitation function for the (a) system. σ_{er} at higher energies are seen to be extrapolated back to the origin (dotted line). Solid circles represent observed σ_f[5] for the (b) system, and open circles are the difference between σ_{fu} and σ_f which do not point to the origin as shown with a dotted line.

proportionality is found to systematically increases as the mass number of the compound system decreases.

The reason of the systematic deviation is very likely to lie in σ_{fu} in the energy region where $\underline{l}_{max} > \underline{l}_{crit}$ predicted by Bass model. Then it follows that the fusion reaction mechanism in the region of $\underline{l} > \underline{l}_{crit}$ is not so simple as Bass model specifies. In the consideration of the effect of high angular momenta on the fusion mechanism, one can not disregard existence of quasi-fission as a competing process against fusion. The mechanism of quasi-fission or direct fission is qualitatively classified into the following three types depending on the collision depth; i) deep inelastic scattering with longest dissipation times[6] following the peripheral collision, ii) the so-called quasi-fission as a consequence of deeper collisions, and iii) direct fission of a composite system failed to surmount the non-conditional saddle[2].

Of the above-mentioned three types of direct fission, the second and third ones are considered to affect a bit the fusion cross section. The second type of fission is considered to take place under the condition that the fission barrier disappears because of the high angular momentum. Characteristics of quasi-fission with no barrier are not clear in a sense how they are different from those of the fusion fission. Grégoire et al.[6] discuss that the width of the product mass distribution would become broad abruptly and demonstrate an observation which does not contradict their estimated trend with respect to the angular momentum. However, the observed widths are consistent also with a smoothly increasing trend without any abrupt break at $\underline{l} = \underline{l}(B_f=0)$. Therefore, we should say there is no experimental evidence of quasi-fission of the type.

Viola has measured[7] the fission fragment angular correlation for the ($^{14}N + ^{238}U$) system over the energy range from $\underline{E}/\underline{A}$ = 7 to 45 showing that the fraction of the linear momentum transferred from projectile to composite system decreases gradually from 1.0 to 0.7 with the energy. Furthermore, the folding angle distribution becomes significantly broad at high incident energies where the full momentum transfer is not attained. The results are likely to be the consequences of intrusion of quasi-fission at high energies because broadening of the folding angle distribution seems to diminish the possibility of precompound fission or incomplete fusion fission.

Recently, we devised a method[4] of extracting a particular J-window for sub-actinide nuclei, a critical value J_{ER} at which the partial level width for fission becomes equal to the width for neutron emission. This critical J-value is characteristic of individual fused nuclide and, therefore, one should obtain the same value of J_{ER} for different combinations of projectile and target leading to the same compound system. It was then really found to be the case for heavier nuclides close to the actinide region, whereas there were large discrepancies in the value of J_{ER} in some lighter nuclides. The resulting J_{ER} value was found to become significantly large with heavy projectiles. Such an abnormally high J_{ER} value is very likely to arise due to quasi-fission and, if so, it can be a probe for the occurrence of quasi-fission.

References

1. R. Bass, Nucl. Phys. A231 (1974) 45.
2. W. J. Swiatecki, Nucl. Phys. A376 (1982) 275.
3. T. Sikkeland et al., Phys. Rev. 135 (1964) B669.
4. S. Baba et al., to be published.
5. J. van der Plicht et al., Phys. Rev. C28 (1983) 2022.
6. C. Grégoire et al., Nucl. Phys. A361 (1981) 443.
7. V. E. Viola, Nucl. Phys. A471 (1987) 53c.

19. Electron Capture from K Shells in Heavy Atoms by 72, 62 and 52 MeV $^{3}He^{2+}$ Beams

I. Katayama*, T. Noro*, H. Ikegami*, F. Fukuzawa**, K. Yoshida**, Y. Haruyama***, A. Aoki***, H. Ogawa**** and I. Sugai*****

*Research Center for Nuclear Physics, Osaka University, **Department of Nuclear Engineering, Kyoto University, ***Laboratory of Applied Physics, Kyoto Prefectural University, ****Department of Physics, Nara Women's University, *****Institute for Nuclear Study, University of Tokyo

Electron capture at intermediate energies where the cross section shows increasing to the maximum remains the subject of interest in atomic collision problem. Especially the experimental study of K shell electron capture by light projectiles is particularly of importance from a couple of reasons, i.e., i) experimental data are indispensable to test the several calculations in the SPB (Strong Potential Born) theories[1,2] ii) single electron model has been employed historically for the K shell electron in the theory, nevertheless the multi-electron effect or the shielding effect in the capture process has not yet been established.[3]

Up to now, the experiment aimed to separate the contributions of different shell electrons in the target atom was done in the p+Ar system at 10 MeV proton energy by Horsdal-Pederson et al.[4] They performed the coincidence measurements between electron capture yield i.e., neutral hydrogen H^{0} and deexcitation KX rays from the residual atom. As the increase of incident energy and of target atomic number, the method is found to be less effective by the fact that the accidental coincidence due to relatively growing yields of KX rays by the ionization process becomes serious. We have reported that a high resolution magnetic spectrograph can be successfully applied to separate the target K shell in electron capture by 72 and 52 MeV $^{3}He^{2+}$ beams for Sn and Ag targets.[5,6]

The $^{3}He^{2+}$ beams were accelerated by the RCNP AVF cyclotron. The resolution of the beam after the momentum analysis was 2×10^{-5}. The electron capture products were measured by the magnetic spectrograph RAIDEN at zero degree. Fig. 1 shows the energy spectra of $^{3}He^{1+}$ which is the electron

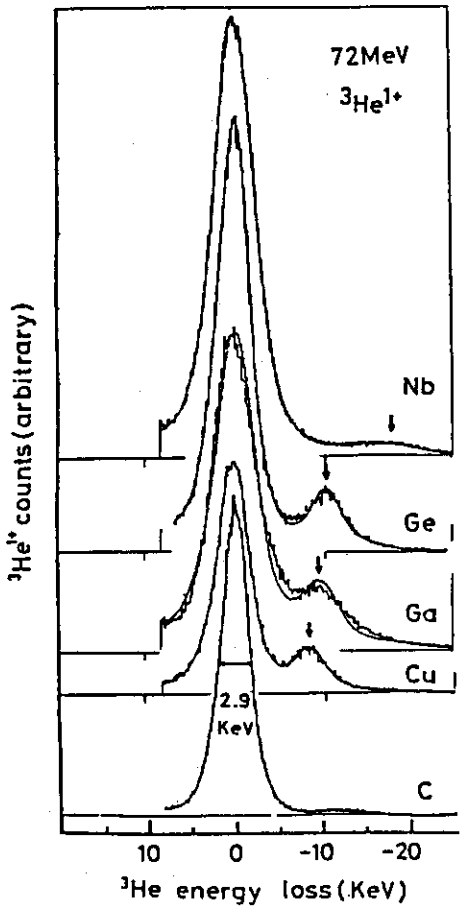

Fig. 1 Energy spectra of electron capture yields $^3He^{1+}$ from several targets at 72 MeV. The arrows denote the K shell position of each target atom.

capture yield of $^3He^{2+}$ in C, Cu, Ga, Ge and Nb targets at 72 MeV. The energy calibration showed that the difference in energy between the carbon peak and the small peak seen at the right part in each spectrum corresponds to the K binding energy of each target atom. The peaks denoted by arrows in fig. 1 were then assigned to those due to electron capture from the K shell in the target atom. Combining these results with another measurements in which the total $^3He^{1+}$ yields were counted as a function of the target thickness, we could deduce the capture cross section of K shell electrons.

One of the present results is shown in fig. 2. The target atomic number dependence of the K shell capture cross sections seems reasonablly well explained by the SPB calculation. Publications of the this experiment up to now are found in refs. 5, 6, 7 and 8.

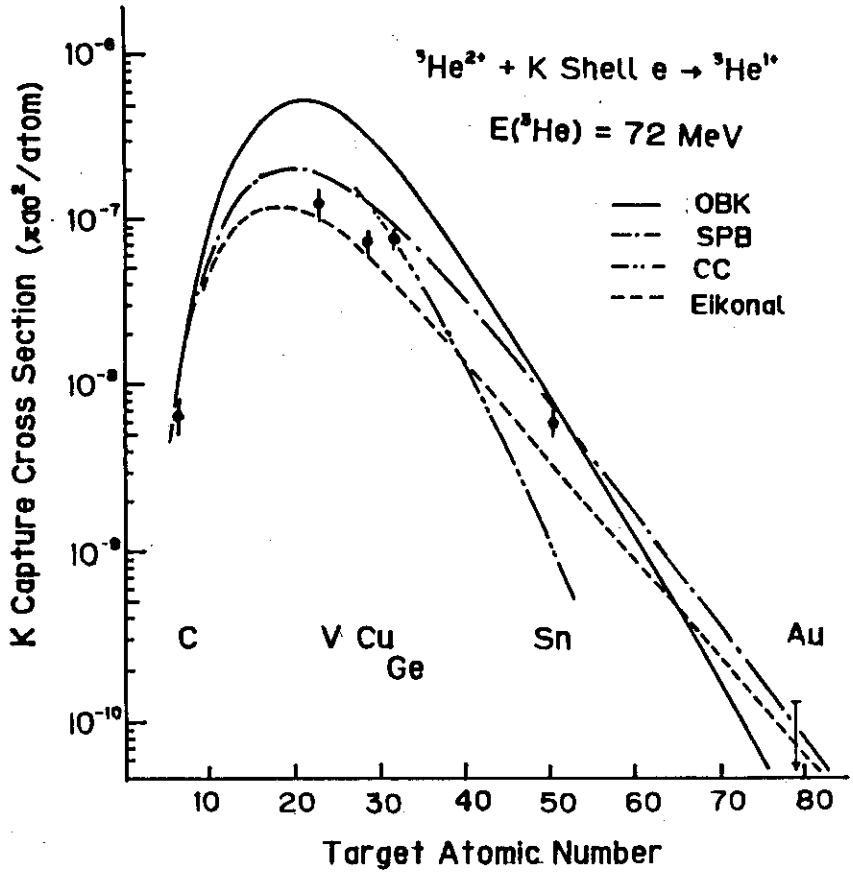

Fig. 2 The target atomic number dependence of the target K shell capture cross sections by ^{3}He of 72 MeV.

References

1) J. Macek and K. Taulbjerg, Phys. Rev. Lett. 46 170 (1981).
2) J.H. Mcguire, R.E. Kletke and N.C. Sil, Phys. Rev. A32 815 (1985).
3) J.H. McGuire, Private communication.
4) E. Horsdal-Pederson, C.L. Cocke, J.L. Rasmussen, S.L. Verghese, and W. Waggoner, J. Phys. B16 1799 (1983).
5) I. Katayama, M. Fujiwara, S. Morinobu, T. Noro, H. Ikegami, F. Fukuzawa, and I. Sugai, Proceedings on the Second Asia-Pacific Physics Conf., Bangalore 1986, ed. S. Chandrasekhar (World Scientific, Singapore 1987) p.622.
6) I. Katayama, M. Fujiwara, T. Noro, H. Ikegami, F. Fukuzawa, K. Yoshida, Y. Haruyama, A. Aoki, H. Ogawa and I. Sugai Proceedings on the Int. Seminar on Dynamic Processes of Highly Charged Ions (Fuji susono, Japan, Aug., 1986) IPPJ-AM-48, p. 75.
7) H. Ogawa, I. Katayama, Y. Haruyama, T. Noro, H. Ikegami, F. Fukuzawa, K. Yoshida, A. Aoki and I. Sugai, Nucl. Instr. and Method A262 (1987) 23.
8) Y. Haruyama, I. Katayama, H. Ogawa, T. Noro, H. Ikegami, F. Fukuzawa, K. Yoshida, A. Aoki and I. Sugai (to be published in N.I.M.)

20. Atomic Capture and the Successive Nuclear Absorption of Stopped-Negative-Pion

Atsushi Shinohara

Department of Chemistry, Faculty of Science, Nagoya University

A negative meson slowed down in the material is captured by the Coulomb field of an atom and forms a mesic atom. The captured meson cascades down by emitting Auger electrons or X rays, and is eventually absorbed by the nucleus when it reaches an inner shell where its wave function overlaps with the nucleus. As for the capture process, currently, the influence of the molecular or atomic structure on it have been a subject of interest for many experimental and theoretical groups, and being explained by means of the large mesic molecule model.[1,2] The nuclear reactions following the absorption of the stopped-negative-meson present a different feature from that of ordinary nuclear reactions induced by bombarding particles giving the equal amount of excitation energy (140 MeV for a pion) due to a different characteristic of the excitation process.

In this report, we describe the results of the measurements of the fission probability and the product yields in the pion absorption reaction in ^{209}Bi and discuss the reaction mechanism.[3] The pion irradiations and the pionic X- and in-beam γ-rays measurements were performed at the 12-GeV proton synchrotron of KEK. Identification and determination of the produced nuclides were carried out by means of the in-beam reaction γ rays and the γ rays of the residual activities. Figure 1 shows the observed yield distributions of lead isotopes with A = 194-207 and thallium isotopes with A = 199-205. The fission event was detected with a mica track detector. The fission probability, W_f, was determined as $W_f = (3.01 \pm 0.34) \times 10^{-3}$ with the aid of the pionic X-ray measurement.

First, we have searched for such an energy distribution of the equilibrium states reproducing both the W_f value and the product yield distribution, and found the distribution having the low excitation energy of about 50 MeV on an average and the wide width of about 35 MeV. The speculation about the equilibrated state supports the reaction mechanism proposed in the previous studies.

Next we carried out a model calculation to further obtain a clear insight into the reaction mechanism. The proposed model consists of four steps as shown in Fig. 2. As for the angular momentum of the nucleus, it was assumed to be induced only by the fast particles emitted in the 2nd and

3rd steps (two extreme cases were considered for two particles emission; one is the case with 180° correlation, and the other is the case with no correlation). Comparisons of the calculated and the observed values for the product yields are given for lead and thallium isotopes in Fig. 1. For lead isotopes, both the solid and the dashed histograms are in excellent agreement with the observed values. The calculation also reproduced the average angular momenta deduced from the observed isomeric ratios.

In conclusion, the absorption process was described by a quasideuteron capture in an extremely peripheral region of the nucleus and the deexcitation was explained by the hybrid model operated along two independent paths and including the escape process of the primary particles followed by the particle evaporation and fission. The motion of the primary nucleon pair and the double particle emission showed an angular correlation peaking at 180° . Furthermore, this model indicates that the angular momentum of the nucleus is qualitatively explained with the vector sum of the angular momenta estimated classically from the linear momenta of emitted particles.

References

1) For example; P. I .Ponomarev, Ann. Rev. Nucl. Sci., 23, 395 (1973).
2) N. Imanishi, et al., Phys. Rev. A, 32, 2584 (1985); 35, 2044(1987).
2) A. Shinohara, et al., Nucl. Phys., A456, 701 (1986).

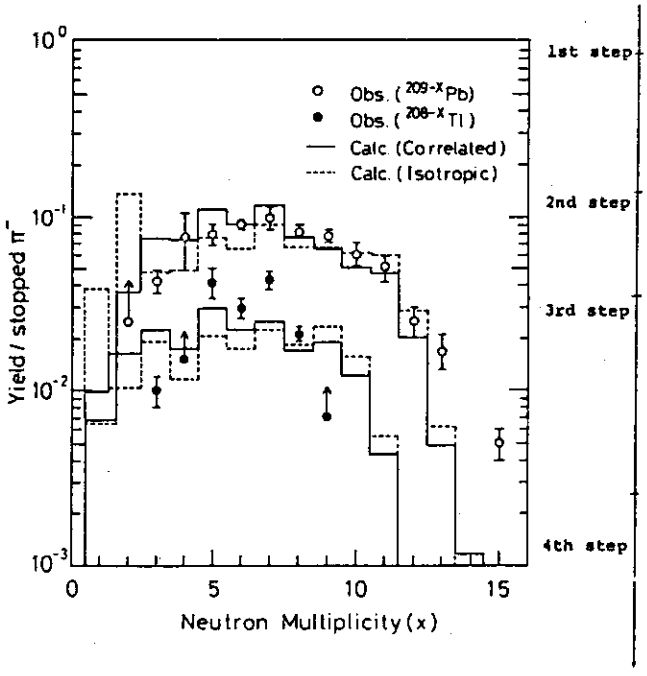

Fig. 1 Observed and calculated yield distributions of lead and thallium isotopes.

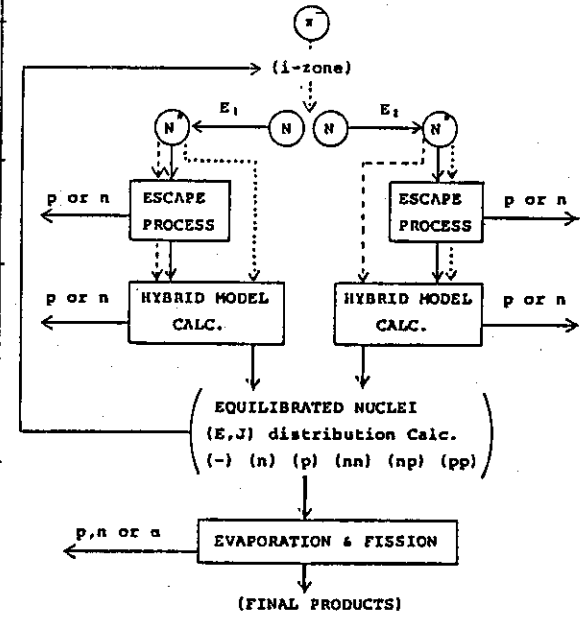

Fig. 2 Flow chart of the model calculation.

21. Muonic Three-Body Problem and Muon-Catalyzed Fusion

Yoshinori Akaishi

Department of Physics, Hokkaido University, Sapporo 060

Since 1977 the muonic three-body system $dt\mu$ has aroused considerable attention in relation to the realization of a useful muon-catalyzed fusion [1]. This bound system must be solved up to 7 digits in energy to establish the formation rate of the $dt\mu$ molecule. Our Japanese group applied a method named ATMS [2] and a coupled-channel method [3] to the Coulomb three-body system and obtained the detailed information on energy levels and wave functions of the bound states. We investigated the effect of nuclear interaction on the fusion rate in the bound states. Figure 1 shows up the main results obtained in our collaborations.

Last year Kamimura obtained very accurate values for the energy levels of $dt\mu$ by using the coupled-channel method [3]. Especially, the energy of the shallowest level is

$$-660.30 + 0.02 \text{ meV}.$$

This value may not explain the experimental formation rate [4,5]. Khin Swe Myint et al.[6] investigated relativistic effects and other corrections and obtained a total correction of about +29 meV. On the basis of these results the $dt\mu$ formation rate should be reinvestigated.

The fusion rate in $dt\mu$ is proportional to the probability that d and t comes closer to the range of the nuclear interaction passing through the Coulomb barrier. The d-t nuclear interaction has a near-threshold nuclear resonance, which strongly couples with the $dt\mu$ molecular states, and makes the probabity about 200 times larger than that of Coulomb interaction only. Figure 1 shows up the fusion rates obtained from our calculations [7] together with the interaction potential for the ground state and the energy levels of $dt\mu$. The fusion rate from the (J=0, v=1) excited state is much larger than the transition rates to the lower levels: The $dt\mu$ molecule produced in the shallowest (1,1) state deexcites to the (0,1) state and immediately fuses into $^4He + n + \mu$. This is the fusion mechanism of $dt\mu$.

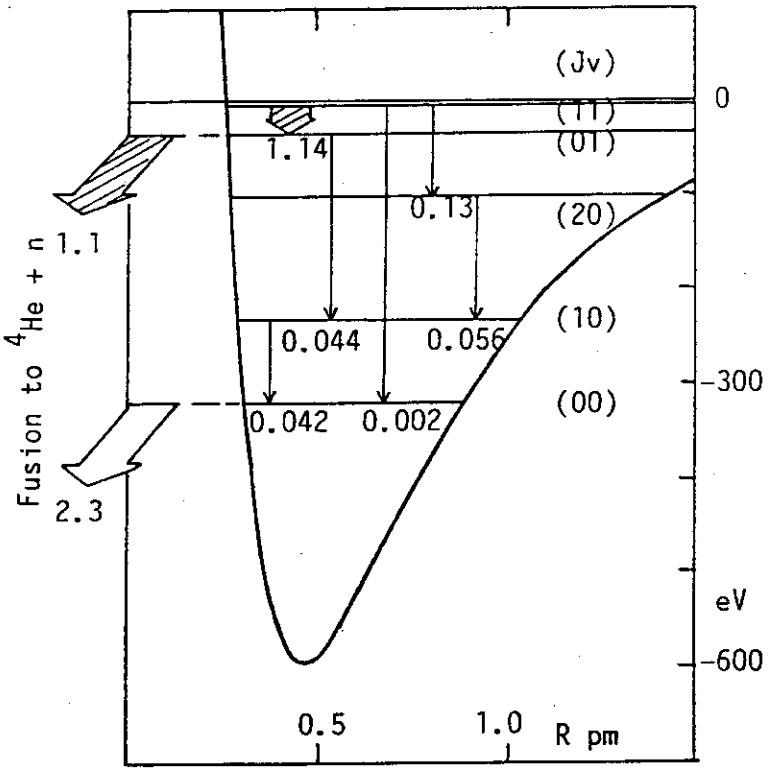

Figure 1
Fusion and electro-magnetic transition rates in the dtμ molecule. (unit in 10^{12} s^{-1})

Finally, we should note a "doubly resonant" feature that the dtμ molecular states of size ~pm resonantly couples with the D_2 molecular states of ~Å and with the d-t nuclear state of ~fm. This is a peculiar property of the dtμ molecule not seen in the case of pdμ or ddμ.

References

1. L.I. Ponomarev, Atomic Physics 10 (1987) 197.
2. Y. Akaishi, Int. Rev. Nucl. Phys. 4 (World Scientific, 1986) 260.
3. M. Kamimura, Talk at Int. Symposium on Muon-C.F. (Leningrad, 1987), and to be published.
4. S.E. Jones et al., Phys. Rev. Lett. 51 (1983) 1757.
5. M. Leon, Phys. Rev. Lett. 52 (1984) 1655.
6. Khin Swe Myint, Y. Akaishi, M. Kamimura and H. Narumi, preliminary cal.
7. M. Teshigawara, Y. Akaishi and H. Tanaka, to appear.

22. Statistics in nuclei

T. YUKAWA

National Laboratory for High Energy Physics (KEK)
Oho, Tsukuba, Ibaraki 305, Japan

ABSTRACT

Statistical methods in nuclear physics are discussed from a new point of view, namely as quantum chaos. There are essentially two directions of research focusing either on the static property or the dynamic property of an isolated quantum system. As for the static property statistics of energy level fluctuations is well-known because of the long history of research on neutron resonance of nuclei. An attempt for justifying the GOE(Gaussian orthogonal ensemble) model of the random Hamiltonian matrix theory is proposed[1]. For the dynamical property time evolution of periodically kicked one dimensional systems has been studied most popularly because their classical properties are known in detail. The localization phenomena found in the kicked rotator is shown to be non-generic for a stochastic system despite popular belief[2]. Possibility of finding quantum energy diffusion in the periodically kicked oscillator is explained[3].

REFERENCES

1. T. Yukawa, Phys. Rev. Lett. **54** (1985) 1883; Phys. Lett. **A116** (1986) 227.
2. T. Yukawa, KEK preprint KEK-TH 193(1988).
3. T. Yukawa, KEK preprint KEK-TH 200 (1988).

23. Ion of Unstable Nuclei in Superfluid Helium

N. Takahashi

College of General Education, Osaka University

It has long been known that a positive ion, when it is introduced in liquid helium, exerts electrostriction on helium atoms surrounding it and forms a charged aggregate, which is referred to as "snowball". Thus the ion acquires effective mass of 50 - 100 times the He mass. Such a snowball has been a versatile probe in studying the elementary excitation in superfluid helium.[1] Lack of proper methods for detection of snowballs other than the conventional measurement of ion current has been a main obstacle for further studies in this field.

In our experiments carried out at the Research Center for Nuclear Physics, Osaka University, we used short-lived beta-emitting nuclei as impurity ions and detected the snowballs by beta rays from them, thus increased the detection efficiency by many orders of magnitude.

Short-lived beta-ray emitters, ^{12}B, sustaining nuclear spin polarization were produced in the $^{232}Th(^{14}N, ^{12}B)$ reaction at 135 MeV and were introduced into superfluid helium. Many of boron ions were neutralized instantaneously, but some survived to form snowballs. The charged snowballs thus formed were transported in a static electric field and were separated from the neutralized ^{12}B. The nuclear polarization of ^{12}B was then observed via measurement of beta-ray asymmetry and was compared with the original polarization which was known through the earlier polarization experiments.[2] Fig. 1 shows the experimental setup and Fig.2 is an example of the beta-ray time specrtum. It was found that the nuclear polarization of ^{12}B after

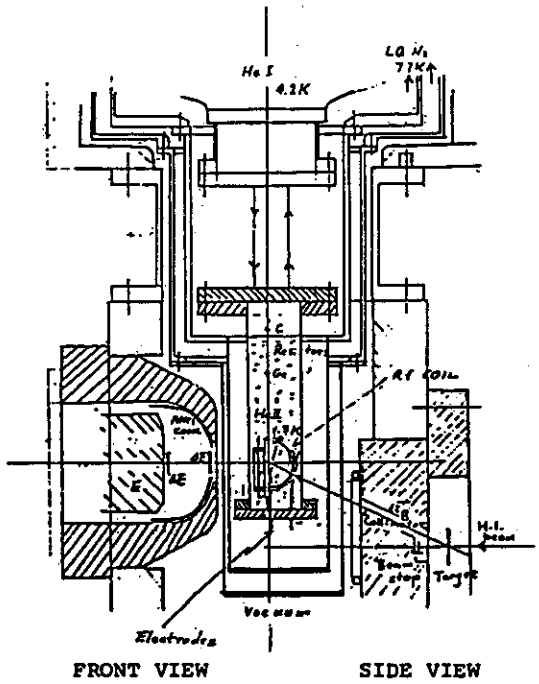

Fig. 1 Experimental setup

transportation in a form of snowball was 7±3 %. We conclude from this result that the nuclear polarization of core nuclei ^{12}B in its snowball was preserved throughout the lifetime (20.3 ms).

This suggests that the snowball produced around an alien ion, constitutes a suitable milieu for preserving (freezing out) the nuclear spin polarization of the core ion and that most likely the solidification takes place at the interior of the aggregate.

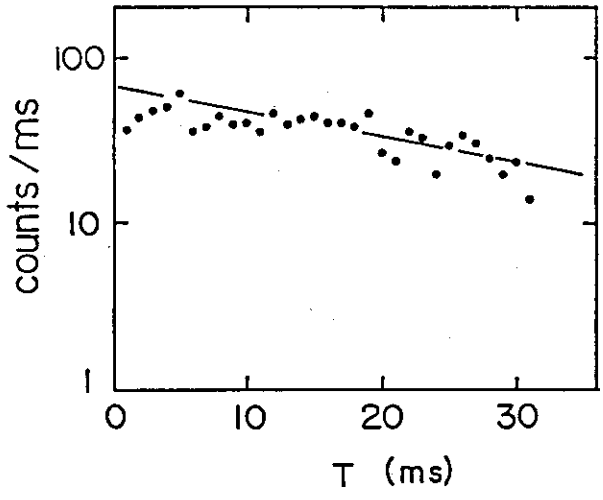

Fig. 2 Beta-ray time spectrum

This novel method of transporting spin-polarized short-lived nuclei and detection of snowballs by beta-rays will open a new way to study nuclear moments of various unstable nuclei by using the freezing-out of polarization. This method will open another new way for investigating, besides properties of nuclei far from stability, basic interactions in superfluid helium. Beams of beta-active nuclei are introduced into the superfluid helium as impurity ions and the snowballs formed around radioactive nuclei are detected by the beta-rays from the short-lived nuclei. One of the interests is the use of ^{6}He and ^{8}He and many other beta-active nuclei to study the transport phenomena related to impurity ions and thus basic interactions in liquid helium.

This work is supported by the Grants in Aid of Scientific Research and Toray Science and Technology Grants.

References

1) L.Meyer and F.Reif, Phys. Rev. 110 (1958) 279L and G.Careri, F.Scaramuzzi and J.O.Thomson, Nuovo Cimento 8 (1959) 1758.

2) N.Takahashi, Y.Miake, Y.Nojiri, T.Minamisono and K.Sugimoto, Proc. INS Intl. Symposium on Nuclear Direct Reaction Mechanism, Fukuoka, Japan, 25-28 October, 1978, INS, University of Tokyo, p. 635 (1979).

24. High Energy γ Rays from Spontaneous Fission of ^{252}Cf

H. Hama, J. Kasagi, H. Takeuchi
K. Yoshida and M. Sakurai

Department of Physics, Tokyo Institute of Technology

Gamma rays from the spontaneous fission of ^{252}Cf have been studied with energies below 20 MeV so far[1),2)]. These γ rays in this energy region have been considered to be associated with statistical γ decays of excited fission fragments, and a observation of a giant dipole resonance (GDR) of the excited states has already reported[2)].

The present work reports the result of measurements of the high energy γ rays up to $\sim$ 100 MeV from the fission of ^{252}Cf. The γ rays were measured by a well calibrated scintillation counter[3)] which is consisted with seven hexagonal BaF_2 crystals separated optically each other. TOF technique was emmployed to reduce the effect of high energy neutrons by using a NE213 scintillator as the starting counter set close to the fission source. A n-γ discrimination method was used to obtain the γ events with the NE213 counter. The time resolution for γ events was 1.4 ns and neutrons with energies up to 55 MeV were separated by 3.8 ns timming gate. The ^{252}Cf source was covered with a SUS capsule and the fission intensity was 3.8×10^4 s^{-1}. The coincidence rate was about 1K events/s in the case a distance between the source and the γ counter was 60 cm. The total measurement time with the source was $\sim$ 5 days, and the background was measured for $\sim$ 3 days.

The background subtructed γ spectrum is shown in Fig. 1. The spectrum apparently consists of two exponentially decreasing components. Fig. 2 shows the low energy part of the spectrum. A weak shoulder arround E_γ $\sim$ 15 MeV can be interpreted as arising from enhanced γ decays by GDR built on the excited states. We carried out statistical model calculations using CASCADE code[4)]

with following conditions ; the average excitation energy of the fission fragments was 20 MeV, only E1 transition was taken account to the statistical γ desays and the standard GDR parameters of ground state GDR were used. The calculations were performed for 12 fission fragments ($100 \leqq A \leqq 150$), and the calculated spectra for each fragment were summed up and folded with responce functions of BaF_2 counter.The solid line in Fig. 2 is the result of calculation. In order to give the best fit to the data, the calculated result is multiplied by 1.8. This value is involving some ambiguities of property of neutron-rich fragments, i.e. the particle separation energies (particularly for neutron) and the excitation energies of low lying state.

We considered the high energy continuum up to $\sim$ 100 MeV would be interpreted as emitting from internal Bremsstrahlung of fragments. The result of a classical Bremsstrahlung during accel-

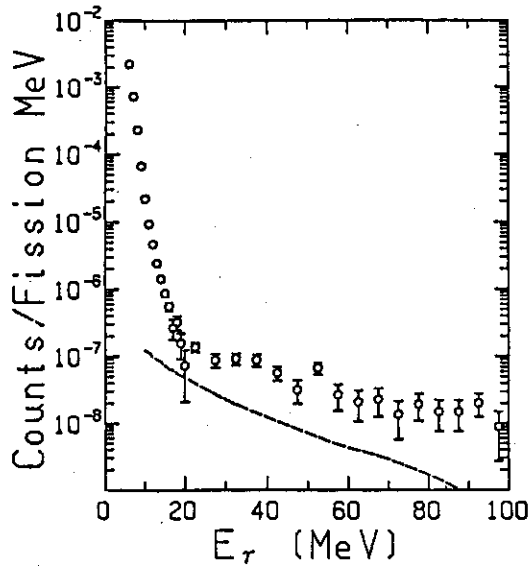

Fig. 1 γ Spectrum from ^{252}Cf
The dushed line shows the result of classical Bremsstrahlung calculation assuming fragments are acclerated by Coulomb potential.

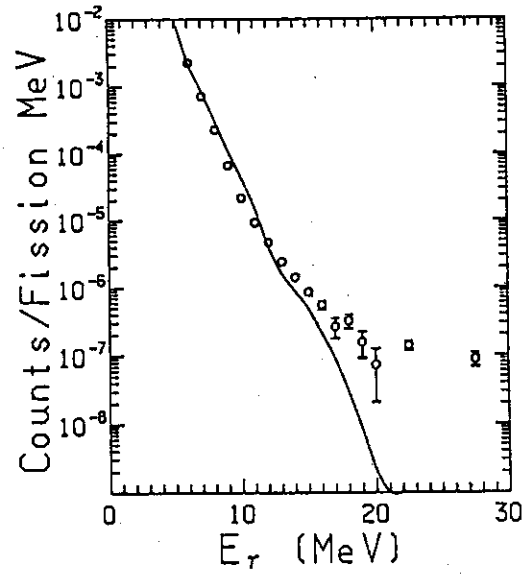

Fig. 2 Low Energy Part
The line shows the result of the statistical mode calculation using a code CASCADE.

eration of fragments in the Coulomb field with static initial condition is shown in Fig. 1 with a dashed line. The general trend of the observed spectrum is reproduced by the calculation except for the absolute yield. The presice measurements of γ rays from ^{252}Cf fission (coincidence measurement of γ rays and fragments, etc.) and quantum mechanical calculations are highly required.

References

1) J. W. Brooks et. al., Phys. Rev. C7 (1973) 1579.
2) F. S. Dietrich et. al., Phys. Rev. C10 (1974) 795.
3) will be published in elsewhere.
4) F. Puhlhofer, Nucl. Phys. A280 (1977) 267.

25. On the α-decays and exotic decays

Shigeto Okabe

Center for information Processing Education, Hokkaido University

Sapporo 060, Japan

What are problems in α-decays now? There are two different theoretical approaches from fission models and cluster models. In fission models one aims to describe a whole process from a compound state of a mother nucleus to its α-particle emission in a framework of collective motion. A lot of investigations have been made to determine dynamical variables, mass parameters and potentials of the collective model. In cluster models, on the other hand, one just deals with relative motion between an α-particle and a daughter nucleus. A hamiltonian for the relative motion which is generally defined by Feshbach's projection method is, however, impossible to be exactly evaluated. If we can get an approximate hamiltonian, then we can derive spectroscopic factors and amplitudes from experimental decay widths by solving a Schroedinger equation under the hamiltonian.

A large value of the spectroscopic factor of about unity means existence of an α-cluster state consisting of an α-particle and a nucleus. Indeed, we have typical α-cluster states in light nuclei such as ^{8}Be and ^{20}Ne. In heavy nuclei , on the other hand, no evidence for the cluster state has been observed up to now. The old experimental data which sometimes show abnormaly large values of the spectroscopic amplitudes in heavy nuclei were reduced in recent accurate measurements[1]. Even if values of the spectroscopic factor are not large, they are useful for selection of nuclear structure models. That is, one expects that qualitative behaviors of the spectroscopic quantities are understood by nuclear structure models. In other words, one assumes that the relative motion outside a nuclear surface is dominated by a weakly state-dependent potential. This is supported by the fact that the experimantal spectroscopic amplitudes obtained with simple optical potentials apparently display shell effects (Fig. 1).[2]

It was striking that Mang first had succeeded to explain ratios of the

spectroscopic amplitudes with simple shell model configurations about a quarter century ago.[3] After this work many nuclear structure models up to a recent IBM model calculation[4] have been applied for expalaining them in a variety of nuclei. A central difficuly in Mang's and similar calculations was quite large discrepancies in the absolute values. As far as spectroscopic factors are concerned, this problem was solved by treating exactly an antisymmetrizaion operator according to definition of a projection operator.[5] In the nuclear reaction theory antisymmetrization is usually treated in a procedure of projection after variation. The above result suggests that we need to reinvestigate a nuclear reaction theory concerning compound-nucleus reactions. Effects of antisymmetrization on the spectroscopic quantities seem to be a matter of normalization, so that the previous results about the relative ratios are expected to be not so largely changed. In order to discuss the absolute values we have to calculate the RGM norm kernel in heavy nuclei. By developements of calculational techniques we now can evaluate the absolute values near closed-shell nuclei[6].

There remain some problems: the spectroscopic factors calculated in a shell model with configuration mixings have no shell effects unfortunately. Further, absolute values of the spectroscopic amplitude are too small, because motion outside the nuclear surface is not well understood. There are two standpoints for solving the problems. One is to improve tail parts of compound nucleus wave functions by taking large configuration mixings into account.[7] The other is to introduce an α-cluster degree of freedom, that is, a hybrid model.[8] We follow the latter idea, because α-clustering is expected to play an important role outside the nuclear surface and the shell effects are considered to be connected to α-particle thresholds. We do not yet have the final conclusion about it. What we are interested in through analyses of α-decay is to see clustering correlations in a wide range of nuclei. For this purpose we also need to make investigations from the light nucleus side such as pf-shell nuclei[9].

Conerning ^{14}C-decay of Ra nuclei, it is not clear whether or not a similar analysis to that for α-decay is effective. Recently many pehnomenological analyses have been carried out from the viewpoint of fission.[10] We evaluated values of a ^{14}C spectroscopic factor in the

cluster model. The calculated values are quite small of about 10^{-6}. An operator of the spectroscopic factor, that is, a projection operator is, however, a 14-body operator, so that a reduced probability per nucleon is about 0.3, which is almost the same as that in α-decay. Further, we get an interesting result that values of the spectroscopic factors are sensitive to deformation of Ra and we can obtain reasonable values with a value of deformation determined phenomenologically. (Fig. 2)

References

1) K. Katori, private communication.
2) K. S. Toth et al., Phys. Rev. Letters 56(1986) 2360.
3) H. J. Mang, Phys. Rev. 119(1960) 1069.
4) H. J. Daley and B. R. Barrett, Nucl. Phys. A449(1986) 256.
5) T. Fliessbach and H. J. Mang, Nucl. Phys. A263(1975) 75.
6) S. Okabe, Nucl. Phys. A427(1984) 87.
7) I. Tonozuka and A. Arima, Nucl. Phys. A323(1979) 45.
8) T. Steinmeiyer, W. Sunkel and K. Wildermuth, Nucl. Phys. 125B(1983)437.
9) S. Ohkubo, private communication.
10) D. N. Poenaru et al. Z. Phys. A325(1986) 435.

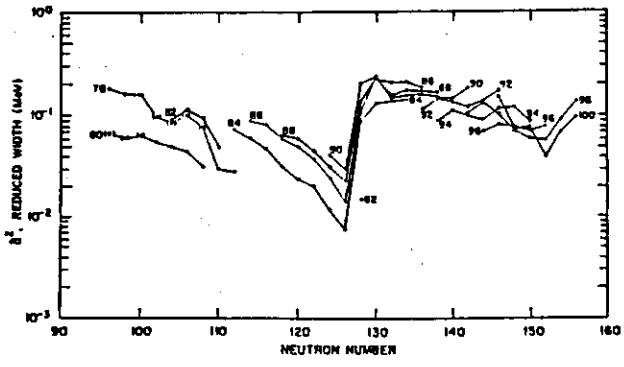

Fig. 1

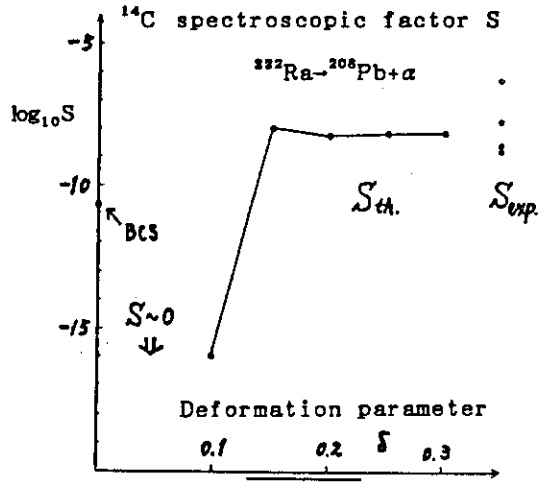

Fig. 2

26. Decay properties of odd mass einsteinium isotopes

Y. Hatsukawa, K. Sueki, T. Ohtsuki, H. Nakahara, I. Kohno*, N. Shinohara**, M. Magara**, S. Usuda**, Y. Kobayashi**, K. Gregorich***, D.C. Hoffman***. Department of Chemistry, Tokyo Metropolitan University. *Cyclotron Laboratory, RIKEN. **Department of Chemistry, JAERI. ***Nuclear Science Division, Lawrence Berkeley Laboratory.

For the studies of nuclear fission and superheavy elements, the nuclear decay properties of nuclei in heavy elements actinide have to be known well. However we have only limited information about actinide isotopes because of their short half-lives or difficulty in producing them. The present report describes the decay properties of odd mass einsteinium isotopes, mainly α decay properties of ^{245}Es. The einsteinium isotopes were produced by the ^{238}U(^{14}N,xn)$^{252-x}$Es, ^{237}Np(^{12}C,xn)$^{249-x}$Es and ^{249}Cf(p,xn)$^{250-x}$Es reactions. The reaction products recoiled out of the targets were stopped in a fast flowing He-jet system[1], and transferred to the low background counting system. The α spectrum were measured by Si(Au) surface barrier detectors. The isotopes obtained by bombardments were identified by the energies of emitted α particles, the half-lives and the excitation functions. The peak profile and energy calibration were determined by using α rays of ^{211m}Po, ^{213}Fr and ^{214}Ra produced by separate bombardments of ^{209}Bi target with ^{14}N or ^{12}C. The α spectrum had a resolution(FWHM) of 27 keV for 7.27 MeV α peak of ^{211m}Po. In the α particle spectrum obtained in the bombardment of ^{237}Np with ^{12}C, the peak at 7.73 MeV of ^{245}Es is seen to be complex. The result of an α analysis of the complex α particle groups at 7.73 MeV by ACSEMP[2] computer program is shown in Fig. 1. The result suggests that ^{245}Es emits four different α rays, 7.78, 7.73, 7.70 and 7.65 MeV. From analogy with ^{255,253}Es and ^{251,247}Bk, and from the energy level diagram of Nilsson[3], the ground states of ^{245}Es and its daughter ^{241}Bk are expected to be 7/2+[633] and 3/2-[521] orbitals, respectively. α Decay between these ground states would be hindered, while the favored decay should take place to the excited 7/2+[633] proton level of the daughter nucleus. Therefore, 7.78 MeV α ray which is substantially hindered and has the maximum transition energy, is considered to be an α transition from the 7/2+[633] level of ground state of ^{245}Es to 3/2-[521] level of that of its daughter

^{241}Bk. The favored α transition, 7.73 MeV α ray, then goes to the 0.05 MeV 7/2+[633] level of ^{241}Bk. The 0.08 MeV level(E_α = 7.70 MeV) and the 0.13 MeV level (E_α = 7.65 MeV) are assigned to the 9/2 and 11/2 member of the 7/2+[633] band, respectively. The tentative α decay scheme of ^{245}Es is shown in Fig. 2. We also found three α peaks, 7.316, 7.275 and 7.210 MeV, in the α spectrum of ^{247}Es in the bombardment of ^{249}Cf with proton beam. From their half-lives, it is concluded that ^{245}Es emits three α rays. More detailed analysis of the data of ^{247}Es is in progress.

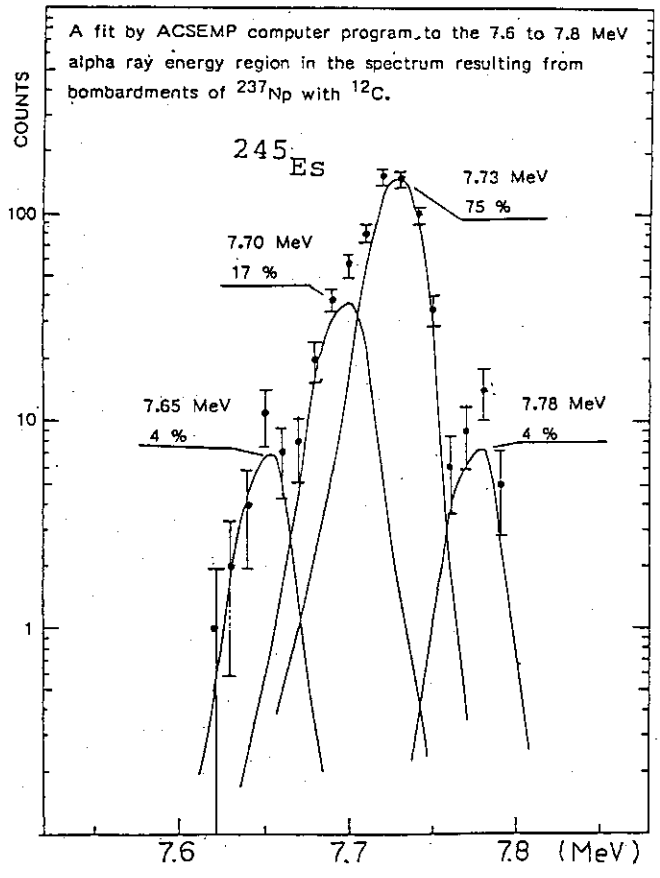

Fig. 1
α Spectrum of ^{245}Es.

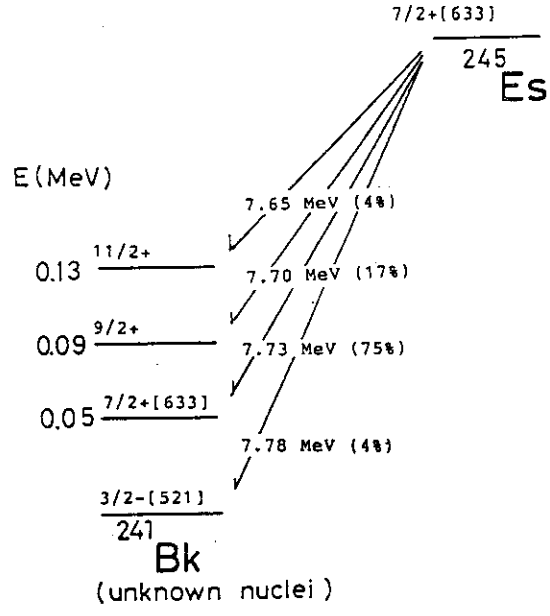

Fig. 2
Decay scheme of ^{245}Es.

References

1)H. Kudo, T. Nomura and J. Fujita: RIKEN Accel. Prog. Rep., 17,127 (1983)

2)M. Fujioka, M. Takashima, M. Kambe, O. Dragon and M. Rysavy: Z. Phys., A299, 287 (1981)

3)C.M.Lederer and V.S. Shirley: Table of Isotopes 7th ed.

27. Alpha-Decay of Mass Separated Isotopes with A=152 to 160

Hiroari Miyatake*, Kenji Katori**, Akio Higashi**, Takashi Oshima**, Atsushi Shinohara***, Nobuo Ikeda****, Syunpei Morinobu*****, Ichirou Katayama*****

*College of General Education, Osaka University, **Laboratory of Nuclear Studies, Osaka University, ***Department of Chemistry, Nagoya University, ****Institute for Nuclear Study, University of Tokyo, *****Research Center for Nuclear Physics, Osaka University

The spectroscopic study of alpha-decay gives us useful information on the nuclear structure. In paticular the reduced alpha-width would be one of the good probes to study the shape transition from spherical to deformed nuclei[1]. Therefore the accurate measurement of reduced alpha width is quite important. Although a large number of experimental data for alpha-decays have been accumulated[2] in the region of $N \geqq 86$, some of them have rather large experimental error to discuss the shape transition.

The recoil mass separator CARP[3] is best suited for this kind of measurement with its high mass resolution. In this report we like to describe a first successful application of the CARP to the measurement of alpha-decay branching ratios in the decay chains starting from $^{157\text{-}160}$Hf.

These nuclei were produced in the ^{144}Sm(^{20}Ne,xpyn) reactions at 120-150 MeV. A 2 mg/cm^2 thick ^{144}Sm foil, enriched to 88%, was bombarded by the pulsed Ne beam from the AVF cyclotron.

By using the CARP placed at 0 degree to the beam, the reaction products which emerged out of the target with recoil energies around 16 MeV and ionic charge states of $q=10^+ \sim 20^+$ were separated from the beam, then mass(A) analyzed and focussed on a 5 cm long position sensitive solid state

detector(PSD). The acceptance angles of the separator were set at 30 mr in the median plane and 40 mr in the transverse plane. The energy acceptance was estimated to be about 4%.

Fig. 1 is the position spectrum obtained by the PSD, showing the A/q distribution of the products. The mass resolution of 750 seen in the figure enabled us to definitely identify the mass number of the products.

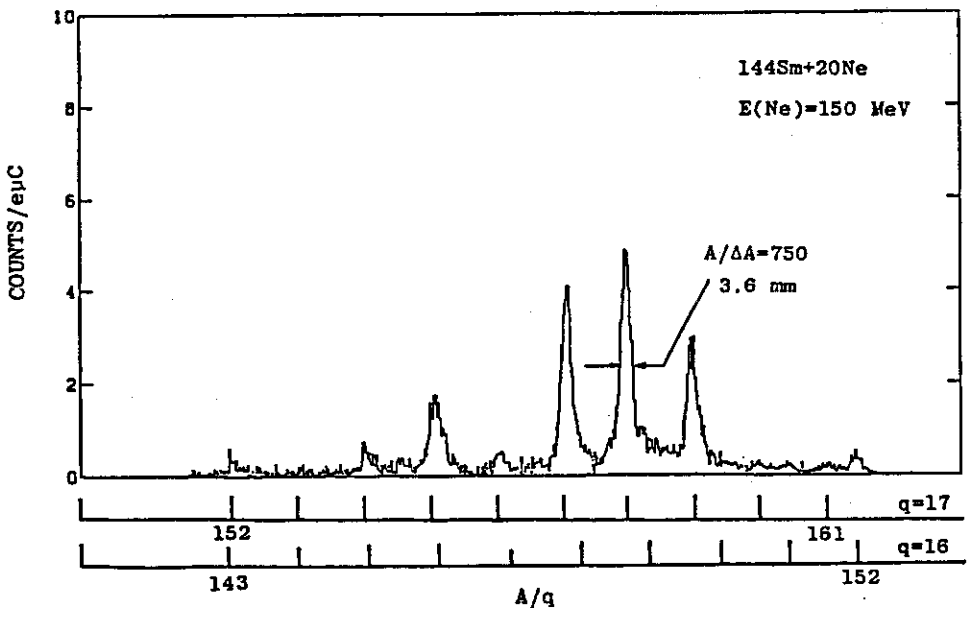

Fig. 1 The A/q spectrum of the recoil products emitted with ^{20}Ne induced reaction on ^{144}Sm at 150 MeV. The recoil energy of the products taken was 18 MeV.

Fig. 2 shows the energy spectrum of the alpha particles obtained for the A=159 group. For the reduction of the background, this measurement was restricted to the beam-off period. Seven alpha lines are observed clearly without any appreciable background counts.

Six alpha lines were uniquely assigned as the transitisions from the parent nuclei appearing in the alpha-decay chain of ^{159}Hf, which are also indicated in fig. 2. The 4.420 MeV line was attributed to the decay of ^{159}Lu.

These assignments together with the relative intensities of the alpha

rays enabled us to calculate the alpha-decay branching ratios for the daughters of ^{159}Hf and ^{159}Lu, as listed and compared with the previous data[2] in Table 1. The experimental data for A=157,158 and 160 groups were also tabulated. We observed 26 alpha transitions and obtained 13 branching ratios for these transitions.

We obtained the first experimental branching ratio for the decay of ^{155}Tm→^{151}Ho. The large ambiguities for the case of ^{151,151m}Ho originate from the lack of the knowledge of their relative production rates in the beta decay of ^{151}Er. For the case of ^{156}Yb→^{152}Er, our value was close to that reported by Mlekodaj et al[4](9±2%).

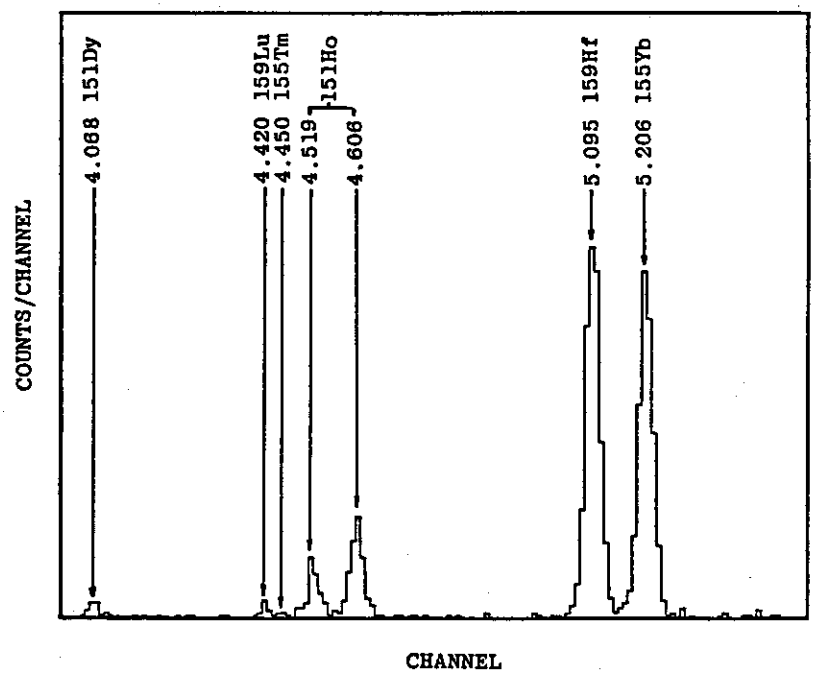

Fig. 2 The energy spectrum of the alpha particles measured in the off-beam period for the A=159 group. The separator was set to the recoil energy of 14 MeV and q= 15^+ for the products.

In the above descriptions, one may see that the mass separation of the reaction products leading to the unique identification of their mass greatly simplifies the observation of alpha decays and the interpretation of the data. A comparison of the experimantal reduced alpha widths and the

theoretical ones is in progress.

Table 1

Summary of alpha decay measurements

Parent	Daughter	E_α(MeV)	Branching Ratio(%) Present	Previous
^{156}Yb	^{152}Er	4.686(10)	5.9(14)	21(6)
^{155}Yb	^{151}Er	5.206(5)	89(6)	84(10)
^{154}Yb	^{150}Er	5.332(5)	95(3)	93(2)
^{155}Tm	^{151}Ho	4.450(10)	7.6(57)	
^{154}Tm	^{150}Ho	4.959(5)	56(30)	44(15)
^{153}Tm	^{149}Ho	5.109(5)	92(10)	93(7)
^{154}Er	^{150}Dy	4.166(3)	7.4(71)	<4
^{153}Er	^{149}Dy	4.674(10)	62(27)	47(3)
^{152}Er	^{148}Dy	4.802(5)	69(60)	93(4)
^{151}Ho	^{147}Tb	4.519(5)	>19	18(5)
^{151}Ho	^{147}Tb	4.606(5)	>31	13(4)
^{151}Dy	^{147}Gd	4.068(10)	6.7(17)	5.9(6)
^{150}Dy	^{146}Gd	4.232(5)	34.5(18)	38(5)

References

1) H. J. Daley and B. R. Barrett, Nucl. Phys. A449 (1986) 256.

2) P. D. Cottle and D. A. Bromley, Phys. Lett. A449 (1986) 129.

3) S. Morinobu, I. Katayama, and H. Nakabushi, CERN 81-09 (1981) 717.

4) R. L. Mlekodaj et al., Phys. Rev. C27 (1983) 1182.

28. Nuclear Moments Studies by Use of Beam-Foil Interactions

Y. Nojiri

Department of Physics, University of Osaka

Polarized nuclei, especially polarized radioactive ones, have been quite useful and important for various studies on nuclear physics. Typically, creation of nuclear polarization of unstable nuclei far from the stability has recently become crucial for the nuclear structure studies through determinations of their nuclear moments.

In our laboratory of Osaka University, polarized short-lived beta-radioactive nuclei have been effectively used to study mainly the following four regimes of physics studies, 1) the nuclear structure through nuclear moments[1,2], 2) the solid-state physics through hyperfine interactions of dilute impurities in crystals[2,3], 3) the weak-interaction of beta-decay[3], and 4) the nuclear reaction mechanism in polarization phenomena[4].

For the creation of nuclear spin polarization of the beta-emitters in this NMR studies, polarization phenomena in nuclear reactions were so far used. On the other hand since 1974 in the field of atomic physics, polarization phenomena of the beam-foil interactions has been investigated extensively[5]. As one of the results, tilted foils are found to be effective for creation of atomic polarization of ions ejecting out of the final foil surface. While passing in free space afterwards, the created atomic polarization is transferred to nuclei through hyperfine interactions, resulting in induction of a polarized nuclear beam.

After the discovery of the atomic polarization produced in the asymmetric collisions of the beam-tilted foil interactions in 1974[6], its applications to nuclear physics began with g-factor measurements of short-lived g radioactive isomeric states ($T_{1/2} < 150$ psec)[7]. In the experiments, polarization of atomic hyperfine fields was created through the beam-tilted foil interaction and used to deduce g-factor informations of these short isomers. The technique extended to the creation of polarization of relatively long-lived isomeric high-spin states ($T_{1/2} > 10$ nsec) to determine signs and magnitudes of quadrupole moments of the states[8]. In these experiments, a stuck of multi-tilted foils were effectively used for polarization creations of high-spin states. A direct confirmation of nuclear polarization, together with multi-foil enhancements of polarization, created by the beam-tilted foil interactions was also done in the measurement

of a ß emitter ^{12}B[9,10]. Unknown g-factor of ß emitter ^{33}Cl was recently determined by the tilted foil technique[10], which was combined with an recoil-mass separator. Nuclear polarization of heavy-ion beams which were directly extracted from accelerators was produced by passing through tilted foils and detected by the Coulomb excitation measurements of polarized nuclei[11].

It has been shown that the beam-foil interaction can be effectively used for estack studies on nuclear moments through creation of nuclear polarization. Especially this is quite useful for studies on radioactive nuclei because of its universal applicability and feasibility to use. Thus, it is expected that application of the beam-foil interaction to nuclear physics will surely open new fields, especially for the studies on nuclei far from the stability.

References

[1] K. Sugimoto, A. Mizobuchi, K. Nakai, and K. Matuda, Phys. Lett. 18 (1965) 38, J. Phys. Soc. Japan 21 (1966) 213. T. Minamisono, J. Phys. Soc. Japan 34 Suppl. (1973) 324.
[2] K. Nakai, Hyp. Int. 21 (1985) 1, and references therein.
[3] T. Minamisono, Hyp. Int. 21 (1985) 103, and references therein.
[4] K. Sugimoto et al., Phys. Rev. Lett. 39 (1977) 323.
[5] H.G. Berry and M. Hass, Ann. Rev. Nucl. Part. Sci. 32 (1982) 1, and references therein.
[6] H. G. Berry et al., Phys. Rev. Lett., 32 (197410 751.
[7] G. Goldring, Hyp. Int., 9 (1981) 115, and references therein.
[8] E. Dafni et al., Phys. Rev. Lett., 50 (1983) 1652.
[9] Y. Nojiri et al., Phys. Rev. Lett., 51 (1983) 180. W. Feber et al., Nucl. Inst. Meth. B16(1986) 439.
[10] W.F. Rogers et el., Phys. Lett., 177B (1986) 293.
[11] K. Sugimoto et al., Ann. Rep. INS, Univ. Tokyo, (1983).

29. Resonating-Group-Method Study of the α+^{40}Ca Elastic Scattering and the ^{44}Ti Structure

Takahiro WADA and *Hisashi HORIUCHI

Research Institute for Fundamental Physics, Kyoto University and
*Department of Physics, Kyoto University

In our previous study[1] we have shown that the calculation by the α+^{16}O resonating group method (RGM) with the introduction of a phenomenological imaginary potential reproduces very well not only the spectroscopic data of the bound and quasi-bound states of ^{20}Ne but also the α+^{16}O elastic scattering cross section in a wide energy range. Furthermore we have shown that the equivalent local potential to the RGM nonlocal potential is very similar to the optical potential of Michel et al.[2]

In order to advance further the RGM study of the inter-nucleus potential, we intend in this paper to make a similar RGM analysis of the α+^{40}Ca elastic scattering. In making the RGM study, there is an important difference between α+^{40}Ca and α+^{16}O systems. The difference is due to the fact that in the present structure-study of ^{44}Ti it is not so much clarified which level have large component of the α+^{40}Ca structure. Therefore unlike the α+^{16}O case it is not easy to use the spectroscopic data of the ^{44}Ti low-lying states in selecting the effective two-nucleon force. We proceed in the case of the α+^{40}Ca system as follows. Contrary to the α+^{16}O case, we first try to fit well the α+^{40}Ca elastic scattering cross section in a wide energy range by the RGM with some suitably chosen effective two-nucleon force, and then by using the same two-nucleon force we calculate the bound and quasi-bound states of ^{44}Ti.

In the following, we calculate the α+^{40}Ca elastic scattering angular distribution by the RGM by using four kind of the effective two-nucleon force, the HNY force with Δ=50 MeV, the Volkov No.1 force with m=0.623, that with m=0.658, and the Brink-Boeker force B1. As seen in Fig.1, use of former two kinds of nuclear force correspond to the standpoint that the ground rotational band of the ^{44}Ti should be reproduced approximately as the lowest rotational band by the α+^{40}Ca RGM, while the use of the latter two correspond to the standpoint that the observed 0^+ state which is to be described by the lowest 0^+ state by the α+^{40}Ca RGM is not the ground state but some excited 0^+ state with large α-strength.

The comparison of the angular distributions between the RGM calculations and the data is shown in FIg.2 for E_{Lab}=29.0, 39.6, 49.5, and 61.0 MeV, and for the adopted four kinds of effective nuclear force. A phenomenological imaginary potential is introduced into the RGM as follows:

$$[\hat{H} + \sqrt{\hat{N}} i W(r) \sqrt{\hat{N}} - E\hat{N}]\chi = 0$$

where E is the scattering energy in the center-of-mass frame. In view of the excellent reproduction of the experimental scattering cross section by the optical potential of Delbar et al.[3], the local imaginary potential $W(r)$ have been taken to be the same as that of Ref.3. We can see that the data fitting in (a) and (b) of Fig.2 is fairly good while that in (c) and (d) in Fig.2 is bad. The large disagreement of the dip positions between theory and experiment in the intermediate angle region of (c) and (d) of Fig.2 has not been able to diminished by changing the parameter values of the imaginary potential $W(r)$.

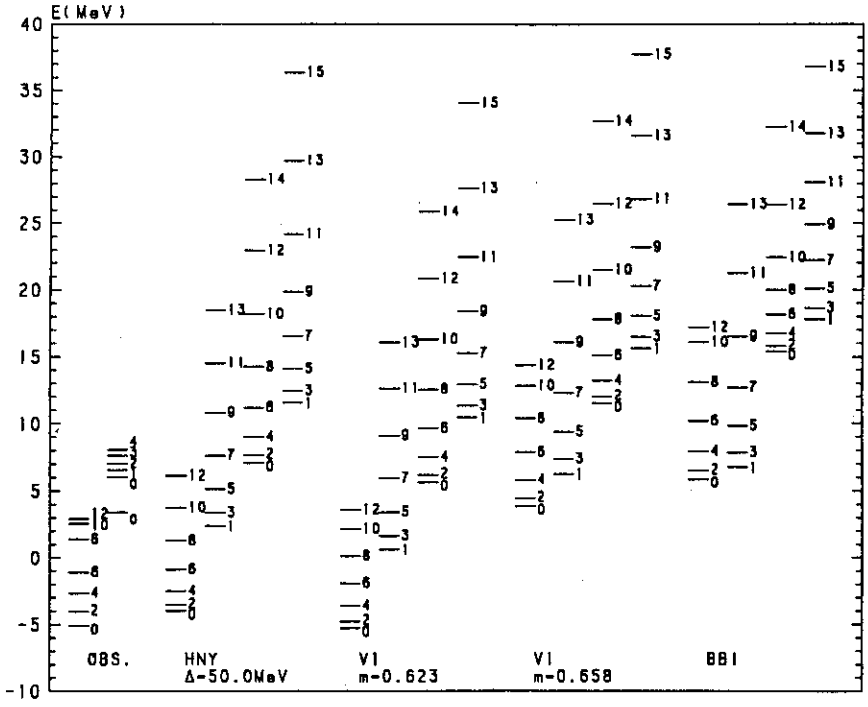

Figure 1 Experimantal and RGM level spectra of ^{44}Ti. In the experimental spectra, only the ground rotational band states and excited states with large α-strength are shown. Energies are measured from α+^{40}Ca threshold energy.

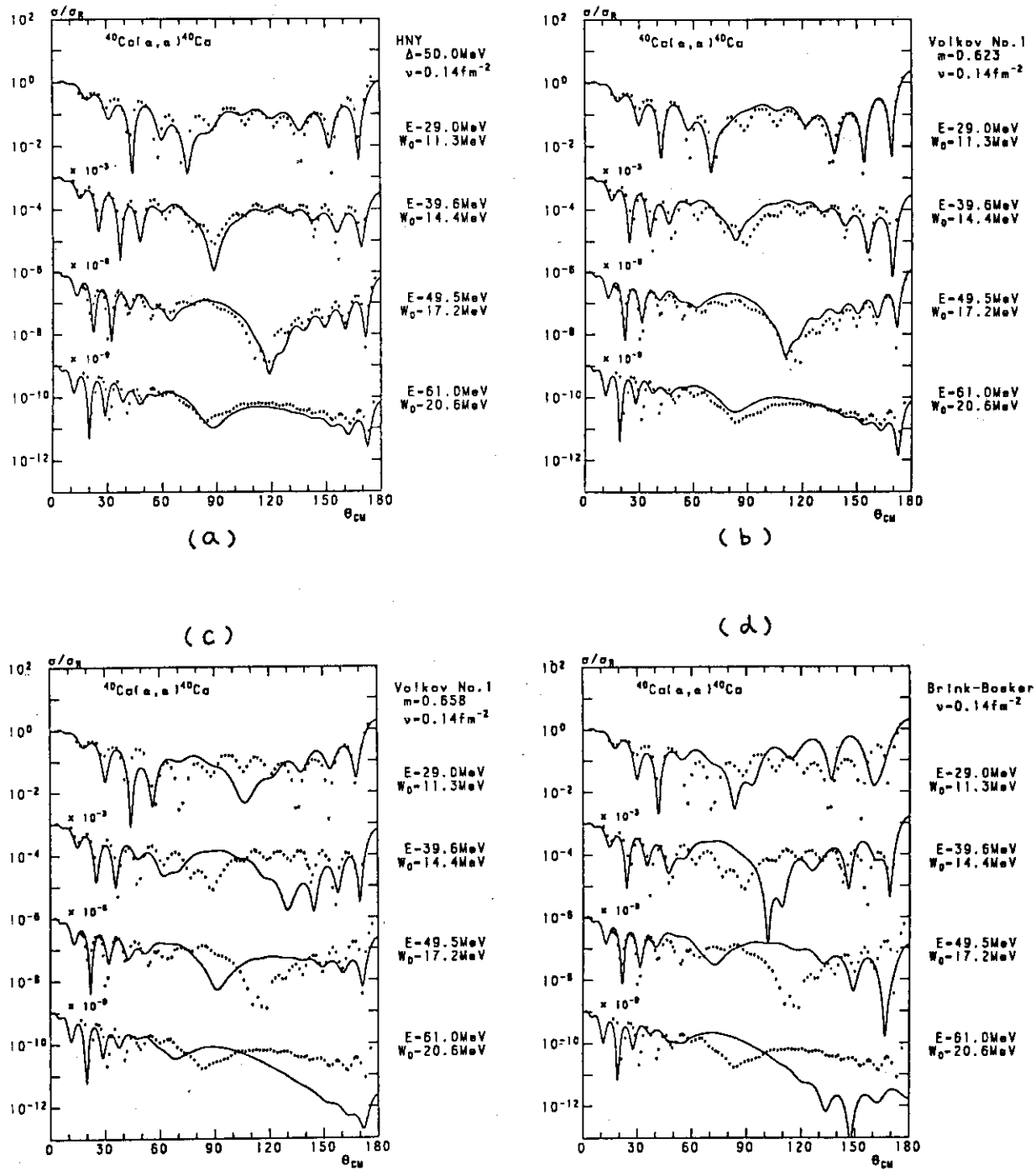

Figure 2 Comparison of the experimental data (dots) for α+^{40}Ca elastic scattering with the calculations (solid curves) by the α+^{40}Ca RGM with four kinds of effective two-nucleon force; the HNY force with Δ=50 MeV(a), the Volkov No.1 force with m=0.623(b), that with m=0.658(c), and Brink-Boeker force B1(d).

The good data fitting in (a) and (b) of Fig.2 leads to the following two conclusions: First, in addition to the α+^{16}O system[1], also in the α+^{40}Ca system the RGM with

fixed effective two-nucleon force has proved to give a good fit to the scattering data in a wide energy range. Furtermore, the angular-momentum-averaged equivalent local potential constructed from the RGM nonlocal potential is found to be very close to the optical potential of Delbar et al. This fortifies our opinion that the RGM is powerful and qualitatively reliable for the microscopic study of the inter-nucleus interaction including the microscopic foundation of the internucleus optical potential. Secondly, when combined with the result that the data fitting in (c) and (d) of Fig.2 is bad, we are forced to support the standpoint that the lowest rotational band by the α+^{40}Ca RGM should be regarded to give us an approximate description of the ground rotational band of ^{44}Ti. The latter conclusion is consistent with that of the recent study of the α+ ^{40}Ca fusion cross section by the optical potential model of Ref.4.

The most serious objection to this conclusion is the fact that the RGM calculation which locates its lowest 0^+ level near the ^{44}Ti ground state cannot avoid the appearance of the negative parity rotational band with its band head 1^- state below the excitation energy 10 MeV although there have been no such experimental indications at all. Our present RGM study predicts the location of the band head 1^- state in the approximate energy region from 0 to 5 MeV above the α+^{40}Ca threshold which therefore should be actively searched for experimentally.

References

1. T. Wada and H. Horiuchi, Phys. Rev. Lett. **58**, 2190 (1987).
2. F. Michel et al., Phys. Rev. **C28**, 1904 (1983).
3. Th. Delbar et al., Phys. Rev. **C18**, 1237 (1978).
4. F. Michel, G. Reidemeister and S. Ohkubo, Phys. Rev. **C34**, 1248 (1986).

30. Polarization in $^{13}C+^{12}C$ Elastic Scattering

O. Satoh, S. Oh-ami and T. yamaya

Department of Physics, Tohoku University

Several experiments have been performed in order to get information on the spin-dependent interactions between composite nuclei ($A \geq 6$). According to these experimental results, the spin-orbit potentials as a spin-dependent term of the optical model potential are much stronger than those obtained from theoretical calculations, that is, folding model calculations. However, there has been no experimental information investigated by direct measurements of the polarization observables in heavy ion scattering except for polarized $^{6,7}Li$ scattering.

In the present work, the polarizations of ^{13}C elastically scattered from ^{12}C were measured at bombarding energies of 52, 56, 60 MeV using a double scattering method. For measurements of the polarization observables in heavy ion scattering, polarized beams are most useful, but the use of polarized ion sources for heavy ions ($A>7$) is not practical in the experiments still today. Under such a circumstance, a double scattering method is commonly thought for polarization measurements.

The experiments were carried out by use of the Tohoku University Model-680 Cyclotron with $^{13}C^{4+}$ beam. The self-supported natural carbon foils of 1.2 mg/cm^2 for the primary target and 2.0 mg/cm^2 for the secondary target were used. Doubly scattered ions were detected with left and right counter systems. The first scattering angle of $\theta_{lab}=8^\circ$ and the second scattering angles of $\theta_{lab}=8.0^\circ$, 9.6°, 11.3° were determined to an accuracy of an order of 0.01°. Detail description of the experimental apparatus and procedure will be given in other publications. The elastic polarizations deduced from the measured left-right asymmetries in $^{13}C+^{12}C$ double scattering are plotted in Fig. 1 together with theoretical curves.

The phenomenological optical model and the microscopic double folding model analyses have been performed for the measured cross section and the polarizations in $^{13}C+^{12}C$ elastic scattering. The results of these calculations are indicated by the solid and dashed curves, respectively, in Fig. 1. In this case, the Thomas-shape spin-orbit potential was used as a

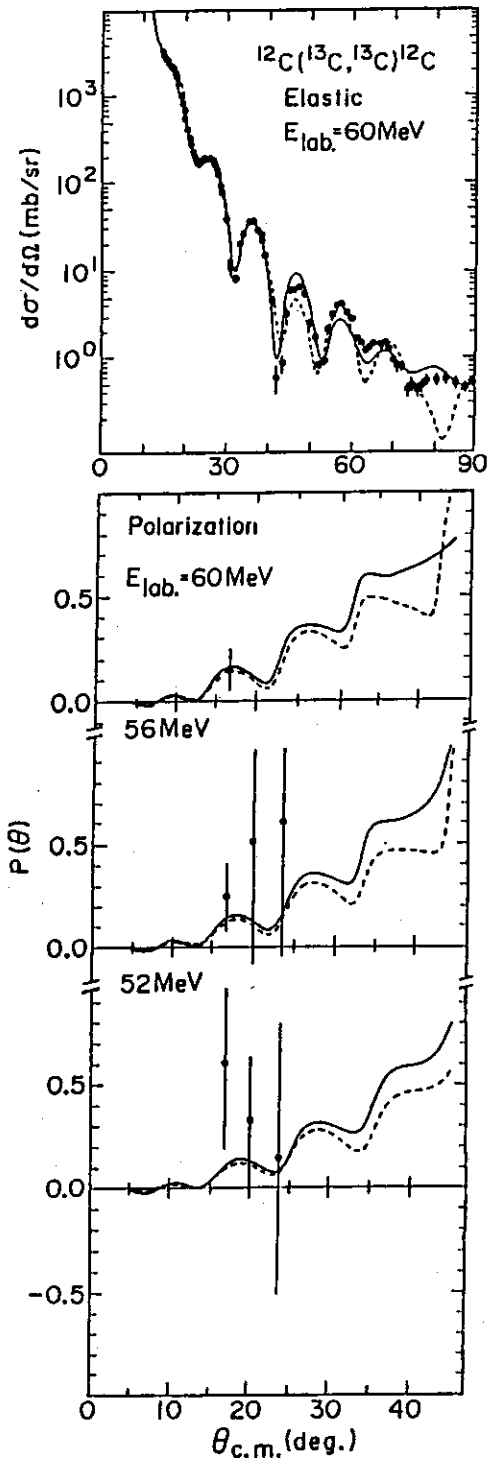

Fig. 1

"effective spin-orbit potential". As shown in Fig. 1, the calculated curves are well reproduced the data, and the potential depth of V_{SO}~0.2 MeV for the spin-orbit term was deduced from the data. This value is mach larger than the theoretical value of V_{SO}~0.03 MeV which deduced from the folding model[1].

In order to investigate an origin of the polarization of ^{13}C at small angles, the measured polarization at 60 MeV was compared with the results of the coupled-channel calculations including inelastic transition channels[2]. The calculations were performed by taking account of the $3/2^-$(3.69 MeV) and $5/2^-$(7.54 MeV) states of ^{13}C and the 2^+(4.44 MeV) state of ^{12}C. The solid-dashed and the dashed curves in Fig. 2(a) indicate the results of the three-channel(only projectile excitation channels) and the four-channel(projectile and target excitation channels) calculations, respectively. In addition to the projectile and the target excitation channels, two mutual excitation channels of $^{13}C^*(3/2^-$ and $5/2^-)+^{12}C^*(2^+)$ were also included in the calculation whose result is indicated by the solid curve. As shown by the theoretical curves, the effect of the inelastic transition channels coupling with the elastic channel is very small in the polarization at small angles, thus it was suggested that the polarization of ^{13}C dose not originate from these inelastic transition channels.

One-nucleon transfer channel is considered as another origin of the polarization in $^{13}C+^{12}C$ elastic scattering[3]. Two-step process calculations were performed using the finite-range DWBA code. The one-neutron transfer processes to the single-particle states of $^{13}C^*(1/2^+$ 3.086 MeV and $5/2^+$ 3.854 MeV) were considered in the calculations as the intermediate states. The calculated two-step amplitudes were summed coherently with the elastic amplitude. The results are shown in Fig. 2(b). The solid-dashed and the dashed curves indicate the two-step process through the neutron transfer channel to the $1d_{5/2}$ and $2s_{1/2}$ states, respectively. The solid curve indicates the results of the coherent sum of these amplitudes. It was found that the polarization of ^{13}C at small angles originates from the one-neutron transfer channels.

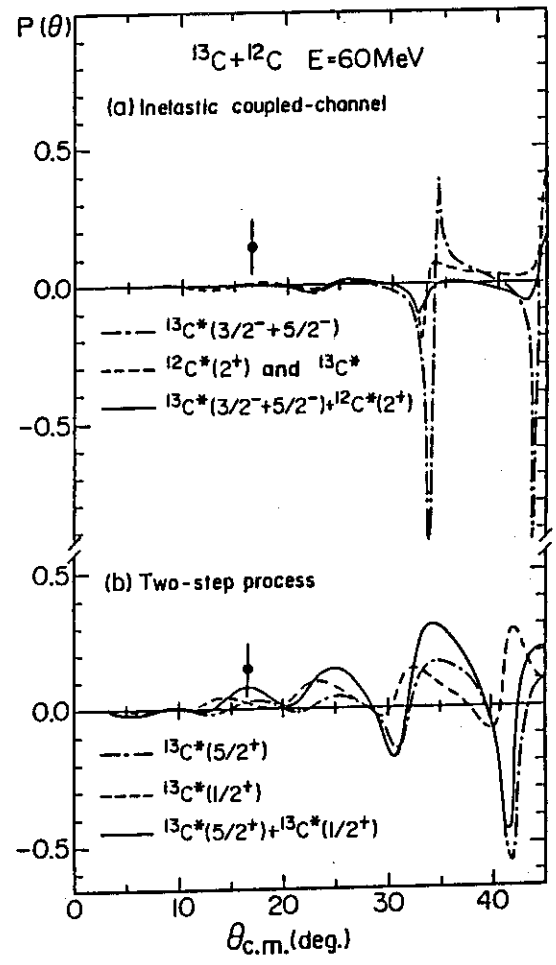

Fig. 2

References

1) H. Amakawa and K.-I. Kubo, Nucl. Phys. A266, (1976) 521.

2) Y. Sakuragi, private communication.

3) B. Imanishi and W. von Oertzen, Phys. Lett. 118B, (1982) 273.

31. Effect of Spin-dependent Force in Heavy-ions Elastic Scattering on ^{28}Si

T. Yamaya and O. Satoh

Department of Physics, Tohoku University, Sendai

In the surface of region where a short-range attraction force begin to at inside nuclear radius, the cross sections in the elastic scattering are expected to be so sensitive that perceive a somewhat of a weak surface-type potential adding to the strong central potential. As a surface-type potential, a spin-orbit force arising from the valence nucleon(s) of the nucleus is commonly thought. The spin-orbit potential for the heavy ion scattering is much weaker in proportion to $1/A^2$ than that for light ions scattering,[1] where A_p is a projectile mass. However, the experimental evidence has been accumulating that a spin dependent effect is much stronger for the transfer reaction.

Elastic and inelastic scattering of ^{12}C, ^{13}C, ^{14}N and ^{16}O projectiles on ^{28}Si have been studied at corresponding bombarding energies to the scattering in region of the vicinity of the strong absorption radius. Optical model and microscopic double-folding model analyses have been performed in order to define the nature of the optical potential depending on the projectile nuclei. For the analyses with the phenomenological optical model potential, the shallow potential such a central real potential depth V_R= 10 MeV not adequate to reproduce both the elastic and the inelastic scattering data because of the unrealstic effective interaction deduced from the shallow potential for the elastic scattering. A distinction with a difference between the central potentials of the spinless projectiles ^{12}C and ^{16}O and the projectiles with spin ^{13}C and ^{14}N was found in the elastic scattering analyses. For the inelastic scattering data, the results of the DWBA calculations using the optical potential obtained from the elastic data well reproduce the data of the spinless projectiles ^{12}C and ^{14}N but not

reproduce the data for ^{13}C and ^{14}N projectiles. A spin-orbit term of the Thomas-shape as an "effective spin-orbit potential" was introduced to the optical model calculation of ^{13}C and ^{14}N elastic scattering. It is a consequence of the introduction of the spin-dependent potential that the central potential of all four 1p-shell projectiles are nearly equal for the elastic scattering data and the calculated DWBA angular distributions reproduced the measured inelastic cross sections for ^{13}C and ^{14}N projectiles.

Usual strongly absorbing heavy-ion optical potentials which yield good fit to low energy data have a central imaginary well depth 1/2 - 1/4 of a real depth. In the present analyses, the ratios of the W_o/V_o and the $W_{1/2}/V_{1/2}$ are plotted in Fig. 1, where $V_{1/2}(W_{1/2})$ indicate the depth of the real (imaginary) potential at the strong absorption radus $R_{1/2}$. Both ratios of W/V at R=0 and $R_{1/2}$ were almost 1/2 for ^{12}C and ^{16}O but are unusual values for ^{13}C and ^{14}N in the six- adjustable parameter analyses(except for the spin-orbit term). As the result of the analysis with the nine-adjustable parameter(including the spin-orbit term), both ratios W/V of about 1/2 at the radius R=0 and $R_{1/2}$ are obtained for all four projectiles. That is, the ratios of W/V= 1/2 keep a good balance in the nearly equal central potential for all four 1p-shell projectiles.

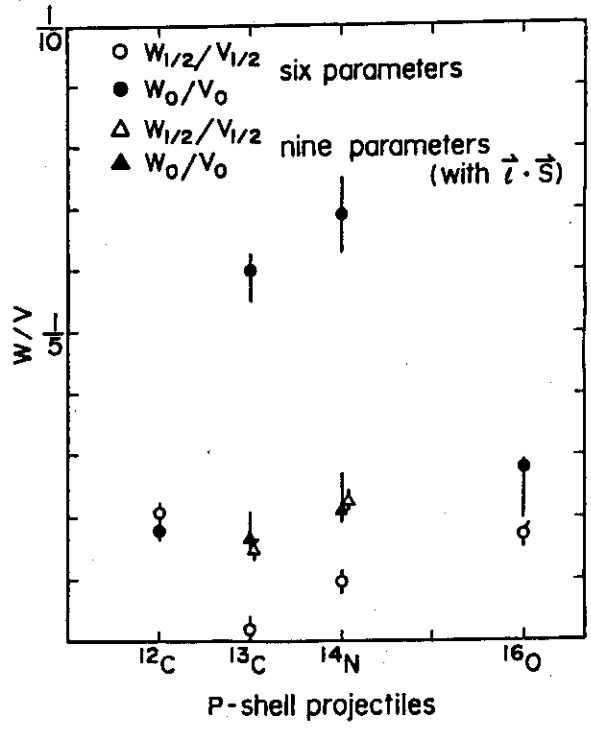

Fig. 1

A necessary of the spin-dependent force in the scattering system ^{13}C and ^{14}N + ^{28}Si was also suggested by the analyses using microscopic

double-folding calculations[2], as same as the analyses using the phenomenological optical model. This results is shown in Table I. It is expected to observe directly polarization of heavy-ions in the elastic scattering.

TABLE IV Optical potential parameters in the double-folding calculations.[a]

Ions	N_R	W_I (MeV)	r_I (fm)	a_I (fm)	V_{so} (MeV)	r_{so} (fm)	a_{so} (fm)	χ^2/N
^{12}C	0.74	43.90	1.12	0.55				8.6
^{13}C	1.0	17.25	1.26	0.73				6.9
(with l.s)	0.74	66.28	0.97	0.87	-0.78	1.40	0.32	4.9
^{14}N	0.97	12.06	1.28	0.65				9.7
(with l.s)	0.87	63.62	0.93	0.83	0.32	1.30	0.52	11.2
^{16}O	0.80	59.31	1.15	0.49				8.8

a. Charge radius is r_c=1.0 fm.

References

1) H. Amakawa and K.-I.Kubo. Nucl. Phys. A266, (1976) 521

2) Y. Sakuragi, M. Yahiro, and M. Kamimura, Prog. Theor. Phys. Supplement No.89 (1986); Y. Sakuragi, private communication.

32. THREE-BODY COUPLED CHANNEL ANALYSIS OF $^{19}F+^{12}C$ AND $^{19}F+^{16}O$ ELASTIC AND INELASTIC SCATTERING

H.Fujita, N.Kato*), T.Sugimitsu*) and Y.Sugiyama**)

Daiichi College of Pharmaceutical Sciences, Fukuoka,
*) Department of Physics, Kyushu University, Fukuoka, and
**) Department of Physics, Japan Atomic Energy Research Institute, Ibaraki

In the $^{19}F+^{12}C$[1,2] and $^{19}F+^{16}O$[3] systems, it is known that the angular distributions of the inelastic scattering to the lowest $5/2^+$ and $3/2^+$ states in ^{19}F at E_{lab} = 30-60 MeV for $^{19}F+^{12}C$ and E_{lab} = 60 and 80 MeV for $^{19}F+^{16}O$ can not be reproduced by the DWBA and coupled channel (CC) analyses with the usual macroscopic rotational model. Recent studies[2,3] show that the CC calculations including the spin-orbit (SO) force of V_{so} = -0.3 and -0.6 MeV for $^{19}F+^{12}C$ and $^{19}F+^{16}O$, respectively, reproduce well the above angular distributions. However, the origin of the residual SO interaction deduced by the CC analyses is not clear. The residual SO interaction may be caused by other coupling effects neglected in the CC analyses in refs.2 and 3.

In the last decade, a marked progress in understanding of the SO interaction between heavy ions has been achieved experimentally and theoretically by the elastic and inelastic scattering of the polarized $^{6,7}Li$ beams. Recent CC calculations[4] with cluster folding interaction reproduce almost all features of the experimental data and make clear the important roles of dynamic effects in the heavy ion polarization phenomena. Ohkubo and Kamimura[5] applied also similar CC method to the elastic scattering of ^{19}F from ^{28}Si, considering the states of ^{19}F as the cluster states of t + ^{16}O configuration.

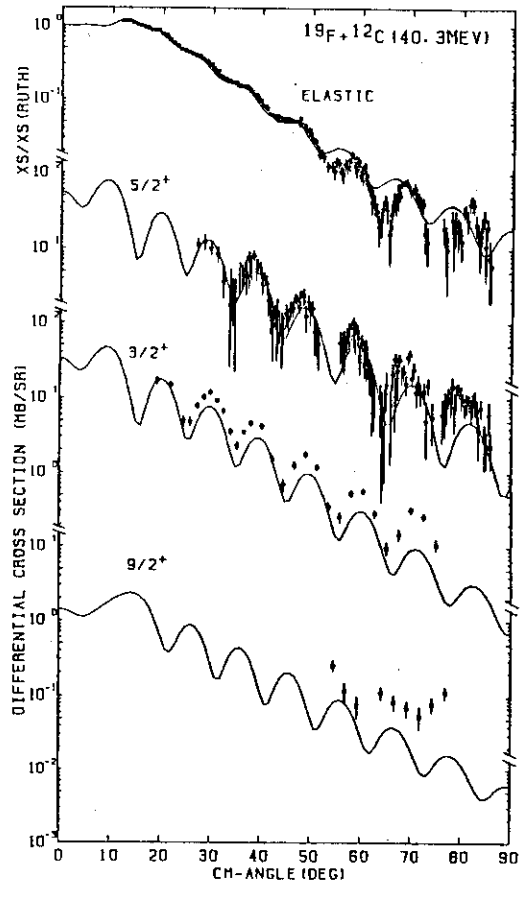

Fig. 1

In this note, we present the preliminary

results of the three-body CC calculations including the excitation of the t + ^{16}O cluster states of ^{19}F. The angular distributions of the differential cross sections for the elastic and inelastic scattering to the 1/2$^+$(g.s.), 5/2$^+$(0.197MeV), 3/2$^+$(1.554MeV) and 9/2$^+$(2.780MeV) states in ^{19}F were calculated with the CC method using a cluster folding model. Wave functions of the ground and excited states of ^{19}F were constructed with the t + ^{16}O cluster model given by Buck and Pilt[6]. Diagonal and non-diagonal ^{19}F + ^{12}C (^{16}O) potentials were calculated by folding the existing t + ^{12}C (^{16}O) and ^{16}O + ^{12}C (^{16}O) optical potentials into the wave functions obtained above. With no adjustable parameter, the 4-channel (1/2$^+$ - 5/2$^+$ - 3/2$^+$ - 9/2$^+$) CC calculations were performed. All calculations were carried out using the codes made by M.Kamimura et al.[7]. Figs.1 and 2 show the results for ^{19}F + ^{12}C at E_{lab} = 40.3 MeV and for ^{19}F+^{16}O at E_{lab} = 59.9 and 80.0 MeV, respectively. The characteristic features of the experimental data for both systems at all energies are reproduced well by the calculations except the elastic scattering of ^{19}F+^{16}O. Especially, the phase relation of the inelastic scattering to the 5/2$^+$ and 3/2$^+$ states is reproduced very well.

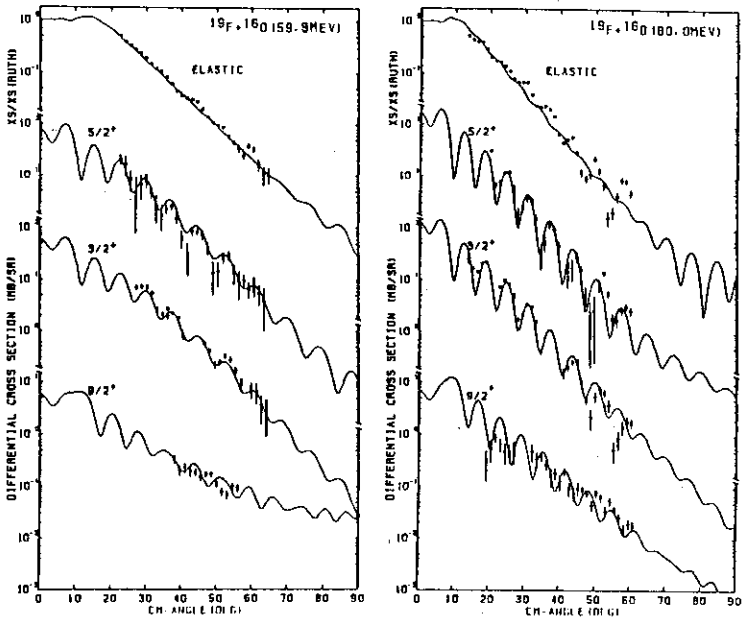

Fig. 2

Next we examined what is the main origin of the success of the CC calculations mentioned above. We first examined the CC effect. Four types of the CC calculations with the 1-channel (1/2$^+$), 2-channel (1/2$^+$ - 5/2$^+$), 2-channel (1/2$^+$ - 3/2$^+$), 3-channel (1/2$^+$ - 5/2$^+$ - 3/2$^+$) and 4-channel (1/2$^+$ - 5/2$^+$ - 3/2$^+$ - 9/2$^+$) couplings were performed. Slight shift of the phase of the angular distributions from the 4-channel coupling for the elastic scattering is observed for only the 1-channel and 2-channel(1/2$^+$ -

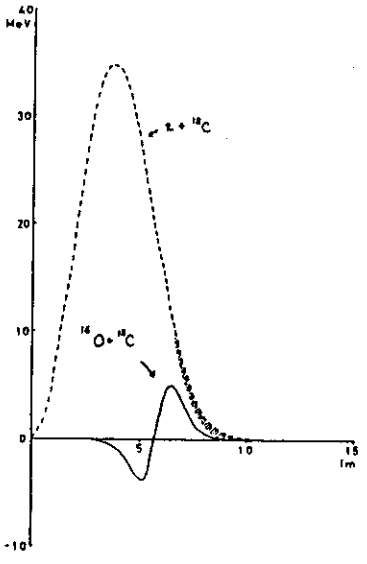

Fig. 3

3/2⁺) couplings, while for the inelastic scattering the shift of the phase is not observed at all, though small change of the yield is observed. In the next step, the effects of the reorientation and folding SO potential were examined. The latter two effects did not affect the phase of the angular distributions almost at all. Thus it is concluded that the effects of the channel coupling, reorientation and folding SO potential are small.

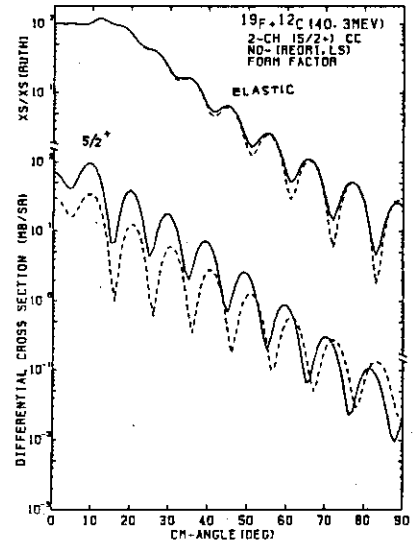

Fig. 4

From that mentioned above we can speculate that the present phase anomaly may come from the shape of the interactions. The present CC calculation uses the different diagonal potential for each state, while the usual DWBA and CC calculations use the same diagonal potential. This effect may contribute to the phase anomaly. However, the diagonal parts of the interactions calculated are very similar each other and this effect is very small. Next the non-diagonal parts of the interactions may be the origin. Then we performed the CC calculations for $^{19}F+^{12}C$ at E_{lab} = 40.3 MeV with the 1/2⁺ - 5/2⁺ coupling but with the reorientation and folding SO interactions switched-off, varying artificially the shape of the transition form factor between the 1/2⁺ and 5/2⁺ states. The form factor between the 1/2⁺ and 5/2⁺ states seems to have a long tail, which arises from the t - ^{12}C part, as shown in Fig.3. The CC calculation was performed with the form factor in which the hatched region of the tail in Fig.3 was removed. The result is shown by the dashed line in Fig.4. The solid line shows the result with the normal form factor. Backward shift of the phase is observed. This suggests that the shape of the transition form factor, which has a long tail, can be a resonable candidate for the origin of the present phase anomaly.

References

1) T.Tachikawa et al., Phys.Lett. 139B (1984) 267.
2) T.Tachikawa et al., Nucl.Phys. in press.
3) H.Fujita et al., to be published.
4) H.Nishioka et al., Nucl.Phys. A415 (1984) 230; H.Ohnishi et al., Nucl.Phys. A415 (1984) 271.
5) S.Ohkubo and M.Kamimura, Phys.Lett. 150B (1985) 25.
6) B.Buck and A.A.Pilt, Nucl.Phys. A280 (1977) 133.
7) M.Kamimura, private communication.

33. Statistical Theory of Precompound Reactions: The Multistep Direct Process

H.Nishioka*, H.A.Weidenmueller** and S.Yoshida***

*Niels Bohr Institute, Copenhagen, Denmark ,** Max-Planck-Institut fuer Kernphysik, Heidelberg, West Germany and *** Faculty of Engineering, Yamagata University, Yonezawa

The precompound process is divided in two parts, the multistep direct (MDS) process and multistep compound (MSC) process. The latter was investigated in the previous paper using novel technique in the statistical theory in the previous paper. The direct interaction effect is removed by the unitary transformation U. To study the former process is the aim of the present paper.

The MSD process is described by the energy averaged effective Hamiltonian in the P-space, and the S-matrix for this process is obtained by solving coupled channel equations with optical potentials. In the MSD process one particle always stays in contiuum. For low energy incident particles the main process is MSC process, but as the energy increases the MSD process becomes important. However if the incident energy is below a couple of hundred Mev, it loses the energy after one or two collisions and drops in a quasi-bound state and it proceeds in MSC process. So it is enough to consider one or two steps in perturbation expansion.

For MSD process the residual nucleus is in highly excited states, whose level spacing is so small that it is impossible to treat individual levels. The cross section is averaged over residual nuclear states, and it contains the level density, which is identical to the one appeared in MSC cross section. If we estimate the collision time of the incident nucleon with nucleons in the nucleus by empirical data of single particle widths, it is shorter than the collision time for nucleons in the nucleus among themselves. So the sudden aproximation is utilized in calculating the two step process. This is in cotrast with Tamura et al who assumed the adiabatic approximation. It is not yet known how the results are differnt in the two approximations, but we expect they may not be so different.

34. Level Density for Fixed Exciton Number in Pre-equilibrium Nuclear Reaction

Kenichi Sato* and Siro Yoshida**

* Division of Physics, Tohoku College of Pharmacy

** Faculty of Engineering, Yamagata University

For pre-equilibrium reactions the level densities with fixed exciton numbers are necessary, and the well-known Ericson-Williams type has been widely used due to its simplicity. Recently Jacquemin and Kataria[1] estimated, in the independent particle model, exactly the level densities with recursive method using realistic single particle energies. In spite of the progress within the independent particle model, there are only a few works on realistic level density which explicitly take into account the residual interaction.

Nishioka et al.[2] suggested the possibility of strong coupling between classes specified with the exciton number, which would imply the modification of the level densities for fixed exciton numbers having so far been used[2,3]. As for the total level density, which is given by the sum of such level densities, Jacquemin and Kataria anticipated the difficulty to fit the experimental level density at the thermal neutron resonances unless the residual interaction is taken into account.

In the present work we study level densities classified with the exciton number m in which the residual interaction is explicitly taken into account. It is done on the basis of NVWY theory[2] which introduced the Gaussian Distributed Ensemble (GDE). The GDE assumes many GOEs, which are specified with the exciton number m and have different centers h_m and different variances M_{mm} , being coupled one another by the off-diagonal GOE random interaction. Then it is characterized by its second moments M_{mn}.

First the nuclear second moments

$$M_{mn} = (N_m N_n)^{-1} \sum_{\mu,\nu} |\langle m\mu | V^R | n\nu \rangle|^2 \qquad (1)$$

are calculated on the basis of the same simple model as Ref.3 using realistic single particle states but adopting the more general type of residual interactions, taking ^{40}Ca and ^{208}Pb as examples. In Eq.1 N_m is the number of states which belong to the class of exciton number m and V^R is the residual interaction. The result indicates that such nuclei are near in the strong interclass coupling situation proposed by Nishioka et al.[2] as an possibility. Then the level density for fixed exciton number ρ_m are obtained first by solving the saddle point equations[3] in the strong interclass

coupling limit given by

$$\frac{\tau_m}{\lambda_m^2} = (E-h_m-\tau_m)^{-1} + \sum_{n(\neq m)} \frac{\lambda_{mn}^2}{\lambda_m^2} \sqrt{\frac{N_n}{N_m}} (E-h_n-\tau_n)^{-1} \qquad (2)$$

using the second moments as the input, and secondly by taking the imaginary part of the propagator as

$$\rho_m = -\frac{N_m}{\pi} \ell_m (E-h_m-\tau_m)^{-1} \qquad (3)$$

Partial level densities ρ_m (m=2,4,6,...) are calculated for ^{208}Pb. In Fig.1 the total level density $\rho(E)$, which is the sum of partial level densities $\sum_m \rho_m(E)$, is shown by a solid curve, and is compared with the sum of semi-circle level densities which is shifted to coincide with the solid curve at the threshold energy.

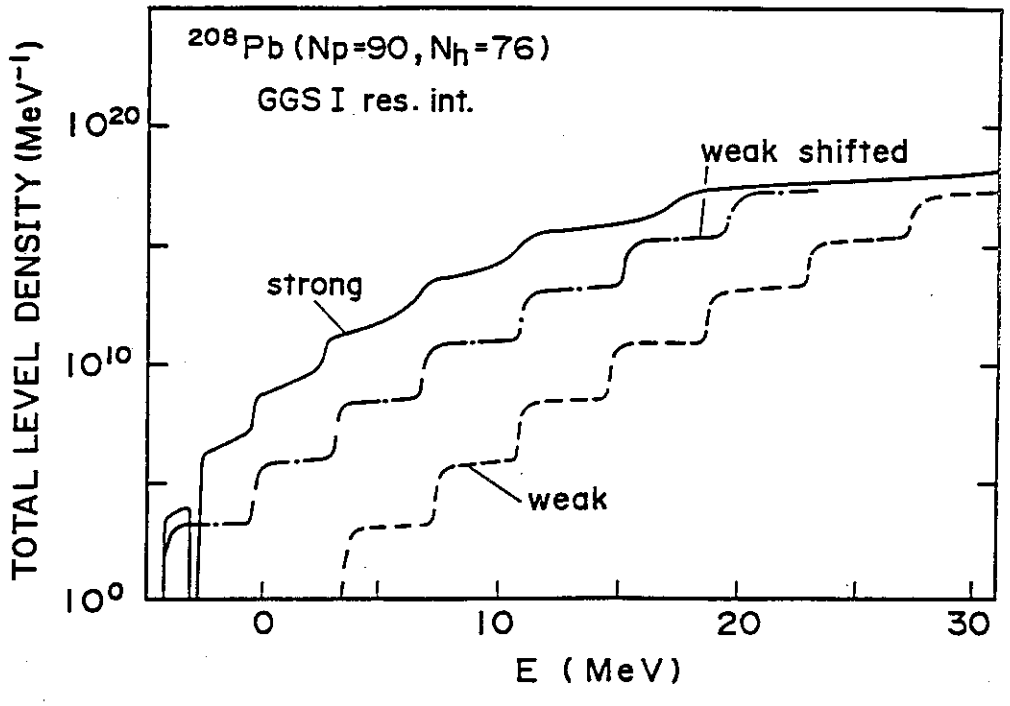

Fig.1 Level Density for ^{208}Pb, which is the sum of level densities for fixed exciton number.

Main results of our investigation for level densities with fixed exciton number are "the enhancement in the low energy region" -- which improve greatly the agreement with the experimental total level density at the thermal neutron resonances, "general trend in their shape change according to the strength of the coupling", "Wigner-like repulsion between semi-circle level densities" and "the occurrence of multimodal distribution" -- which French et al.[4] have already found in another simple system.

Our results for level densities should be regarded as giving qualitative information concerning how the residual interaction changes its behavior, because the present investigation has the unsatisfactory features inherent in the pure GDE such as the unperturbed semi-circle partial level densities for all m -- actually unperturbed partial level density would be similar to the Gaussian form for large m if the two-body nature of the residual interactions is explicitly simulated. It seems to be expected, however, that those results would be common features of level densities when the residual interaction is taken into account.

References

1) C. Jacquemin and S.K. Kataria: Zeit. Phys.,324A, 261 (1986)

2) H. Nishioka, J.J.M. Vervaarschot, H.A. Weidenmuller and S. Yoshida: Ann. Phys.,172, 67 (1986)

3) K. Sato and S. Yoshida: Zeit. Phys.,327A, 421 (1987)

4) J.B. French and V.K.B. Kota: Phys. Rev. Lett.,51, 2183 (1983)

35. Production of Super Heavy Elements by Neutron Rich Beams

N. Takigawa, T. Shinozuka and M. Abe
Department of Physics and Cyclotron Radioisotope Center
Tohoku University, 980 Sendai, Japan

The production of Super Heavy Elements(SHE) in Laboratory is one of the most intriguing subjects of nuclear physics[1,2]. It was stimulated by the theoretical prediction of new magic numbers, Z=114, N=184 etc., in late 1960es. So far, one has succeeded in producing up to Z=109 elements, though the cross section became already very small. It is of the order of ten pico barn for the production of Z=109 element.

In this talk, we discuss the advantages of using neutron rich beams in producing SHE[3]. Before doing so, let us recall that there are two decisive factors in producing SHE. The formation cross section of the SHE has, of course, to be large. In addition, the created SHE has to live long enough as a compound system, say, for a period of the order of milli-seconds. Higher bombarding energy clearly makes the fusion cross section larger. It lowers, however, the survival probability, because the higher bombarding energy makes the decay by fission much more dominant. An optimum condition must, therefore, be sought.

The experiments toward SHE production can be roughly classified into two groups, i.e. the cold fusion and the hot fusion. In the former, one uses relatively symmetric projectile and target. The idea is thus to lower the reaction Q-value and makes the survival probability higher. A serious problem in this approach is the existence of the so called extra-push energy.

One of the comments which we should like to make in this talk is that the extra push energy can be lowered by using neutron rich beams. This is very desirable, because the decay by fission can consequently be reduced. The magnitude and the origin of the extra push energy are not yet fully understood. We, therefore, here base our discussion on a phenomenological systematics clarified in ref. [4]. In Fig. 1, the extra push energy (Exx) for various systems is plotted as a function of an effective fissility parameter (Xm) [taken from Ref. 4, except for K+Am systems]. The dashed line was obtained by the chi-square fit to the "data" points. This was then used to estimate the extra push energy for

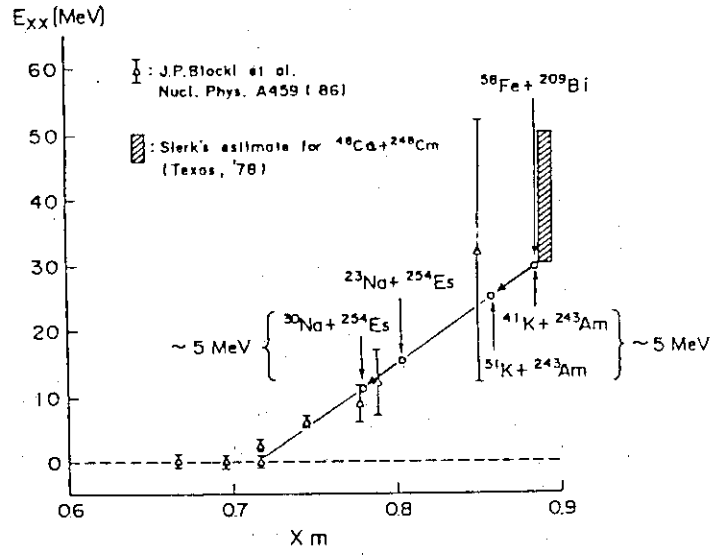

Fig. 1

the K+Am system for two isotopes of K. We see that the extra push energy is lowered by about 5 MeV by using very neutron rich K isotope (51K) as the incident beam compared with the usual 41K beam.

Fig. 2 shows the excitation function of the fusion cross section calculated by the one dimensional potential model. The arrows show the position of the Coulomb barrier for each case. The figure implies that the reduction of the extra push by the amount of 5 MeV, which has been discussed in the previous paragraph, introduces the gain of the fusion cross section of the order of 3 at sub-barrier energies. In this sense, the neutron rich beams have a great advantage.

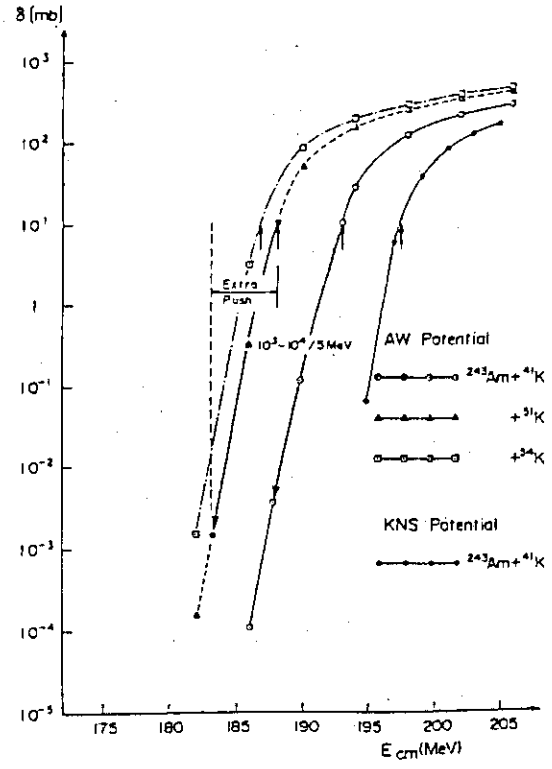

Fig. 2

Another advantage of neutron rich beams is that the survival probability is expected to increase with increasing neutron excess. Fig. 3, which is taken from Ref. 5, supports this expectation. The figure shows how the cross section for 4 neutron decay channel increases with increasing neutron number of the residual nuclei, which are Th isotopes. The figure implies that the survival probability of the compound nucleus becomes larger by about 5 order for the experiments with 10 excess neutrons.

In this talk, we argued that neutron rich beams have advantages of reducing the extra push energy and also of increasing the survival probability of the compound nucleus. There remain, however, many problems to be clarified. The trustworthy estimate of the fission barrier is very important. The dependence of the fission barrier on the excitation energy should be clarified, especially because SHE are shell-stabilized

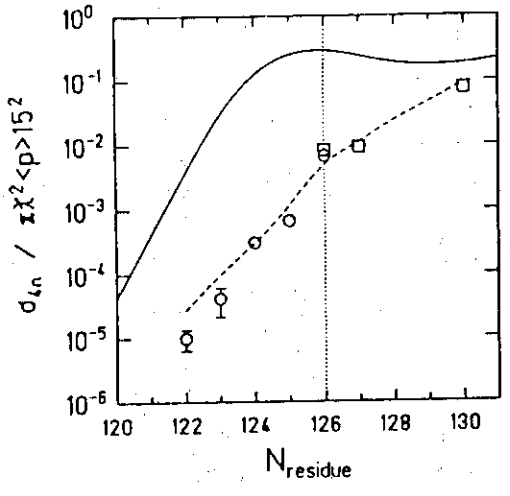

Fig. 3

systems. This is essential in choosing either the hot or the cold fusion. The potential model used in obtaining Fig. 2 should be modified by taking into account reaction dynamics, such as the role of nuclear surface vibrations, which are known to play very important role in enhancing the sub-barrier fusion cross section for medium mass heavy ion collisions. The persistence of the neutron halo, suggested in 11Li, in heavy neutron rich nuclei and its role in fusion would be very interesting. Also, it is not obvious whether the AW (Akyuz-Winther) and the KNS (Krappe-Nix-Sierk) potentials, which have been successful for conventional beams, are still valid in describing the scattering of neutron rich beams. Another important thing is that the technique has to be much developed to supply intense neutron rich beams.

References

[1] P. Armbruster, Ann. Rev. Nucl. Part. Sci. 35(1985) 135.
[2] F.P. Hessberger et al., Proc. of 5th Int. Conf. Nuclei far from Stability, Rosseau, Canada(1987) p.786
[3] T. Shinozuka, N. Takigawa and M. Abe, JHP-7 (1988)117; Proc. of the Symposium "Physics in Japan Hadron Project", INS, Dec. 2-4 ,Tokyo (Japanese mimeograph)
[4] J.P. Blocki et al., Nucl. Phys. A459(1986)145.
[5] C.C. Sham et al., Nucl. Phys. A441(1985)316.

36. Subthreshold Pion Production in Heavy Ion collisions

Toshitaka Kajino, Ken-ichi Kubo and Hiroshi Toki
Department of Physics, Tokyo Metropolitan University

In the free space nucleon-nucleon collisions the threshold energy of pion production (n+n-->n+n+π) is T_{lab} ~ 280MeV. On the other hand, in heavy ion nuclear collisions pions can be procuced below the free space pion production threshold (T_{lab}/A < 280MeV). Hence, such a process is called subthreshold pion production. If we estimate the threshold energy in the quasi free mechanism by taking into account the Fermi motion and the Pauli principle, it comes out $T_{lab}/A \gtrsim$ 30-40MeV. Comparing the model calculations within the quasi-free mechanism and the experimental data, we find the model calculations underestimate the pion production cross sections σ_π by far below T_{lab}/A ~ 50MeV. Questions are then

1. What is the mechanism to push up σ_π?
2. Where is the absolute threshold?

The absolute threshold is given by the pionic fusion, where all nucleons participate coherently for pion production. The threshold energy is simply written as T_{lab} ~ 280MeV (T_{lab}/A ~ 280MeV/A). Therefore, if A = 20, it is T_{lab}/A ~ 14MeV, which is much lower than the quasi-free estimate.

We believe that for T_{lab}/A > 50MeV the quasi-free process dominates in σ_π and for T_{lab}/A ~ 280MeV/A the pionic fusion is important, while for the energy region in between, more complicated processes take place for pion production. As a strategy, we started to study the pionic fusion process for understanding subthreshold pion production in heavy ion collisions.

We published a paper entitled 'Pionic fusion in heavy ion collisions and the clustering correlation' in Phys.Rev.C35(1987) 1370-1381. The A=7 systems (^{7}Li and ^{7}Be) are described very well within the resonationg group method (RGM). In addition to calculating the spectroscopic values (μ, Q, B(E2)..), the application are made also for Astrophysics (Star and Big Bang). The clustering correlations (^{3}He, t, α) in the A=7 systems are found extremely important for explaining various quantities.

Hence, we expect the same importance also for pionic fusion.

The pionic fusion cross section is written as

$$d\sigma/d\Omega \sim \Sigma |\langle \phi_\pi \psi_7 | O_\pi | A(\phi_4 \phi_3 \chi) \rangle|^2$$

The A=7 systems (scattering and bound states) are obtained by solving the RGM equations. With the use of only the p-wave pion production interaction for O_π, we find the results very close to the experimental data for $^4He(^3He,\pi^+)^7Li$ at E_{lab}/A =88.8MeV. The clustering correlations make the cross sections by a factor 30 larger. Estimates are made also for heavy nuclei such as $^{12}C + ^3He \dashrightarrow ^{15}N + \pi^+$. See the details for this process in the published paper.

In clonclusion, we find the clustering correlations extremely improtant to enhance the pion production cross section in order to cause the required coherence of many nucleons for pion production. In this respect, the pionic fusion process should reveal the clustering states in heavy nuclei in the pionic fusion cross section. As a further study, we want to include the s-wave π-N interaction. In addition, we want to apply our method for the continuum spectra in the pionic fusion cross section and for the incident energy dependence.

37. Shell Model Calculation of Light Neutron-rich Nuclei

T.Hoshino, H.Sagawa and A.Arima

Department of Physics, University of Tokyo,
Hongo 7-3-1, Tokyo 113, Japan

Experimental data of properties of neutron-rich nuclei, e.g. masses, rms radii and electromagnetic moments, become available recently. Data, which were obtained in projectile fragmentation reaction of Heavy Ion in Bevalac[1], show an anomaly; the rms radii of ^{11}Li and ^{11}Be are much larger than those which are obtained by the spherical Hartree-Fock calculation. We show the radii of the Li isotopes in Fig. 1. Theoretical curves in Fig. 1 are calculated

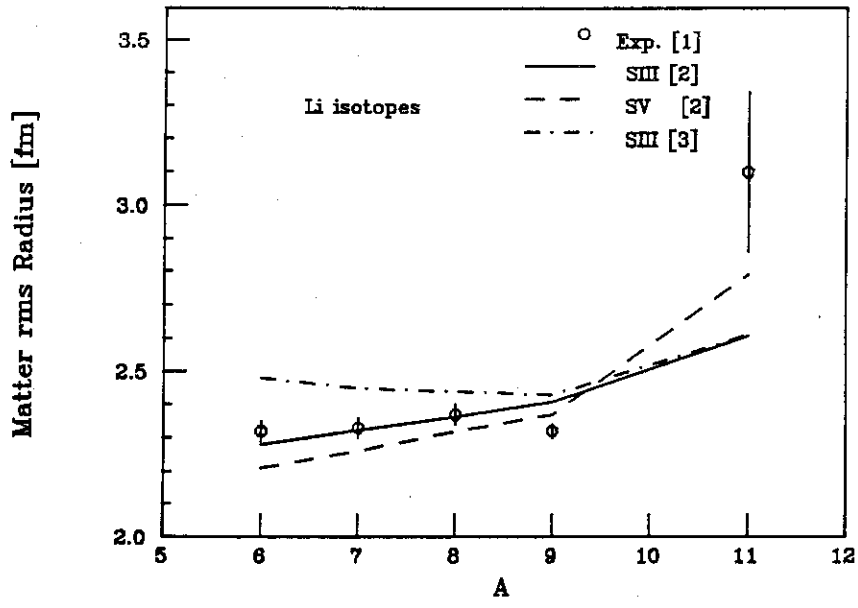

Figure 1 Matter radii of Li isotopes

by the spherical Hartree-Fock calculations, using the Skyrme-type density dependent force. Two different ways for these open-shell nuclei are adopted to give the density-matrices in these calculations [2][3]. The value of ^{10}Li is not available because it is unstable. In Fig. 1, one can see the anomaly of the radius of ^{11}Li.

We consider a mixing of sd-shell components to the ground states of ^{11}Li because they make the ground state of ^{11}Be be $\frac{1}{2}^+$ in the shell model calculations, suggested by the Talmi and Unna[4]. We take a configuration space upto $2\hbar\omega$ excitations as a model space and calculate the ground state wave functions of Be and Li isotopes using Millener-Kurath interaction[5], This interaction reproduces the energy of the $\frac{1}{2}^+$ state near that of the first $\frac{1}{2}^-$ state.

Utrecht group[6] has already calculated the p-shell nuclei by using a phenomenological interaction in full $(0+2)\hbar\omega$ configuration space. However, one has a large admixture of 1p-1h components (e.g. $(0p)^{-1}(1p)$ component,in ^{16}O) in the ground state of a closed shell nuclei by this calculation. We do not go into details this problem [1]

We take the model space of 0p-0d1s shells instead of full $(0+2)\hbar\omega$ space. As mentioned before, the Millener-Kurath interaction does not reproduce the ground state spin $\frac{1}{2}^+$ of ^{11}Be correctly, though it is very close to $\frac{1}{2}^-$ state. Thus, we change the single particle energy $\epsilon_{1s_{1/2}}$ of $1s_{1/2}$ state as a free parameter to interchange the sequence of the energies of $\frac{1}{2}^+$ and $\frac{1}{2}^-$ states. The modified single particle energy is defined as

$$\epsilon'_{1s_{1/2}} = \epsilon_{1s_{1/2}} - \Delta\epsilon_{1s_{1/2}}. \tag{1}$$

We show the number of particles in sd-shell nuclei in Fig. 2. The value of

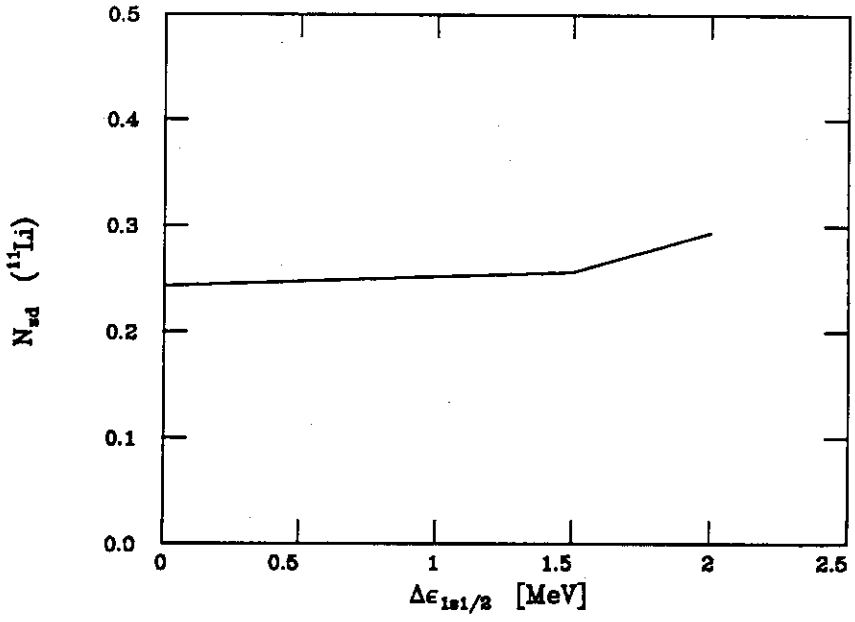

Figure 2 Particle number in sd-shell in ^{11}Li

$\Delta\epsilon = 2.0$MeV gives rise to invert $\frac{1}{2}^+$ and $\frac{1}{2}^-$ states in ^{11}Be, but the number of particle in sd-shells in ^{11}Li is not too large (it is 0.3). This fact suggests that we cannot obtain the enhancement of the rms radius of ^{11}Li when we use a harmonic oscillator (H.O.) single particle wave functions. We use the Hartree-Fock wave function, calculated by using Skyrme-type density interaction (SII), instead of the H.O. wave function. We adopted a way that is, the density-matrix was given by the occupation probability obtained by the shell model calculation[3]. When we use the $0\hbar\omega$ model space, this calculation

[1]Detailed discussions will be found somewhere else [7]

gives 2.61fm (c.f. 2.41fm by the H.O. wave function). On the other hand, when $(0+2)\hbar\omega$ model space is taken, it gives 2.81fm (c.f. 2.47fm by the H.O. wave function). However, since we do not check the convergence of this value, we have to calculate them in a self-consistent way.

We can obtain the enhancement of the rms radius more easily if we take into account the deformation of ^{11}Be predicted by the deformed Hartree-Fock calculation. One-neutron separation energy confirms the breakdown of N=8 closed core near ^{11}Be (see Fig. 3). Measurements of the quadrupole moment of these nuclei will be a crucial test in the investigation.

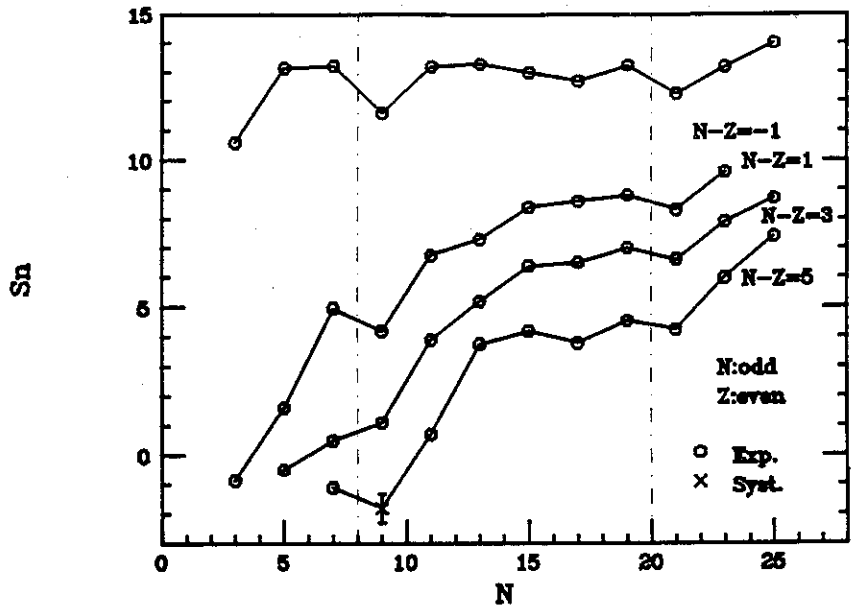

Figure 3 One neutron separation energy

References

[1] K.Sugimoto, O.Yamakawa,T.Kobayashi and I.Tanihata, Phys. Rev. Lett. **55**(1985)55

[2] H.Sato and Y.Okuhara, Phys. Rev. **C34**(1986)34

[3] H.Sagawa, private comminucation.

[4] I.Talmi and I.Unna, Phys. Rev. Lett. 4(1960)469

[5] D.J.Millener and D.Kurath, Nucl. Phys. **A255**(1975)315

[6] P. W. M. Glaudemans, in Proceeding of International Symposium on Nuclear Shell Models, Drexel University, Philadelphia. 1984, p. 2

[7] T.Hoshino, H.Sagawa and A.Arima, Nucl. Phys. **A**(1988) in press.

38. Dynamical Decay of a Hot Nucleus

M. ABE AND N. TAKIGAWA

Department of Physics, Tôhoku University, Sendai, Japan

Introduction Recently, the conventional inputs in statistical decay codes are claimed to be inadequate in the analysis of evaporation spectra of α particle: (1) the level density parameter a is reduced from a=A/8 (the empirical value at low excitations) to A/13 at T$\simeq$ 5 MeV [1], (2) the Coulomb barrier compiled from the energy spectra is systematically lower by 2–3 MeV than the fusion barrier[2]. We have to, however, refine these inputs for high excitations before drawing definite conclusions such as the change of the nuclear property at high excitations. First, the saddle point approximation for the level density is inadequate at high excitations. Second, the transmission coefficient for the particle-decay from a hot nucleus differs from that for the reactions between cold nuclei.

Level density parameter at high excitations The saddle point approximation for the nuclear level density is adequate only at low excitations, when the spacing of single particle levels around the Fermi energy is strongly energy dependent. Therefore, the dynamical bunching of the levels discussed in ref.[3] would have a significant effect on the approximation. The dynamical effect on the level density parameter can be extracted from the energy-dependent optical potential, of which we use the Brown-Rho parametrization for the imaginary part,

$$W(E) = \frac{KE^2}{E^2 + E_0^2}, \tag{1}$$

where E is the energy measured from the Fermi energy. The analyses of spreading widths and optical potentials for light nuclei give K =12.0 MeV, E_0 =22.4 MeV. The dispersion relation between the real and the imaginary parts of the optical potential leads to the following energy-dependent effective mass,

$$\left(\frac{m^*(E)}{m}\right) = \left(\frac{m_k}{m}\right) \cdot \left[1 + \frac{KE_0(E_0^2 - E^2)}{(E_0^2 + E^2)^2}\right]. \tag{2}$$

The $m_k = (0.6-0.7)\cdot m$ is the effective mass due to the nonlocality of the nuclear potential and is known to be weakly energy dependent. The specific heat at low temperature is given by

$$\left(\frac{C(T)}{C_0(T)}\right) = \frac{3}{\pi^2}\int_{-\infty}^{\infty} \frac{\frac{m^*(E=xT)}{m^*(E=0)}\cdot x^2 dx}{(1+e^x)(1+e^{-x})} \tag{3}$$

where $C_0(T) = \frac{\pi^2}{2}(T/\varepsilon_F^*)$ is the specific heat of the Fermi liquid with constant effective mass $m^*(E=0)$. Fig.1 shows the temperature dependence of (C/C_0) for three different values of E_0 (solid lines) and that for the normalized level density parameter(points with bar) reported in ref.[1]. The parameter set $K = 12MeV, E_0 = 22.4MeV$ gives the level density parameter reduced by 30 % at T = 5 - 6 MeV, which is close in magnitude to that claimed in ref.[1].

· Transmission coefficient for the particle decay from a hot nucleus We calculate the transmission coefficient for the particle evaporation from a hot compound nucleus, by assuming that the particle couples to one low lying collective vibration of the residual nucleus populated according to the canonical distribution of temperature T. The resulting expression is

$$t(E,T) = \int_{-\infty}^{\infty} \frac{dx}{\sqrt{2\pi}} e^{-x^2/2} \quad t_0(E, V(R) + x\alpha_T f(R)), \tag{4}$$

where $t_0(E, V(R))$ is the transmission coefficient for the one dimensional potential V(R), E the kinetic energy of evaporated particle, $f(R)$ the coupling form factor to the intrinsic vibration. The effective coupling strength α_T is related to the amplitude of the zero point vibration α and the excitation energy of the intrinsic phonon $\hbar\omega$ as follows,

$$\alpha_T^2 = \alpha^2 \cdot \Big[1 + 2n_B(\omega, T)\Big], \tag{5}$$

with the Bose distribution $n_B(\omega, T) = [\exp(\hbar\omega/T) - 1]^{-1}$. Fig.2 shows the s-wave evaporation spectrum of light particle A (= α, ^{16}O, ^{40}Ca) from the

compound nucleus A+^{198}Pt. The slope parameter was assumed to be 1 MeV for all lines in Fig.2. The line (1) is the result of 1-dimensional potential model which ignores the dynamical effects. The line (2) was dynamically calculated by setting the temperature of the intrinsic phonon T=0. This corresponds to the result of the conventional Weisskopf formula. The line (3) incorporates the dynamical coupling to the thermally fluctuating intrinsic phonon at T=1MeV. We see that the dynamical coupling to the low lying vibrational boson affects the evaporation spectrum below the Coulomb barrier, especially for heavy cluster evaporations. The "thermo"-dynamical effect due to the primary excitation of the residual nucleus becomes more significant for higher excitations.

REFERENCES

1. G. Nebbia *et al.*, Phys. Lett. **B 176** (1986) 20
2. L. Vaz and J. Alexander, Z. Phys. **A 305** (1982)313; **A318**(1984)231
3. C. Mahaux *et al.*, Phys. Rep. **120** (1985) 1

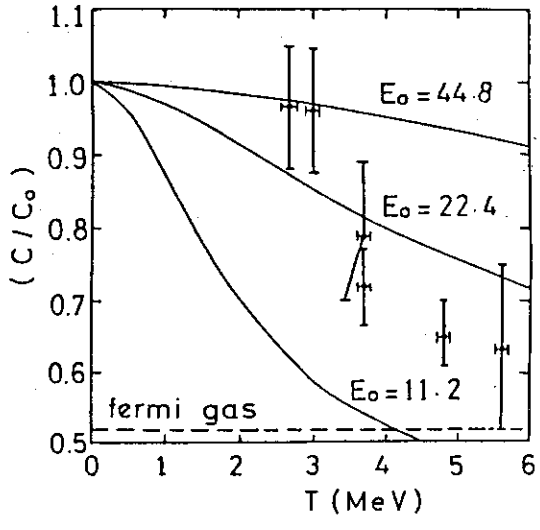

Fig. 1

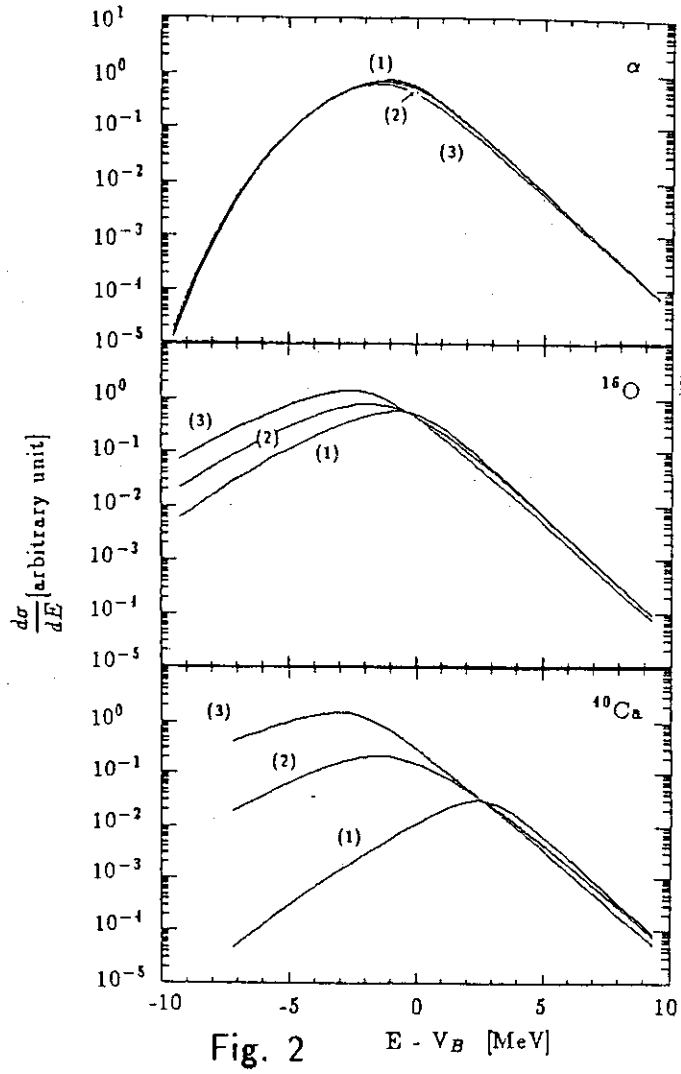

Fig. 2

39. Mass Distributions of Fission Fragments in the ^{19}F + ^{197}Au Reaction

Hiroshi Ikezoe, Naomoto Shikazono, Yoshiaki Tomita, Yasuharu Sugiyama, kazumi Ideno, Wataru Yokota, Yuichiro Nagame, S.M.Lee*, Mitsuhiko Ogihara*, S.C.Jeong*, Hideaki Fujiwara* and David J.Hinde**

Department of Physics, Japan Atomic Energy Research Institute, Tokai, Ibaraki, *Institute of Physics and Tandem Accelerator Center, University of Tsukuba, Ibaraki, and **Research Center for Nuclear Physics, Osaka University, Osaka

This is a report of measurements of the mass distributions for fission fragments produced in the ^{19}F on ^{197}Au reaction. The experiment was performed at the JAERI tandem accelerator. A 450 $\mu g/cm^2$ thick ^{197}Au target was bombarded by ^{19}F beams with beam energies from 100 to 160 MeV. Fission fragments were measured by three time-of-flight (TOF) telescopes. In order to calibrate the absolute mass of the fission fragments, ^{81}Br beams with a beam energy of 200 MeV were used to bombard targets of ^{nat}Ag, ^{nat}Sb and ^{nat}Ba. The recoil nuclei and the scattered ^{81}Br ions were detected by these TOF telescopes at various scattering angles. The ^{81}Br beam energy and the target masses were chosen so as to obtain recoil nuclei covering the ranges of mass and energy of the fission fragments.

The typical mass distribution corrected for neutron emission is shown in Fig.1. The centroids of the mass distributions are shown in Fig.2 as a function of the mean center-of-mass scattering angle. The present data show a weak but distinct angular dependence of the mass centroids, which increases with bombarding energy. The shift from forward to backward angles is ~3 a.m.u. at the highest bombarding energy (E_{Lab}=160 MeV), which is much greater than the systematic uncertainty.

Figure 3 shows the relative angular distributions (normalized to one at θ_{cm}=86.5°) for the two different mass bins at the bombarding energy of 160 MeV. From this figure we can see the enhanced (weakened) yields of the heavy fragments compared with those of the light fragments at the forward angles (at the backward angles). These asymmetric angular distributions of specified fragments are also reported in [1,2] as an evidence of the quasi-fission process.

Forward-backward mass centroid shifts have been observed for heavier reaction systems and have been interpreted in the framework of the extra-push model [3]. According to this model, an "extra-extra push energy" is required

for a heavy reaction system to form a compound nucleus inside the true fission saddle point. If the bombarding energy is not high enough, a fission-like (quasi-fission) process occurs, without the formation of a compound nucleus inside the saddle-point, which may result in a forward-backward mass asymmetry, depending on the reaction time and angular momentum. For the present reaction, the extra-extra push energy is zero according to Back's systematics [4]. Nevertheless the present results indicate a small but a definite occurrence of the quasi-fission process in addition to the dominant compound fusion-fission process in the ^{19}F on ^{197}Au reaction.

References

1. Keller, H., Lutzenkirchen, K., Kratz, J.V., Wirth, G., Bruchle, W., Summerer, K.:Z.Phys.326,313(1987)
2. Lutzenkirchen, K., Kratz, J.V., Wirth, G., Bruchle, W., Summerer, K., Lucas, R., Poitou, J., Gregoire, C.:Nucl.Phys.A452,351(1986)
3. Swiatecki, W.J.:Phys.Scr.24,113(1981)
4. Back, B.B., Betts, R.R., Gindler, J.E., Wilkins, B.D., Saini, S., Tsang. M.B., Gelbke, C.K., Lynch, W.G., McMahan, M.A., Baisden, P.A. :Phys.Rev.C32,195(1985)
5. Cohen, S., Plasil, F., Swiatecki, W.J.:Ann.Phys.(N.Y.) 82,557(1974)

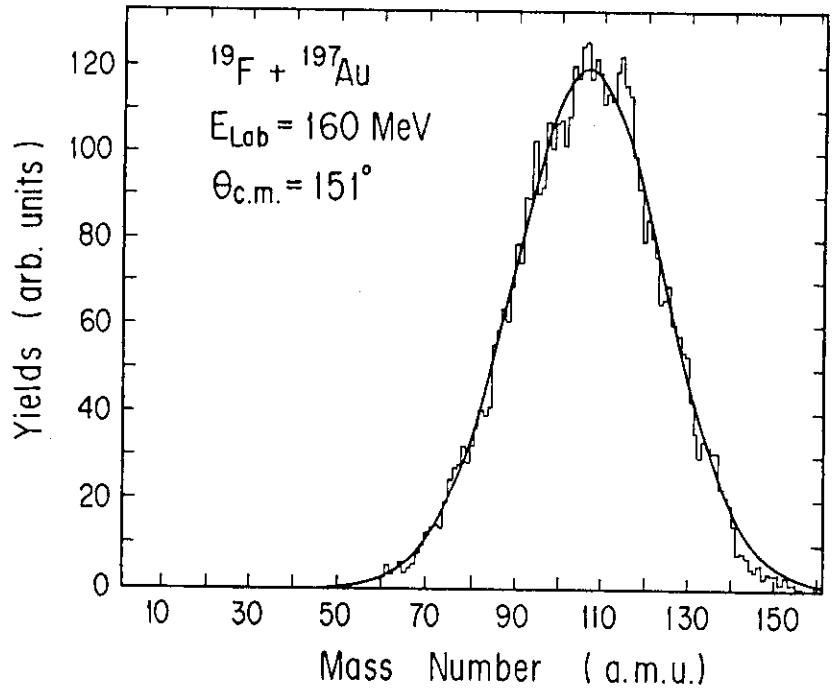

Fig.1 Typical mass distribution of the fission fragments corrected for neutron emission. The solid line is the fitted curve assuming a gaussian function.

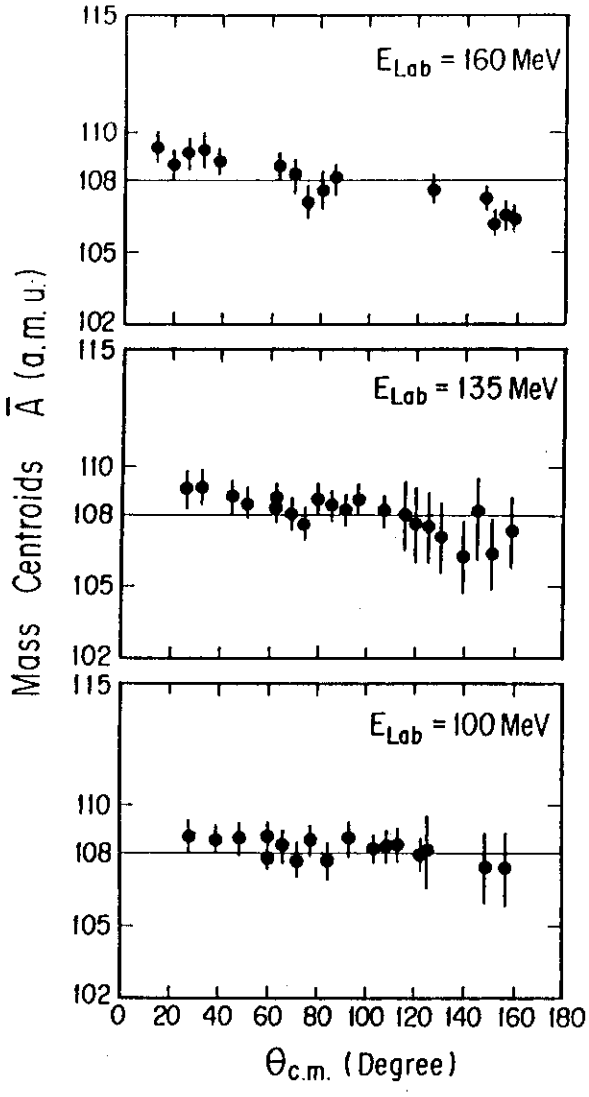

Fig.2 Centroids of the mass distributions of the primary fission fragments at three bombarding energies as a function of the center-of-mass scattering angle.
The horizontal line is the half mass of the compound nucleus.

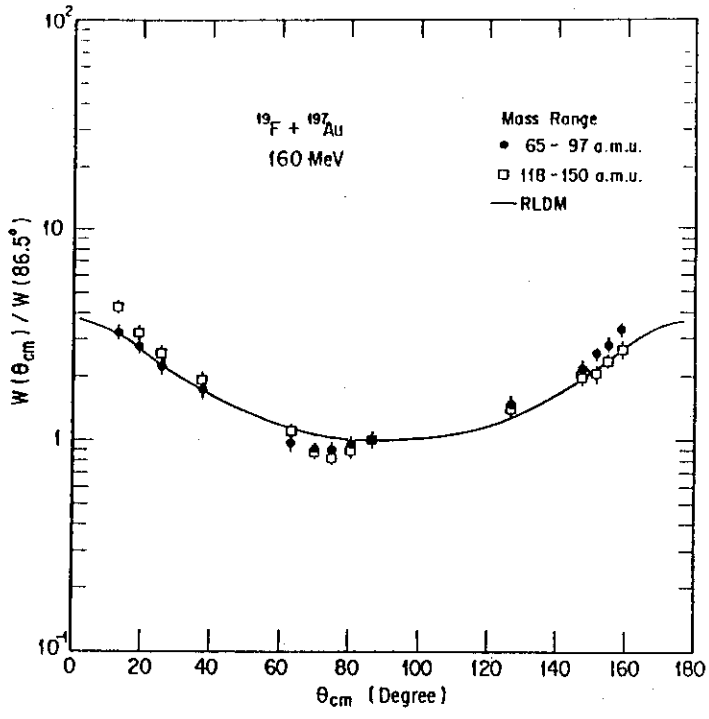

Fig.3 Relative angular distributions of the specified fragments indicated in the figure. Two angular distributions are normalized to one at θ_{cm}=86.5°. The Solid lines are calculations of the standard fission theory using the rotating liquid drop model[5].

40. Large Fragment Emission from the ^{105}Ag Compound Nucleus

Yuichiro Nagame, Sumiko Baba, Kentaro Hata, Toshiaki Sekine, Shin-Ichi Ichikawa, Hiroshi Ikezoe, Kazumi Ideno, Akihiko Yokoyama*, Yuichi Hatsukawa** and Masaaki Magara***

Japan Atomic Energy Research Institute, *Department of Chemistry, Osaka University, **Department of Chemistry, Tokyo Metropolitan University, ***Department of Nuclear Engineering, Nagoya University.

The statistical decay of the compound nucleus has been described in terms of two different modes: light particle evaporation and fission. However, the unity of both the decay modes of highly excited compound nucleus has been emphasized by Moretto[1]. This model treats the two decay modes as a continuous transition from light particle emission to symmetric fission; large fragments intermediate between alpha particles and symmetric fission fragments are produced in the decay of the compound nucleus. The decay widths of various fragments are mainly controlled by the potential energy surface(emission barrier) to binary decay into appropriate masses. This emission barrier is considered to be the energy of the saddle-point shape with constrained mass-asymmetry[1,2].

The present work is devoted to the understanding of the angular momentum dependence of this emission barrier by using the heavy-ion reactions. We present the experimental results on the measurement of large fragments($6 \leqq Z \leqq 29$) produced in the reaction of ^{37}Cl+^{68}Zn. The possibility of large fragment emission from the compound nucleus ^{105}Ag is discussed by comparing the yields of the large fragments with the equilibrium statistical model calculation which takes into account the emission barriers depending on mass-asymmetry and angular momentum.

The 170MeV ^{37}Cl beam with an intensity of $\sim 10^{10}$ particles/s delivered by the JAERI tandem accelerator was used to bombard a self-supporting enriched ^{68}Zn target(755 μg/cm^2). The reaction products were detected by two counter telescopes with ion chambers as the ΔE detectors and Si(Li) as the E detectors.

In the kinetic energy distributions obtained for each element Z, the mean kinetic energies of the relaxed component roughly corresponded to the Coulomb repulsion energy between two touching spheres; for the symmetric

mass-splitting products, the total kinetic energies were well reproduced by the Viola's empirical formula[3]. The angular distributions of the relaxed kinetic energy component for the products with Z=6 to 29 are shown in Fig.1. The forward peaking of the angular distributions observed for the products with Z close to that of the projectile is typical for the shorter interaction time, indicating the contribution of deep inelastic scattering. Since the angular distributions of the products with $Z \leqq 10$ and $Z \geqq 20$ are essentially flat in $d\sigma/d\theta_{cm}$, these products are considered to be either products of a long-lived dinuclear system or decay products from a compound nucleus. The component with $1/\sin\theta_{cm}$ angular distribution for each Z will be discussed in the following.

Figure 2 shows the integrated cross section of each element over the flat region in the angular distribution of Fig.1 together with the charge distribution given by the equilibrium statistical model calculation[1,4]. As shown in Fig.2, the experimental charge distribution clearly exihibits the features expected from the mass-asymmetry and angular momentum dependence of the emission barriers(Fig.3). It seems that the lighter fragments($Z \lesssim 9$) are produced by asymmetric mass divisions at lower angular momentum region, while the heavier fragments around $Z_{CN}/2$ are favorably produced by symmetric mass divisions at higher angular momentum region. The calculation, however, underestimates the yields of lighter fragments($Z \lesssim 9$). This discrepancy may be attributed to the unsuitable emission barriers in extreme mass-asymmetry, since we deduced the emission barriers from a simple model of two touching spheres of the liquid drop masses. For better understanding of the emission barriers depending on the mass-asymmetry and angular momentum, measurements of the excitation functions for the large fragments and of the widths of the mass distributions for the symmetric mass-splitting products are in progress by varying the projectile energy in wider range.

References

1). L.G.Moretto, Nucl.Phys.A247(1975)211.
2). K.T.R.Davies and A.Sierk, Phys.Rev.C31(1985)915.
3). V.E.Viola,Jr., Nucl.Data Tables A1(1966)391.
4). L.G.Sobotka et al., Phys.Rev.Lett.51(1983)2187, and 53(1984)2004.

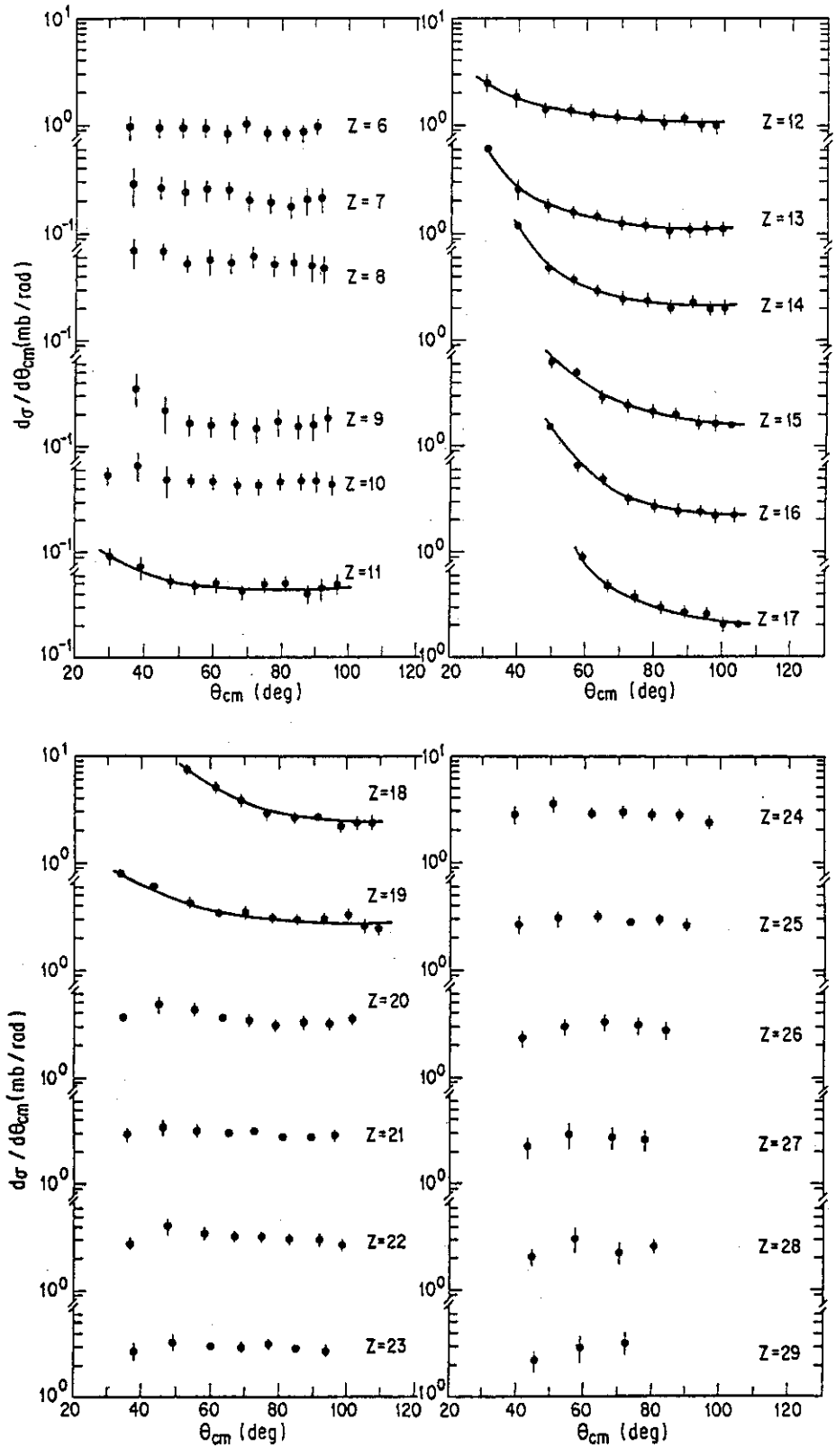

Fig.1 Center-of-mass angular distributions integrated over the relaxed kinetic energy components. The solid lines are drawn to guide the eye.

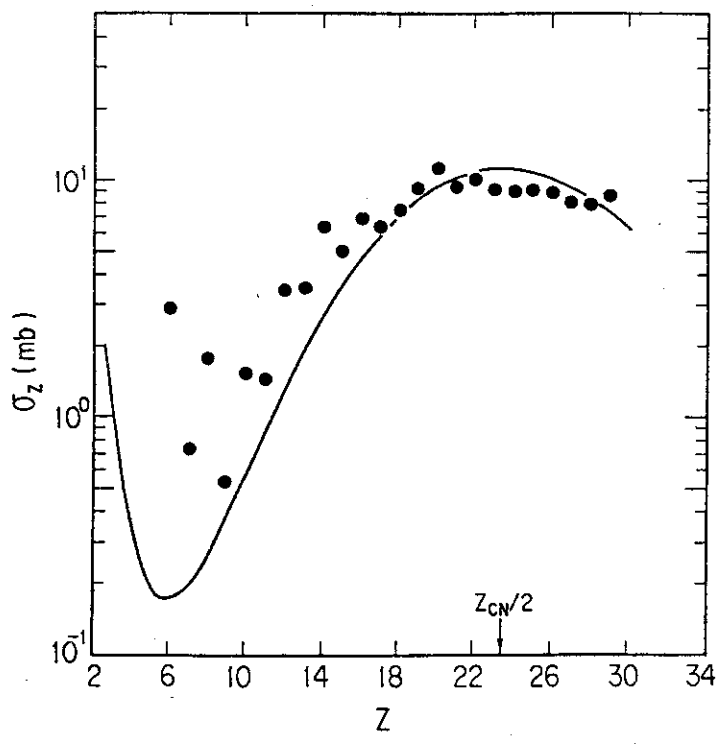

Fig.2 Integrated cross sections over the flat region in the angular distribution of Fig.1. The solid line is the result of the statistical model calculation. Z_{CN} is the atomic number of the compound nucleus.

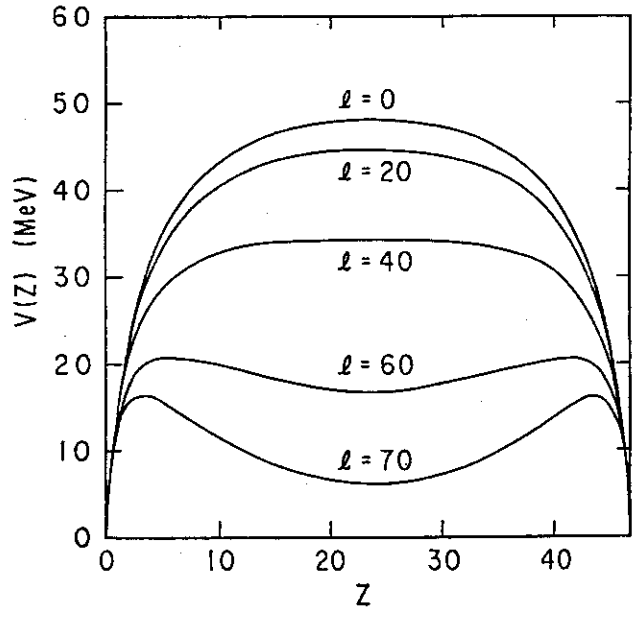

Fig.3 Potential energy surfaces(emission barriers) as a function of mass-asymmetry Z for different angular momenta for the decay of ^{105}Ag compound nucleus.

41. DYNAMICAL EFFECTS ON THE NUCLEAR MOLECULAR ORBITALS

S.Misono and B.Imanishi
Institute for Nuclear Study, University of Tokyo, Tokyo

When we study the nuclear molecular orbitals in heavy-ion collisions, we have to take dynamical effects into account, which are absent in the treatment of the electron molecular orbitals. One of these effects is the recoil effect. The origin of this effect lies in the finite mass of the transferred nucleon. Unlike the electron molecular orbitals, the ratio of the mass of the valence particle to the one of the core particle is not negligible and the molecular axis changes when the valence particle transfers from one core to the other.

Rotational coupling is another dynamical effects. It reflects the breakdown of the adiabaticity in the heavy-ion collisions. This adiabaticity is pretty well satisfied in the atomic collisions. In the heavy-ion collisions, on the other hand, the ratio of the characteristic time of the single particle motion to the scattering time is at most 3 even at the low bombarding energies. Thus the rotation of the molecular axis during the collision have to be considered.

Those two dynamical effects are examined through the numerical analysis on the ^{12}C-^{13}C and the ^{16}O-^{17}O scattering system.

When we treat the recoil exactly in our coupled-reaction-channel formalism, the transfer form factor becomes non-local. We apply the local approximation to this form factor with use of the momentum expansion and take only the 0th order term. Then the local form factor of the 0th order becomes to have J(total spin)-dependent property and K (projection of J along the molecular axis) -mixing terms if expressed in the helicity representation.

The rotational coupling also has K-mixing terms, namely the Coriolis K-mixing terms. Compared to these, the recoil K-mixing terms are much smaller and their contribution to the cross section is indeed negligible. One signature of the molecular orbitals is that the K number of the states becomes a good quantum number. The recoil K-mixing terms have little effect on these pure-K states. Those pure-K states are mainly destroyed by the Coriolis K-mixing terms at higher bombarding energies.

The main part of the recoil effect is contained in the J-dependence of the local form factor. Neither does this part cause significant change in the molecular orbitals themselves. Rather the interactions between the molecular orbitals are affected by the recoil. And the significant change is caused by the recoil when the Landau-Zener transition is involved as in the the ^{12}C-^{13}C system. Since the interaction of the Landau-Zener type has very sharp shape, a slight change in its location or in its width due to the recoil causes considerable change in the cross section. In such a case the inclusion of the recoil effect is necessary for the quantitative analysis of the molecular orbital formation.

The rotational coupling, on the other hand, affects the molecular orbitals themselves. This is illustrated in the $^{17}O(^{16}O,^{16}O)^{17}O^{*}(1/2^{+})$ reaction. When we calculate the conventional adiabatic potentials for the negative parity of this system, we find a pseudo-crossing at r=7.5fm between the ground and the 1st excited molecular orbital. This crossing is quite similar to the one found in the two-center shell model diagram for $^{12}C+^{17}O$ system and has been claimed to be the main source to feed the 2s1/2 state.

However, when we define the molecular orbitals with the inclusion of the rotational coupling (rotating molecular orbitals), another pseudo-crossing appears outside the Coulomb barrier. The characteristic property of this second crossing is that the corresponding potential energy remains almost constant for all J, whereas its location is strongly J dependent. Thus even the higher partial waves can reach this crossing. This is in contrast to the effective Coulomb barrier, whose height increases as J. And if we think that the inelastic transition occurs mainly at this second crossing, we can understand the early rise of the integrated cross section to the 2s1/2 state just above the Coulomb barrier energy and the saturation property at the following energy region. Thus we can say the second pseudo-crossing induced by the rotational coupling plays a dominant role in the inelastic transition.

In conclusion the dynamical effects are important both in the quantitative and in the qualitative argument on the nuclear molecular orbitals.

42. Quasi-Elastic Scattering Near The Coulomb Barrier: $^{16}O+^{144,148,152}Sm$

Yasuharu SUGIYAMA, Yoshiaki TOMITA, Hiroshi IKEZOE, Kazumi IDENO, Norihisa KATO*, Tsuyoshi SUGIMITSU*, Hiroshi FUJITA** and Shigeru KUBONO***

Department of Physics, JAERI, *Department of Physics, Kyushu University, **Daiichi College of Pharmaceutical Sciences, ***INS, University of Tokyo

The correlation between quasielastic reaction and the enhanced subbarrier fusion attracts much interest in heavy-ion reactions near the Coulomb barrier. So far fusion reactions for $^{16}O+^{144,148,150,152,154}Sm$ have been carried out and strong isotope dependence has been observed in subbarrier fusion cross sections[1,2]. The effect of the quadrupole deformation has been taken into account in order to explain the isotope dependence.

In this report we describe results of the quasielastic reaction for the systems of $^{16}O+^{144,148,152}Sm$ carried out at the JAERI tandem accelerator. The ^{16}O beam energy was 72MeV which was about 10% higher than the Coulomb barrier. The energy spectra were measured with an energy resolution of 200 keV by using the heavy-ion spectrograph[3] "ENMA". Mass number, atomic number, Q-value and atomic charge state q of reaction products were determined unambiguously from a measurement of the total energy E, energy loss δE and momentum P. Six nuclei ^{17}O, ^{18}O, ^{15}N, ^{12}C, ^{13}C and ^{14}C were observed in addition to elastically scattered ^{16}O. Other reaction products could not be identified because of their small yields.

The angular distribution of the elastic scattering for $^{16}O+^{144}Sm$ were measured at the incident energy of 71.4MeV[4]. The optical potential parameters which reproduced the data were obtained with the code Ptolemy.

Energy spectra obtained at $\theta_{lab}=95°$ from the reactions $Sm(^{16}O,^{17}O)$ and $Sm(^{16}O,^{15}N)$ are shown in fig. 1. Angular distributions for the ground state transition of these reactions are shown in fig.2. In the reaction $^{152}Sm(^{16}O,^{17}O)^{151}Sm$ the angular distribution for the energy-integrated cross sections (total) is shown. Absolute values of the reaction cross sections were derived by normalizing the yields to those of the elastic scattering which were measured simultaneously. The absolute value of the elastic scattering cross sections for $^{16}O+^{148,152}Sm$ was taken from the data by Weber et al[5].

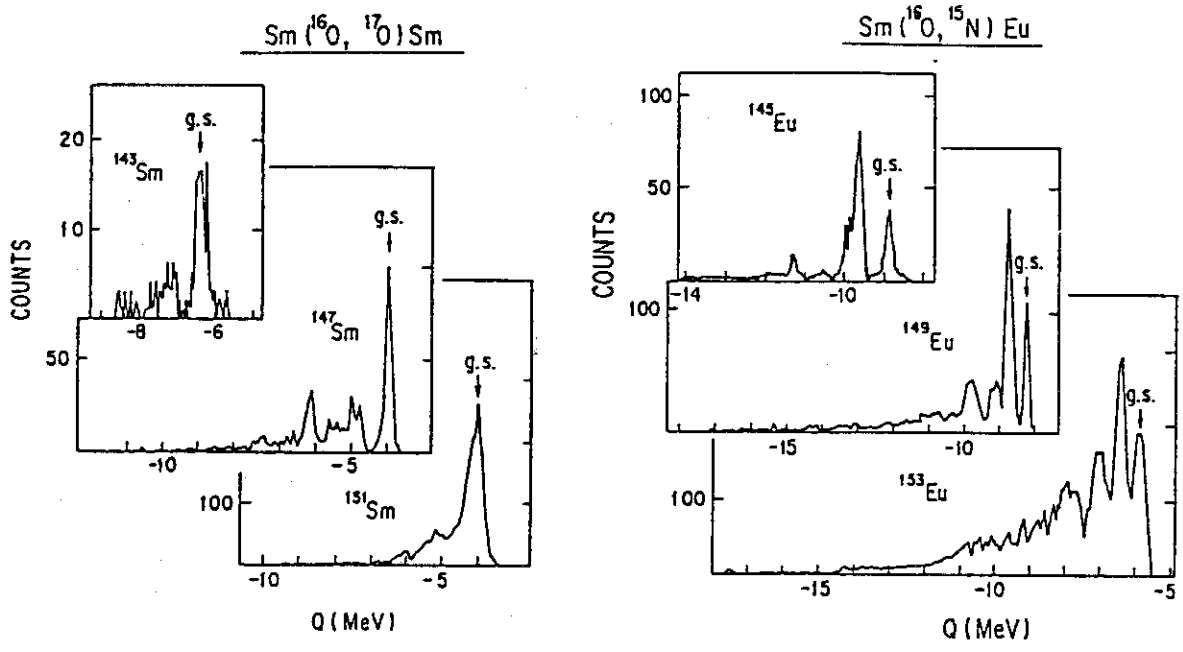

Fig.1 Spectra obtained from the (^{16}O,^{17}O) and (^{16}O,^{15}N) reactions on ^{144}Sm, ^{148}Sm and ^{152}Sm .

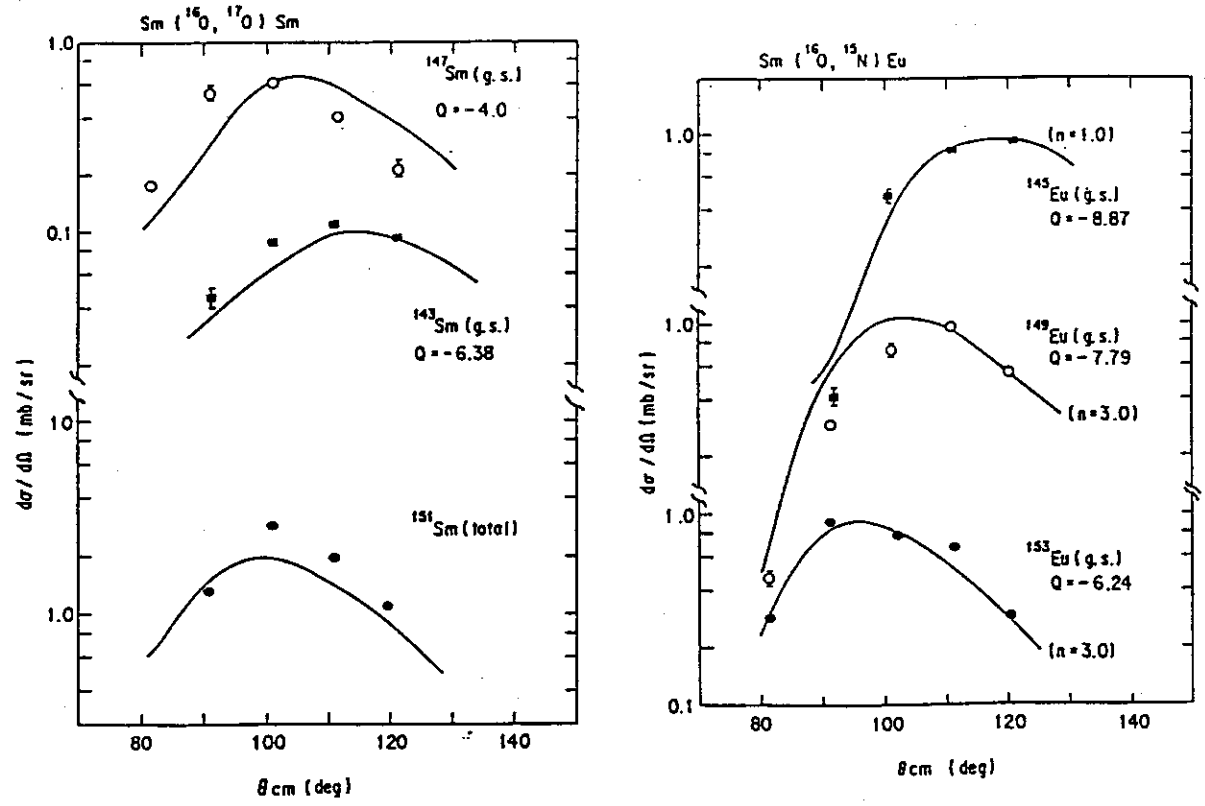

Fig.2 Angular distributions obtained from the (^{16}O,^{17}O) and (^{16}O,^{15}N) reactions on ^{144}Sm, ^{148}Sm and ^{152}Sm. Solid lines are DWBA calculations.

DWBA calculations for one-neutron pickup and one-proton transfer reactions were performed with the code Ptolemy. We used the optical potential parameters which were obtained through the coupled-channel analysis for the elastic scattering[4,6]. For the spectroscopic factors we used the values obtained by the light-ion induced reactions such as (p,d), (d,p), (^{3}He,d) and (d,^{3}He) etc. Solid lines in Fig.2 are the results of the DWBA calculations. For the one-neutron pickup reaction (^{16}O,^{17}O), angular distributions are well explained by the DWBA calculations with a normalization factor of n=1. On the other hand a normalization factor of n=3.0 is required for the one-proton transfer reaction of ^{148,152}Sm(^{16}O,^{15}N).

The sum of the measured quasielastic and fusion cross sections at E_{lab}=72 MeV is compared in Table 1 with the optical-model calculation using parameters which reproduce the elastic scattering data. The optical model calculation reproduces well the total reaction cross sections.

Table 1 Measured quasielastic and fusion cross sections at E_{lab}=72 MeV. The sum of measured cross sections are compared with the total reaction cross sections calculated from the optical model.

	target		
	^{144}Sm	^{148}Sm	^{152}Sm
$\sigma_{transfer}$	34	51	87
σ_{fusion}	220	270	330
$\sigma_{inelastic}$	124	505	1896
Sum	378	826	2313
σ_{R}^{c}	359	831	2300

References

1) R.G.Stokstad et al., Phys.Rev.C21(1980)2427.

2) D.E.Di Gregorio et al., Phys.Lett.B176(1986)322.

3) Y.Sugiyama et al., Nucl.Instrum.& Methods 187(1981)25; Z.Phys. A322(1985)579.

4) Y.Sugiyama et al., to be published.

5) D.J.Weber et al., to be published.

6) R.G.Stokstad et al., Phys.Rev. C23(1981)281.

43. On the Subbarrier Fusion of $^{74}Ge + ^{74}Ge$

Akira Iwamoto* and Noboru Takigawa**

*Department of Physics, Japan Atomic Energy Research Institute and
**Department of Physics, Tohoku University

Enhancement of the subbarrier fusion cross section over the one-dimensional barrier penetration calculation occurs commonly for the reaction when both projectile and target are heavy. The amount of the enhancement is closely related to the size of the system. When the effect of the intrinsic excitation is taken into account by the coupled channel calculation, the data for Ni+Ni or for lighter systems can be reproduced fairly well. For heavier systems, however, the experimental data become much larger than what are calculated by using coupled channel model.

In Ref.1, the above problem was attacked by starting from the semiclassical neck-formation mechanism. The enhancement of the cross section in this model is closely related to the lowering of the effective barrier due to the formation of neck part. Later in Ref.2, the similar model was used to calculate the potential energy systematically. In Fig.2 of Ref.2, we see clearly the systematic trend of the cross section data as a function of the size of the colliding system. Semiclassical liquid-drop-model calculation assuming the neck formation mechanism is found to be powerful to reproduce the general trend of the data as a function of the size of the system. On the other hand, there are some data which show deviation from the general trend. Among them, the system $^{74}Ge+^{74}Ge$ and $^{40}Ar+^{154}Sm$ show large deviations.[1,2] For the latter system, the Ar induced subbarrier fusion data on other Sm isotopes suggest[3] that the ground state deformation of ^{154}Sm plays the important role for the anomaly. In this talk, we concentrate on the anomaly seen in $^{74}Ge+^{74}Ge$ system.

The characteristic of the $^{74}Ge+^{74}Ge$ system is the following. The nucleus ^{74}Ge is spherical in ground state but it is soft against

deformation. Another point is that the compound system ^{148}Gd lies in the mass region of nuclei which shows the super-deformed band. To take into account the effect of the shell structure, we used the Strutinsky procedure to calculate the fusion barrier. The potential energy is obtained by the sum of the liquid drop energy and the shell correction energy. We applied this method to calculate the fusion barrier corresponding to the neck-formed configuration.

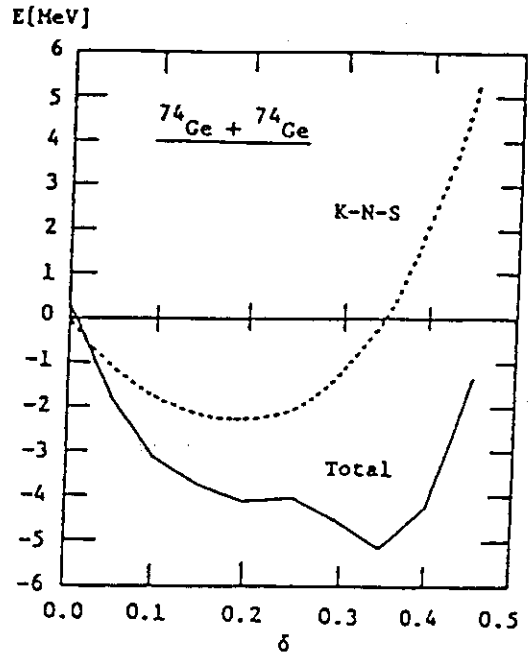

Change of the fusion barrier height as a function of the deformation of the fragment deformation.

Addition of the shell correction caused little effect on the resultant barrier height. The situation changed drastically, however, when we included the freedom of the deformation of two Ge. In the figure, we show the fusion barrier height as a function of the deformation δ of two Ge (same deformation for both of them is assumed). The dotted line is the Yukawa-plus-exponential-model calculation[4] normalized at δ=0. Inclusion of the deformation δ≈0.2 lower the barrier height by about 2.3 MeV. Addition of the shell energy to the dotted line results in total energy shown by the solid line. Due to large negative shell correction energy at large deformation, the barrier height is lowered by about 5.1 MeV at δ≈0.35. Shell correction energy near the barrier is roughly equal to the twice of the shell correction energy of isolated ^{74}Ge. In the isolated ^{74}Ge case, the liquid-drop energy rises so sharply as a function of the deformation that addition of the shell correction energy causes no remarkable change. The situation is quit different in the barrier region where the liquid-drop energy itself decreases as deformation increases up to δ≈0.2. Thus addition of the shell correction energy, which shows decreases sharply as a function of deformation, causes drastic change in the potential energy.

The same kind of the calculation was performed for the reaction of Ni+Ni systems. In this case, irrespective of the isotopes of Ni, we found no big change of the barrier height by inclusion of the freedom of the deformation together with the shell correction energy. In $^{74}Ge+^{74}Ge$ case, the decrease of the barrier height about 5 MeV shown in the figure explains the discrepancy between the data and the liquid-drop-model calculation of Ref.1. Thus the shell structure of the fragment is essentially responsible to the anomaly of the subbarrier fusion cross section. The point is that this shell correction plays a role explicitly when the freedom of fragment deformation is taken into account. On the other hand, the structure of the compound nucleus is not directly related to the change of the barrier height. In this sense, the relation of the exsistence of the super-deformed band to the anomaly of the subbarrier fusion cross section is not seen in this model.

In summary, the model calculation including the freedom of the deformation together with the shell correction energy can explain the anomalous enhancement of the subbarrier fusion cross section seen in $^{74}Ge+^{74}Ge$ system. Systematic calculations of the other systems are in progress.

References

1) A. Iwamoto and K. Harada: Z.Phys. A326 (1987) 201.
2) C.E.Aguiar et al.: Phys.Lett. 201 (1988) 22.
3) W. Reisdorf et al.: Nucle.Phys. A438 (1985) 212.
4) H.J. Krappe, J.R. Nix and A.J. Sierk: Phys.Rev.C20 (1979) 992.